

# Optical Fiber Mechanical Reliability

## Review of Research at Corning's Optical Fiber Strength Laboratory White Paper

WP8002

Issued: July 2017

Author: Dr. G. Scott Glaesemann

ISO 9001 Registered

### “Striving for Failure”

#### 1 Introduction

This is a review of many years of research at Corning into the mechanical reliability of optical fiber beginning in 1986. It begins with an introduction to the fairly complex science of flaw initiation, growth, and potential failure for optical fibers. Theoretical models for crack growth will be reviewed as well as the extensive body of experimental data generated to position the models for practical use. The purpose behind this research is realized in the creation of reliability design diagrams and allowable stress rules to guide use of optical fiber both in communications systems and photonic devices. While investigations refining our basic knowledge of optical fiber fracture will likely continue for many years, the knowledge gained since 1986 coupled with well-controlled manufacturing and installation processes have resulted in a communication network that has proven extremely reliable.

#### 2 Stress

##### 2.1 Residual Stress

Stress is required for the mechanical failure of fiber and it is convenient to separate stress into residual and applied stress. Residual stress develops over the entire fiber length from thermal expansion mismatch between core and cladding as well as draw-induced stress.<sup>1,2,3</sup> In conventional single-mode fiber, these stresses are small compared to the proof stress. However, manufacturing-induced residual stresses can affect physical parameters like fiber curl<sup>4</sup> and optical behavior like polarization mode dispersion.<sup>5</sup> The core of multimode fiber is under sufficient residual stress to cause localized fracture of the core during end polishing if one uses too large a polishing grit. These stresses are permanent, but have little influence on the fiber lifetime. Localized tensile residual stress is created when contaminants, in the form of particulate, attach themselves to the preform or fiber surface and cool during draw.<sup>6</sup> The coefficient of thermal expansion for zirconia, a known contaminant, is twice that of silica. The resulting residual stress decays rapidly ( $1/r^3$ ) as one moves away from the particle. Contamination has the added feature of being a flaw site. Localized residual stress is also generated when the glass surface is damaged by contact with a hard object.<sup>7,8,9</sup> This stress aids in the formation of subsurface flaw systems.

The Corning logo is a blue square with the word "CORNING" in white, uppercase, serif font centered within it.

CORNING

## 2.2 Applied Stress

Applied stresses are those imparted to the fiber by bending, pulling or twisting during processing, handling, and deployment. The stress created by applying a tensile load to the fiber is shown in Figure 1 for several different glass diameters. Note that conventional protective polymer coatings bear less than 3% of the load. In the case of proof testing, the small load borne by the coating is typically accounted for, but under long term tensile loading, the coating will relax and the entire load will eventually be supported by the glass.

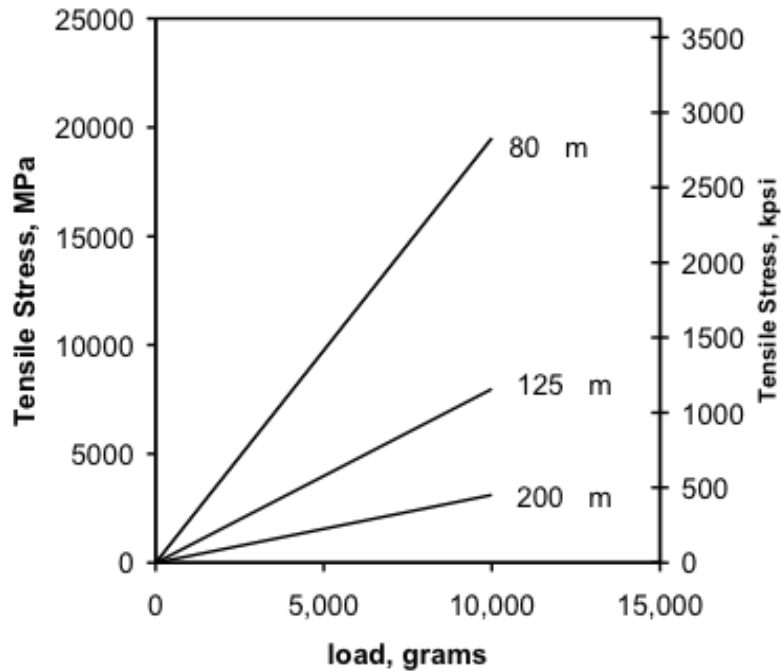


Figure 1. Tensile stress generated by loading for a range of glass diameters.

In bending, the stress is determined from the configuration of the fiber. Figure 2 illustrates that only half the volume of glass is in tension. From simple beam theory, the stress increases linearly from zero at the neutral axis to a maximum at the surface. The stress on the surface of the glass is of particular importance since surface flaws are susceptible to fatigue.

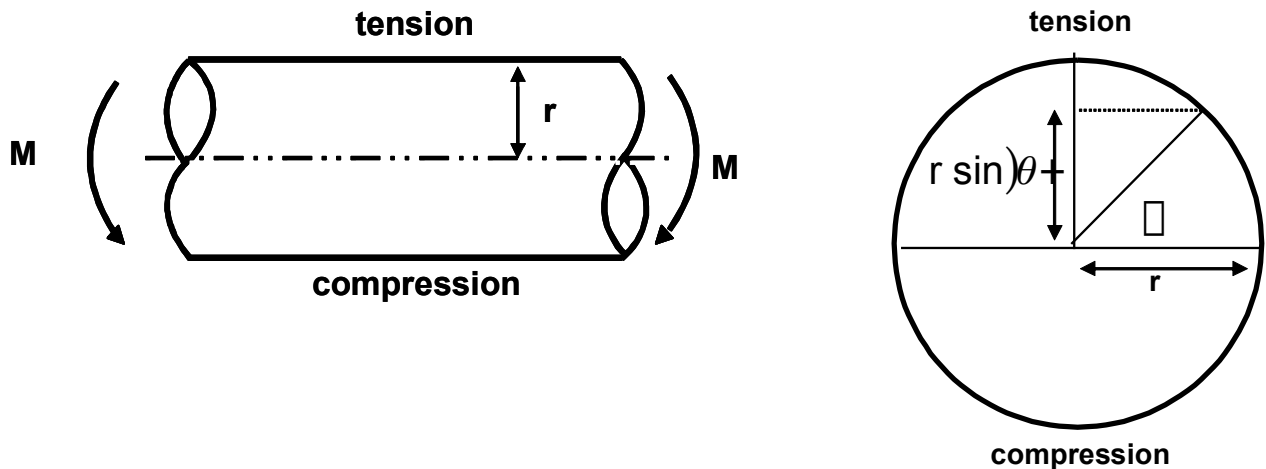


Figure 2. Fiber subjected to a bend of constant radius.

The surface stress decreases from the maximum bend stress at  $\theta=90^\circ$  to zero at the neutral plane according to,

$$\sigma = E \frac{r \sin(\theta)}{R} \quad (1)$$

where  $E$  is the elastic modulus,  $r$  is the radius of the glass portion of the fiber, and  $R$  is bend radius. Silica is a non-linear elastic material and the elastic modulus is dependent on the applied strain.<sup>10,11</sup> For engineering usefulness, the elastic modulus for silica fiber is most commonly expressed as the secant modulus,

$$E = E_o \left(1 + \alpha \varepsilon + \beta \varepsilon^2\right) \quad (2)$$

where  $E_o$ , Young's modulus at zero strain, is 70.2 GPa ( $10.2 \times 10^6$  psi),  $\alpha$  is 3.2 for tension and 2.3 for fiber in bending, and  $\beta=8.48$ .<sup>12</sup> The second order term is generally ignored as its contribution is small. Equation (2) is based on data up to 6% strain. For constant radius bending, the bend-induced strain is  $\varepsilon=r/R$ . The stress at the maximum bend radius,  $\theta=90^\circ$ , is then,

$$\sigma = E_o \frac{r}{R} \left[ 1 + \alpha \frac{r}{R} + \beta \left( \frac{r}{R} \right)^2 \right] \quad (3)$$

The maximum bend stress for 80, 125, and 200  $\mu\text{m}$  diameter fiber is shown in Figure 3 for a range of bend radii. Note that for typical strain levels of less than 1%,  $\sim 6$  mm bend radius or 700 MPa, Young's modulus changes little from the zero strain value and is, for practical purposes, constant.

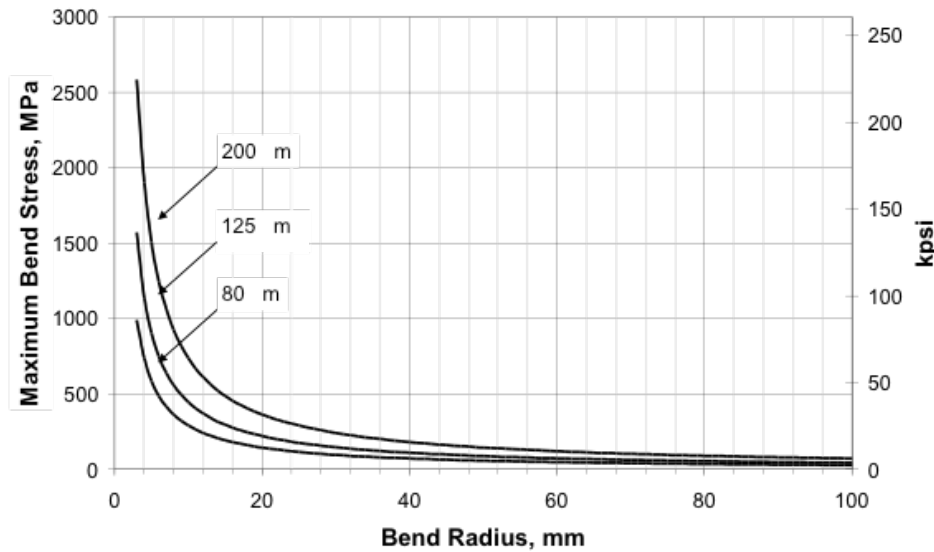


Figure 3. Maximum stress on the surface of fibers of varying diameters due to bending to a constant radius.

When fiber is bent, half the volume of the glass is in compression and not at risk for failure. The maximum tensile stress generated by the bend is a thin line along the length of the fiber. Thus, the risk of failure on the tensile side depends upon the circumferential location of the flaw in addition to the size of the flaw. A large flaw near the neutral plane can be at a lower risk of failure than a smaller flaw near the maximum bend stress. This has statistical consequences as well. Consider two fiber lengths, one is coiled and the other placed straight under tension such that the maximum bend stress of the coiled fiber is equal to the applied tensile stress in the straight fiber. Half of the flaws in the bent fiber are in compression and not at risk of failure, and most of those in the tensile side experience a stress less than the maximum bend stress. Thus, a considerably longer length of bent fiber is required in order to have the same risk of failure. In Figure 4 the equivalent tensile length,  $l_{eq}$ , for a given bend length,  $l_b$ , is shown for a range of Weibull moduli,  $m$ .<sup>7</sup> For typical  $m$  values near the proof stress of 3 to 5, the equivalent tensile length is about 20% of the length in bending.<sup>13</sup> Twenty kilometers of fiber in bending is equivalent to sampling flaws from three to four kilometers in tension. This analysis is useful from a testing perspective in that tensile testing is more efficient when sampling long fiber lengths than bend strength testing.

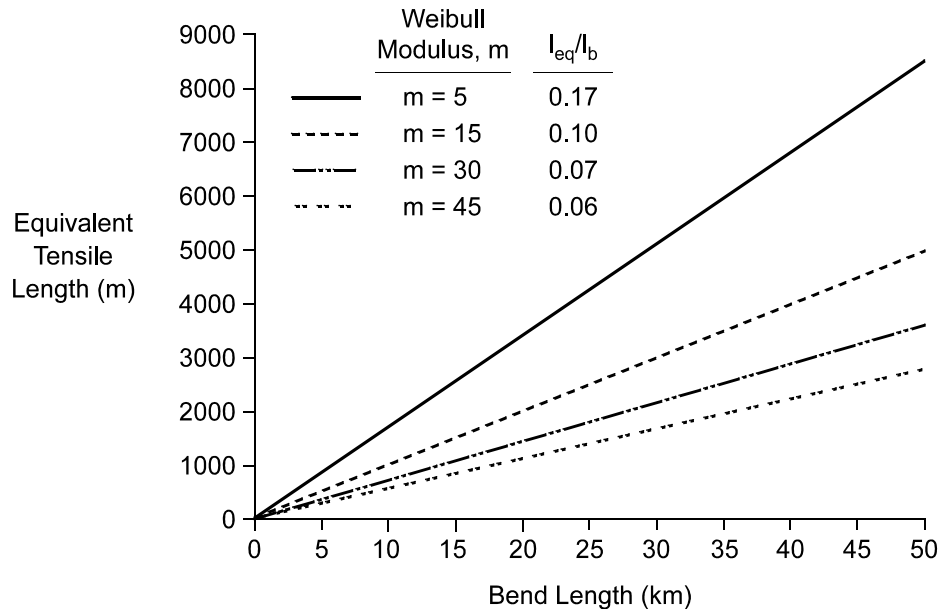


Figure 4. Equivalent tensile length,  $l_{eq}$ , for a given bend length,  $l_b$ .<sup>13</sup>

Torsional stresses are common during any fiber processing or cabling event where fiber is moved from one reel to another. Shear stress is related to the degree of twist,  $\gamma$ , shown in Figure 5 through the shear modulus,  $G$ , which is approximately 31 GPa (4500 kpsi) for silica,

$$\tau = G \frac{r\gamma}{L} \quad (4)$$

where  $r$  is the fiber radius and  $L$  is the length under twist. Fiber twists when it rides up the side of a pulley or when a roller rotates out of plane with the fiber direction. A  $2\pi$  revolution of fiber over a one meter length produces only 12.4 MPa (1.8 kpsi) of shear stress. Failure solely due to torsion is rare, but twist can accumulate during processing. Consequently severely twisted fiber can knot and fail in high stress bending. A limit of no more than three twists per meter is given as a general rule.

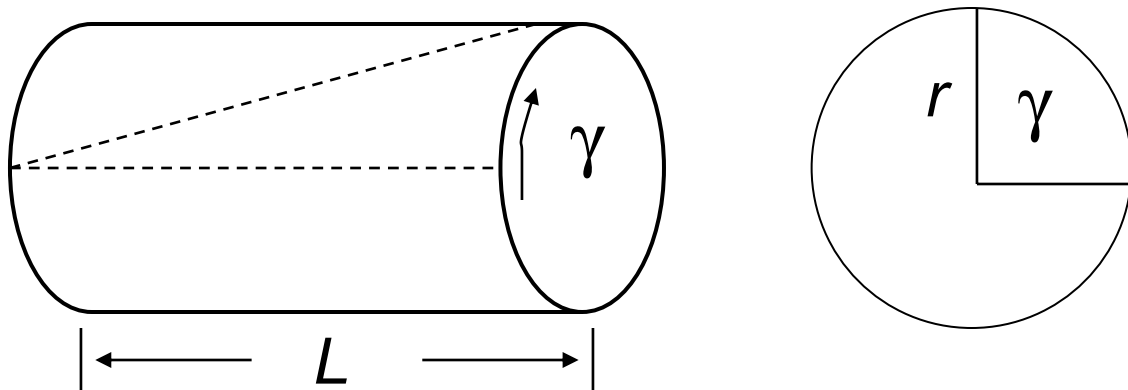


Figure 5. Stress induced by twisting fiber.

<sup>f</sup>The Weibull modulus,  $m$ , represents the spread in the data similar to that of the standard deviation for a Normal distribution. An  $m$  value in the range of 2-5 is typical of fiber strengths near the proof stress level. For more on Weibull distributions, see ASTM C1239-06.

### 2.3 Stress During Processing and Handling

The drawing of fiber is performed under relatively low stress. For standard single-mode and multimode fiber, the magnitude of the draw stress affects the optical behavior more than the mechanical behavior. The residual surface tension on standard single-mode fiber is several MPa. After drawing, fiber is wound onto rather large diameter spools under low wind tension. It is common for fiber to be guided by pulleys and rollers 2 to 3 centimeters in diameter during processing. When coupled with the wind tension, the maximum bend stress can easily reach 350 MPa or half the typical proof stress of 700 MPa (100 kpsi). There are opportunities for inadvertent high stress events during fiber processing. If the tension is too high during fiber payout from a spool, the fiber can pull into the underlying pack, become trapped, and break under a high stress bend as the spool continues to rotate.

Proof testing is used to establish a minimum fiber strength. The most common proof stress is 700 MPa (100 kpsi), but higher stress levels have been used for special applications where high deployment stresses are required. The fiber is proof tested over its entire length, but there are some instances, like splicing, where a localized proof test is also performed.

Figure 6 is a schematic of the three stages of proof testing, loading ( $t_l$ ), dwell ( $t_d$ ), and unloading ( $t_u$ ). Flaws stronger than the proof stress are intended to survive deployment and in-service stresses. Flaw “a” has a pre-proof strength lower than the proof stress and it fails during loading to the proof stress. Note that it experiences some small amount of strength degradation from fatigue prior to failure. Most flaws that fail during proof testing are of this type. Flaw “b” is initially stronger than the proof stress, but fatigue during proof testing weakens it enough to cause failure during the dwell time. Note that initially this flaw had enough strength to pass proof testing and would have been “saleable” if not for fatigue during dwell time. By extending dwell time more flaws will fail due to fatigue. Consequently, the post proof test fiber will have fewer flaws near the proof stress. Some lifetime models that incorporate the effect of proof testing will predict lower failure probabilities for longer dwell time. The logic here is that fatigue during proof testing is meant for controlling the post proof test strength distribution. If one desires to rid the fiber of flaws just above the proof stress, then simply increase the proof stress level.

Note that historically, proof stress requirements were tied to a dwell time of 1 second. This was because early proof test machines were slow and a one second dwell was typical. Today’s machines are capable of dwell times of less than 0.1 seconds. The rare case of flaw “c” is strength degradation from fatigue at the end of the dwell time and the flaw follows the stress during unloading and fails. Even more remote is the “d” where the flaw grows to a level below the proof stress during unloading and survives. Fuller et al.<sup>14</sup> as well as others deduced that the strength of the weakest flaw after proof testing was governed by unloading from the proof stress as well as the proof stress itself. This understanding is integral to present day standards for proof testing fiber.<sup>15,16</sup> Crack growth during unloading is rare and further suppressed by unloading from the proof stress as quickly as possible. A slow unloading time gives opportunity for flaws to grow and follow the stress as it decreases; and therefore, an unloading time of  $\leq 0.1$  seconds is recommended. This is typically accomplished by higher processing speeds and consequently, a minimum dwell time is no longer included in today’s standards and specifications concerning proof testing.

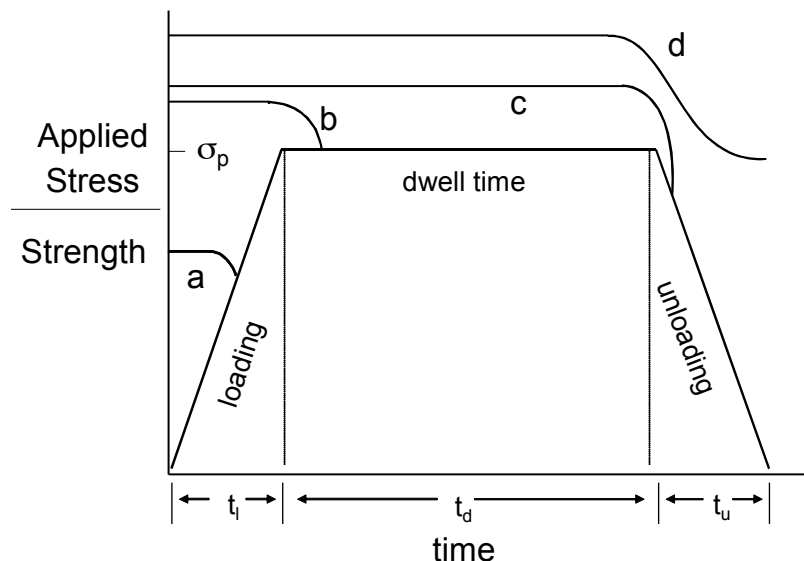


Figure 6. Proof testing optical fiber.

Fiber stress induced during coloring and cabling processes is generally low. There are a few process conditions that can produce elevated fiber stress levels. Small diameter rollers, pulleys, and guide dies are frequently used to position fiber during coloring and cabling. When bending and process tensions are added, fiber stress on the order of 350 MPa (50 kpsi) can easily be achieved. To encase fiber in a loose tube, the fiber is placed in tension as it passes through the tube die. As the buffer material cools it shrinks and buckles the fiber to create excess fiber length in the tube. Thus, the fiber proceeds from tension to a persistent bend induced stress state in a typical loose tube cable. Most often these stresses are kept below required levels for reliability, but it is possible to put too much excess length in a tube and consequently bend the fiber beyond recommended stress levels. There are published examples of cabling processes capable of placing stress in excess of 350 MPa (50 kpsi) on the fiber. Each case is unique and illustrates the importance of measuring and/or modeling applied stresses for each step of the cable manufacturing process.

## 2.4 Stress During Installation

Installation and in-service stress varies by cable design, deployment, and environmental factors. In loose tube cables, excess fiber length is included in the tube. This allows the cable to be stretched before the fiber straightens and experiences tension. The bend-induced stress in loose tube cables extends over the entire fiber length, but is typically well below the maximum allowable stress to ensure long-term reliability. The invention of the loose tube cable was key to the early reliability success of optical fiber.

There are cable designs with little or no excess fiber length where the fiber is constrained to follow the strain in the cable. Here, the cable designer must make wise use of reliability models for fiber and have clear knowledge of cable deployment conditions. In slotted core ribbon cables, fiber ribbons are stacked in channels helically stranded about the core of the cable. When the cable is bent, it is hypothesized that excess ribbon on the compression side slides to alleviate stress on the tensile side. This was confirmed by several studies where fiber Bragg gratings were employed as the means for measuring fiber strain in cables.<sup>18,19</sup>

Opportunities for generating fiber stress during deployment and in-service life include:

- Stressing loose tube cables past the safe strain window
- Ice/wind loading of aerial cables
- Removing sag in aerial cables<sup>20</sup>
- Cable bending and tension when pulling through a duct<sup>21</sup>
- Storage of excess cable in tight loops
- Lightning strikes on aerial cables
- Cable weight of drop cables

At the end of every deployed cable is a termination most often in the form of an enclosure. The cable enters the enclosure where the fiber is distributed, spliced or connectorized. Excess fiber length is typically stored by winding fiber into small coils or by following a raceway within the enclosure. Bending is the primary form of applied stress in these situations. The risk of failure from inherent flaws is low due to the short fiber length involved and the relative infrequency of these flaws in most standard commercial fiber. The most common cause of fiber failure at terminations and enclosures is handling induced damage. In all cases where fiber is spliced or connectorized, it is first stripped of its coating and then cleaned. During stripping of the coating, operators often tilt the tool in an effort to minimize residual coating on the glass surface, thereby, creating high bend induced stress that can be in excess of 2000 MPa (~300 kpsi). It is also difficult to keep from damaging the fiber surface. Once spliced, the coating is either reconstituted or a protective sleeve is placed over the fiber. Proof testing is recommended for fiber splices that are not completely shielded from external tension and bending.

More recently, fiber based devices have become common. Fiber pigtailed enter the device package and are stripped, spliced, and glued depending on the device. Bending is, again, the primary mode of loading within the device package. Also, it is difficult to isolate delicate and often uncoated fiber strands inside the package from external tensile loads on the fiber pigtailed.

From a system reliability point of view, it is important to quantify the applied stress in fiber based cables and devices during manufacturing, installation, and in-service life. Knowledge of applied stress is needed in the determination of the overall reliability of fiber in a given deployment.

## 2.5 Measuring Applied Stress

Direct measurement of length and length change cannot always be performed on cabled fiber. The applied stress on cabled optical fiber can be measured using either optical properties of the glass itself or fiber sensors. The two most common optical methods are the phase-shift and time-of-flight.<sup>22,23</sup> Both methods are based on measurement of the transit time of a pulse of light traveling down the length of fiber. Fiber strain,  $\varepsilon$ , is determined from the measured difference in travel time between stretched and unstretched cable,  $\Delta\tau$ ,

$$\varepsilon = \left(\frac{1}{L}\right)\left(\frac{c}{N} \cdot \frac{1}{k}\right)\Delta\tau \quad (5)$$

where  $L$  is the fiber length,  $c$  is the speed of light in a vacuum,  $N$  is the group index of the fiber, and  $k$  is the stress optic factor which accounts for the dependence of refractive index on strain. The time-of-flight and phase-shift methods, as well as others, are based on variations on the measurement of  $\Delta\tau$ . Note that these strain measurement techniques yield the average tensile strain over the entire length of cabled fiber. Therefore, they are best suited for cable designs where the fiber is straight before or after cable tensioning. If used for fiber in stranded cable designs, one must account for additional stress from bending. Stimulated Brillouin scattering has also been used extensively to measure fiber strain in cables.<sup>24,25</sup> This method has better length resolution than the two previous methods, but still averages strain over meters of fiber.

Due to the complex configuration of fiber in most cables and fiber based devices, it is often desirable to measure fiber stress over lengths on the order of centimeters. Fiber Bragg gratings (FBG) are ideally suited for these more discrete measurements. The FBG is a wavelength selective device created by forming a grating in the core of the fiber that modulates the index of refraction of an optical fiber. A broadband light source is launched from one end and the grating period and effective index of refraction determines the wavelength ( $\lambda_{\text{Bragg}}$ ) of the reflected optical spectrum.<sup>26,27</sup> This is shown schematically in Figure 7.

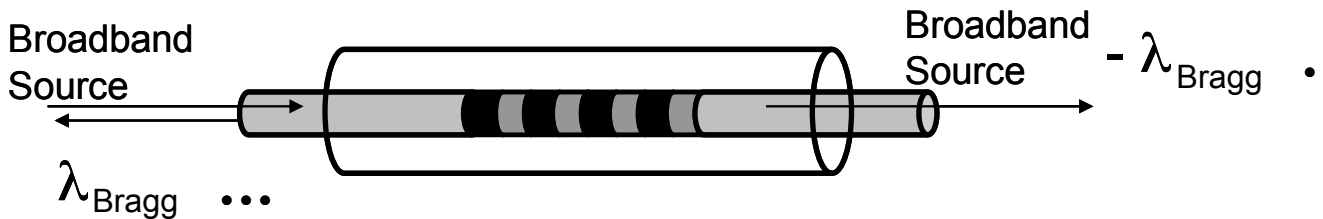


Figure 7. Fiber Bragg grating as a wavelength selective device. The reflected wavelength depends on the temperature and the strain applied on the grating.

The change in the return wavelength ( $\Delta\lambda_{\text{Bragg}}$ ) is linearly related to the stress applied to the fiber containing the grating.<sup>19</sup> The light spectra, reflected by the grating sensors, are captured by an optical spectrum analyzer. A typical grating is approximately 1 cm in length. The relationship between longitudinal strain and Bragg wavelength at a constant temperature is given by,<sup>28</sup>

$$\varepsilon = \frac{\Delta\lambda_{\text{bragg}}}{\lambda_{\text{bragg}}} \cdot \frac{1}{k} \quad (6)$$

where  $k$  is the stress optic factor. The experimental results, illustrated in Figure 8, demonstrates linear dependence for a grating loaded to 700 MPa (100 kpsi) or about 1% strain. Several studies have shown the usefulness of FBG in quantifying fiber strain in ribbon<sup>18,19</sup> and aerial cables<sup>29</sup> as well as fiber in a connector.<sup>30</sup> Figure 9 is an example of FBG used to measure the strain distribution in a bent ribbon cable. The outside fibers in a ribbon are in tension as they have a longer path length after stranding. The center fibers balance the resulting force by going into compression.<sup>18</sup>

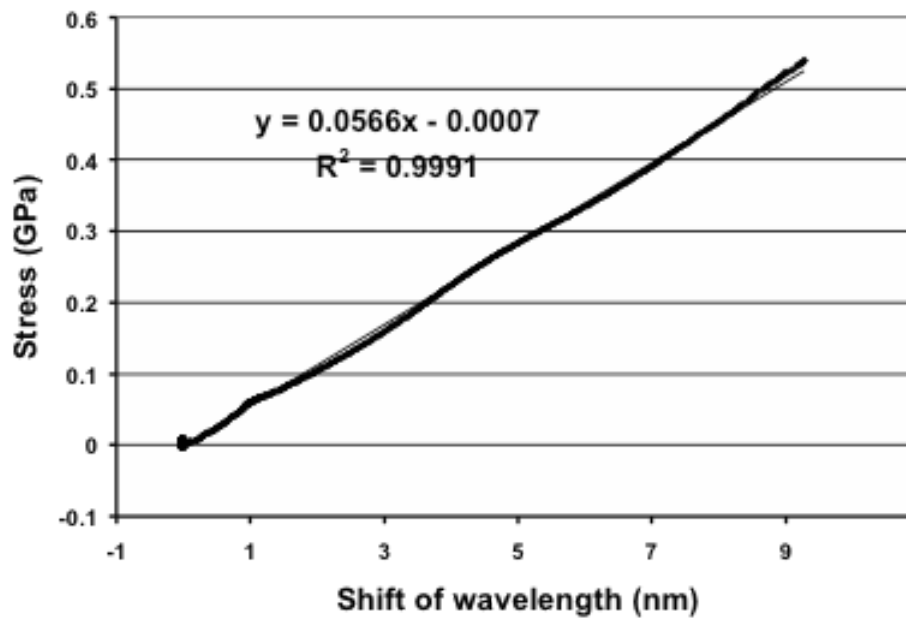


Figure 8. The effect of applied tensile loading on the center wavelength shift of a fiber Bragg grating.<sup>31</sup>

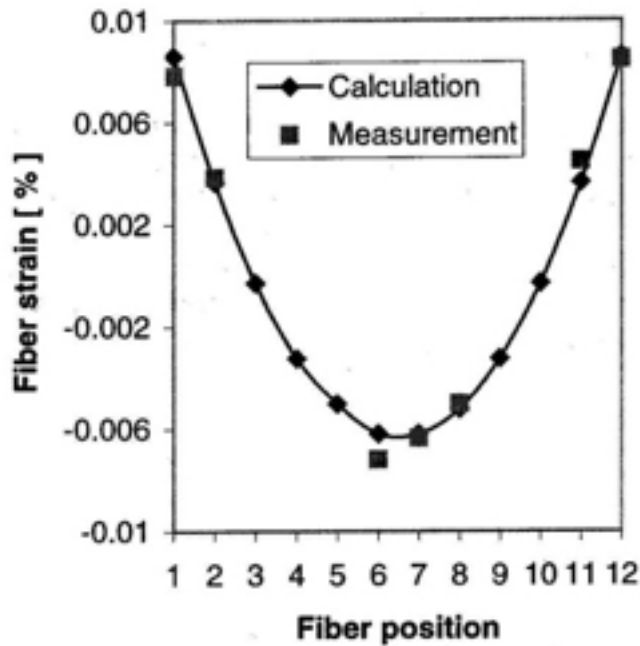


Figure 9. Measured and predicted fiber strain in a twelve fiber ribbon with a stranding pitch of 500 mm.

More recently, FBGs have been used to measure real-time changes in fiber strain.<sup>31,32</sup> Since access to only one end of the fiber is needed for strain measurements with a FBG, fiber containing the FBG can be passed directly into process equipment while one end of the fiber is used for optical interrogation. The stress history of a fiber being proof tested to 700 MPa (100 kpsi) at 15 meters per second is shown in Figure 10.<sup>33</sup> The loading, dwell, and unloading events are clearly observed. The fiber loads to the maximum stress level in 7 milliseconds and is held at that stress level for approximately 95 milliseconds. There is a low amplitude ripple in the stress, except when traveling over pulleys and capstans where the fiber position is more constrained. Unloading occurs in 2.6 milliseconds. Figure 11 shows the effect of loading rate on the proof test stress history of a conventional fiber splice proof testing machine. With this particular proof test machine, the total proof test time decreased and the maximum stress increased with increasing loading rate.<sup>33</sup> It was hypothesized that the device “over shoots” the intended proof stress at fast loading rates. Fiber Bragg gratings can also be used to measure the stress imparted to packaged fiber. Figure 12 shows the stress history of four gratings in fiber wound inside a dispersion compensation module and subjected to temperature cycling. This study demonstrated the ability to examine the effect of packaging on fiber applied stress and reliability.

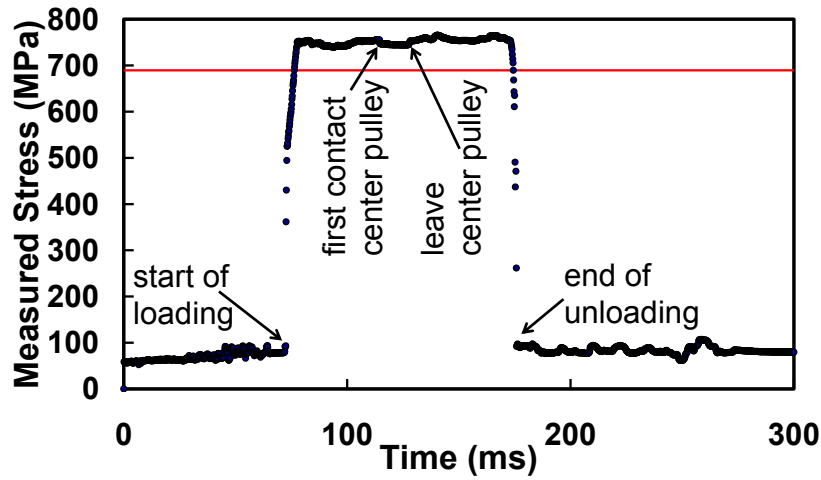


Figure 10. The stress history of a fiber sensor as it passes through a proof test machine at 15 meters per second. The horizontal line represents the specified proof stress level.<sup>33</sup>

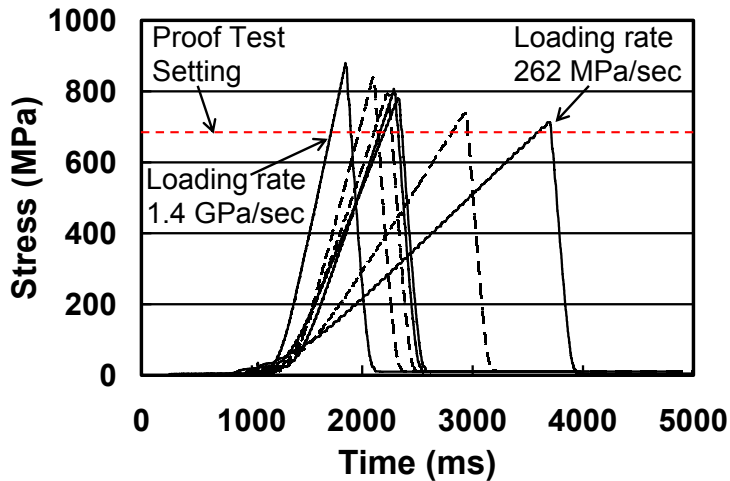


Figure 11. Graph showing measured proof test events for increasing ramp rate settings on the splice proof tester.

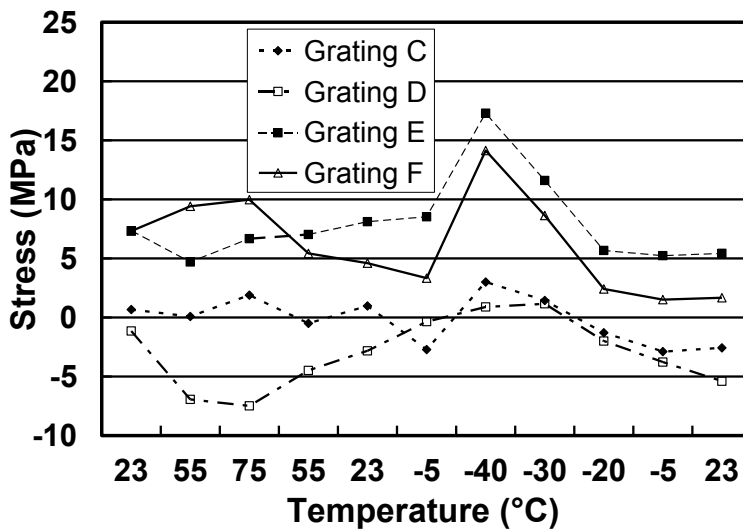


Figure 12. The stress history for each of four gratings in a dispersion compensating module during a thermal cycling event. This particular DCM package places low stress on the fiber over the range of temperatures. This is useful in quantifying the effect of the package design on thermally-induced microbending.<sup>34</sup>

Abraded fiber has been used to obtain discrete strain measurements of cabled fiber. Fiber is continuously damaged during the draw process before application of the protective polymer coating. It is possible to control the strength distribution such that the strongest flaws have a strength close to that of the typical proof test stress of 700 MPa (100 kpsi) and the weakest near 210 MPa (30 kpsi). If the abraded fiber breaks during cabling or post-process manipulation of the cable, the ends of the broken fiber are retrieved and failure stress is estimated from fracture surface features. Note that the estimated stress may not be the peak stress experienced at that location as the stress may have been increasing to a higher value when the fiber broke. Nevertheless, knowledge that the applied stress was at least that of the measured value can be extremely valuable. Ma<sup>17</sup> used this method to estimate stress applied to fiber during the common process step of extrusion. Failure stresses of 490 to 560 MPa (70 to 80 kpsi) were determined from fracture surface markings and compared well with the calculated value of 540 MPa (77 kpsi).

### 3 Flaws in Optical Fiber

The ultimate strength of inorganic glass estimated to be about  $E/5$ .<sup>35</sup> This places the intrinsic strength of silica at about 14 GPa (2000 kpsi). From the classic work of Proctor et al.<sup>36</sup> Figure 13 shows measured strengths near this level on short lengths of silica fibers tested in tension at liquid nitrogen temperatures. These fibers are essentially flawless and fundamental knowledge about glass strength and structure has been gleaned from such experiments.<sup>37,38</sup> In fact, most of the length of today's optical fiber is essentially flawless. However, there are occasional flaws or defects along the length of the fiber. Flaw sources can be roughly categorized as either contaminants or glass surface damage.

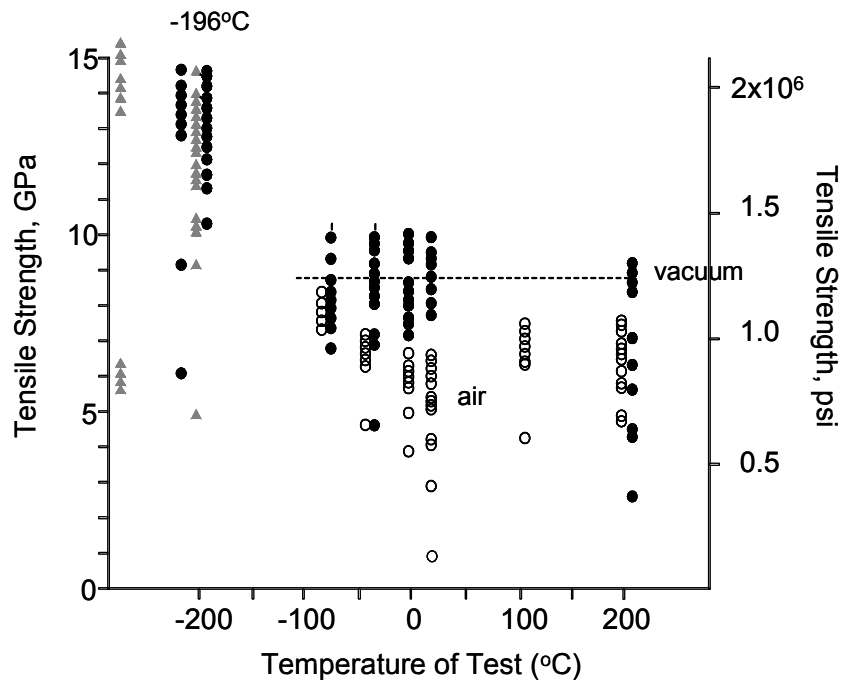


Figure 13. Tensile testing flawless silica fibers in air, vacuum, and at low temperature, from Proctor et al.<sup>36</sup>

### 3.1 Contaminants

The most common location for contaminants is surfaces; for example, preform centerline, over-clad and sleeve interface(s), and outer surface of the preform. The composition of surface contaminants can vary widely and simply depend on the exposure of these surfaces to direct contact events, decomposing equipment materials, and the overall processing area. Contaminants in the soot stream usually originate from the delivery system. Examples of historical contaminants are shown in Figure 14 and Figure 15.

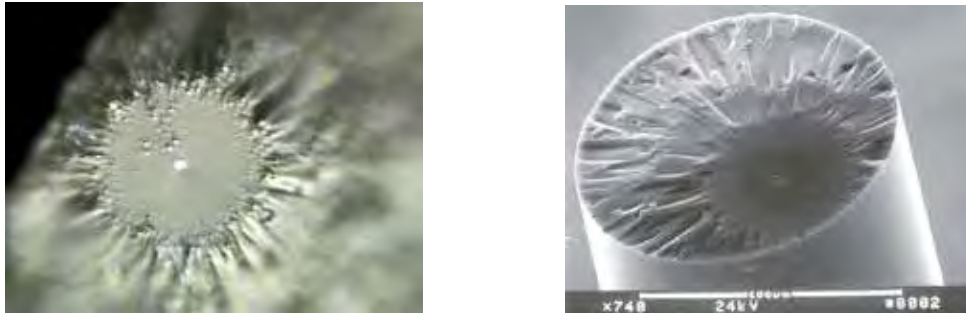


Figure 14. Internal chrome contaminant deposited during the soot deposition process.



Figure 15. Surface Zirconia (left) and Chrome (right) contaminant. The presence of troughs extending from the particle indicates the particle to have a high melting temperature.

Contaminants embedded in the glass are usually low in strength and most are eliminated during proof testing. Those on the centerline and strong enough to pass proof testing are often detected during optical inspection. It is important to note that internal particulates do not pose much of a reliability risk as they do not experience strength degradation from fatigue. Surface particles, however, are exposed to the outside environment and can experience fatigue. With a few exceptions,<sup>39</sup> protective polymer coatings are not a barrier for the moisture required for the fatigue phenomenon.<sup>40</sup>

Visual examination of contamination is initially performed using optical microscopy as particulate color and shape help identify composition. The presence of a trough in the underlying glass yields clues to deposition history as well as composition. Scanning electron microscopy, fitted with an x-ray spectrometer, allows one to determine the elemental composition of surface contaminants.

### 3.2 Contact Damage

Glass surface damage from mechanical contact has been studied extensively.<sup>8,41,42,43,44,45</sup> Glass surfaces can plastically deform upon contact and, depending on the mechanical properties and shape of the contacting material, multiple subsurface crack systems can emanate from the contact origin. Figure 16a shows median/radial cracks,  $m_c$ , extending from the corners of the contact site down into the glass, n-p-n. These crack systems control the strength of the glass. Whereas the shape of the flaw has some influence on strength, it is the flaw depth that is primarily responsible for controlling glass strength.<sup>46,47</sup> Lateral cracks,  $l_c$ , form almost parallel to the surface and are the source of glass chips. Hertzian cone-shaped cracks can emanate from the zone of crushed glass beneath the contact origin, Figure 16b. Some or all of these crack systems form when fiber is impacted, scratched or rubbed.

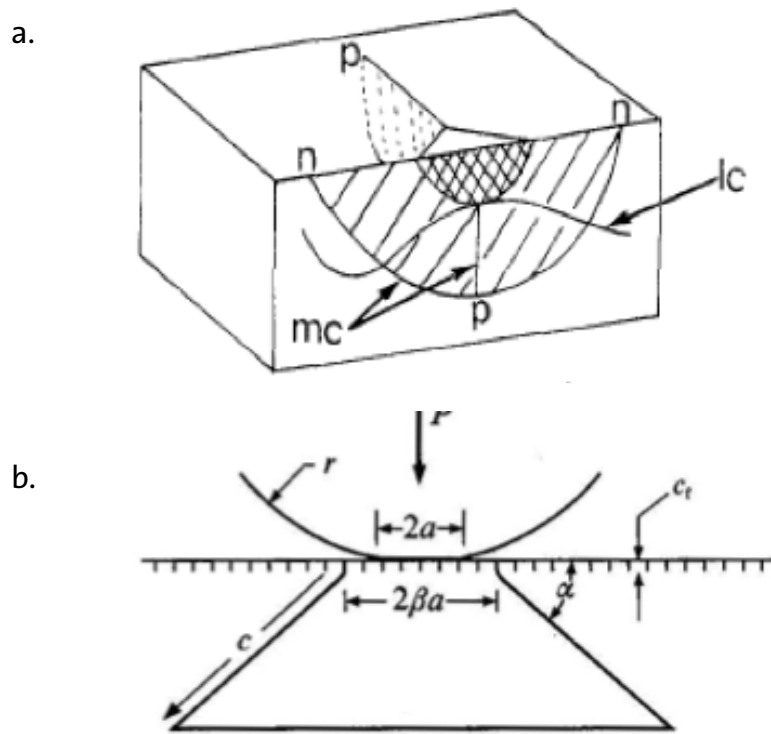


Figure 16. Crack systems resulting from mechanical contact: (a) shows crack systems resulting from sharp contact<sup>48</sup> and (b) shows Hertzian cracks generated by contact with a blunt object.<sup>49</sup>

Note that Hertzian cracks can also form from plastic zones created by sharp contact.

The mechanical damage of optical fiber surfaces constitutes a special category of glass and ceramic reliability. The first observation being that the glass surface is pristine prior to contact. This means that there are no additional effects from surface roughness or from previous damage events. Second, the strength regime of interest is unique among structural glasses and ceramics. Even submicron flaws can result in instant or premature failure. In other words, any contact with the glass surface is certain to create a flaw of reliability interest. Third, the fate of the glass surface is tied to the mechanical properties and integrity of the protective polymer coating.

One of the more persistent failure modes for optical fiber is glass damage through the protective polymer coating during fiber processing and handling. Fiber with standard coating dimensions can be handled without damaging the coating; however, it is necessary to regularly clean and maintain pulleys, rollers, and guides that come in contact with fiber. With the advent of photonic devices, fibers are handled significantly more than in cabling and coating damage resulting in fiber breaks can be a significant cost of manufacturing. Figure 17 shows a typical fiber break resulting from direct puncture through the coating. When sufficient concentrated pressure is applied, the coating will rupture and sometimes split. Common sources of such damage are damaged or contaminated belts and pulleys, contamination in coloring dies, and contact with tools, work surfaces, and operators. Pieces of broken fiber from previous breaks or fiber termination events can easily puncture the fiber coating as well.

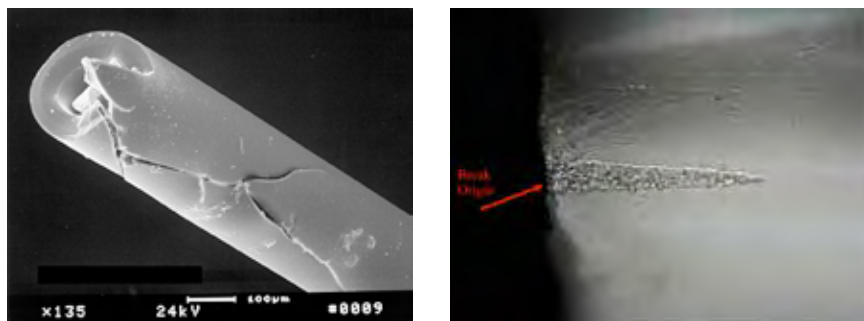


Figure 17. Puncture of the polymer coating and the underlying glass damage.

Another source of mechanical damage to the glass is “whipping”. If spooled fiber ends are not secured during high speed processing, the loose fiber end can “whip” the surface of the fiber pack. Damage can extend down several layers depending on the impact velocity. Figure 18 shows the typical signature of a whip event. The protective polymer coating is damaged and often removed at an oblique angle as the direction of the whipped end is usually not aligned with the longitudinal axis of the fiber. Damage to the glass shows evidence of plastic deformation. The prevailing hypothesis is based on the work of Hockey and Wiederhorn<sup>50</sup> where the impact velocity is sufficient to cause localized heating and melting of the glass. The glass surface in Figure 18 appears to have been “plowed”.

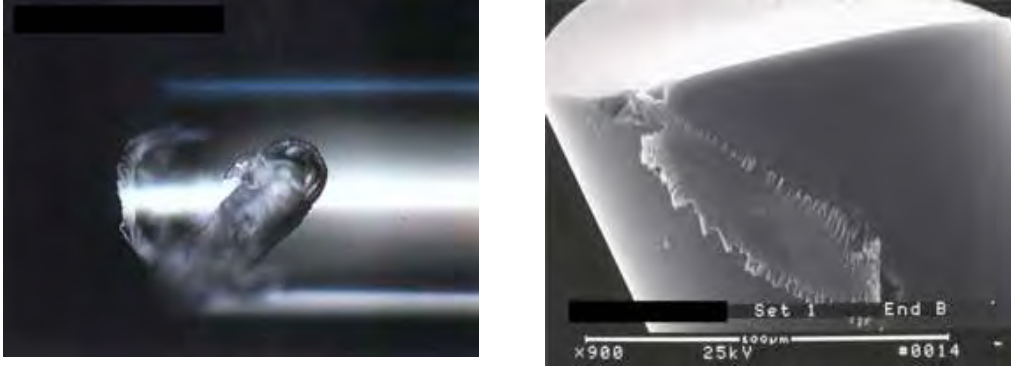


Figure 18. Coating and glass damage from fiber whipping.

Sliding contact during coating stripping is a common cause of surface damage. The metal blade of the tool invariably makes contact with the glass surface during coating removal. Figure 19 is an example of this common flaw inducement event.

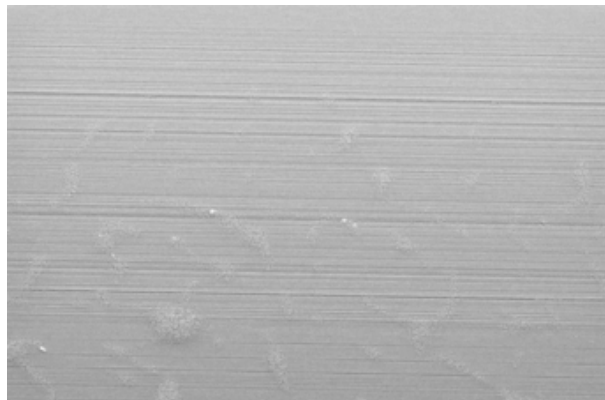


Figure 19. Glass surface damage from stripping tool. Bar represents 1 μm.

Scribing and breaking the fiber end in preparation for termination, cleaving, is one of the few events where the glass surface is intentionally damaged. The purpose is to create a fully mirrored surface with minimal surface damage in the form of chips (lateral cracking) and contamination so that optical measurements or terminations can be made. Figure 20 shows a nicely cleaved surface with the origin clearly identifiable. Field et al.<sup>51</sup> show the effect of pressure and blade shape on the formation of the flaw responsible for fracture in Figure 21.

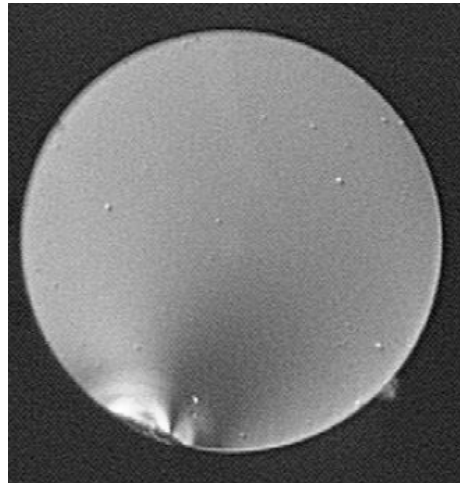


Figure 20. Full mirrored fracture surface from cleaving. Notice origin and evidence of subsurface crack systems after scribing.

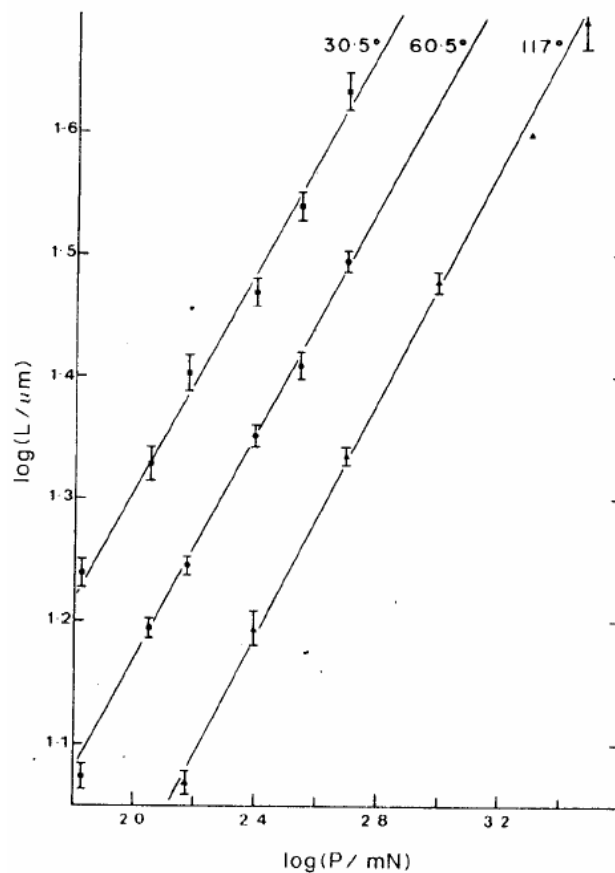


Figure 21. Crack length,  $L$ , depends on indentation load and shape of the scribing blade.<sup>51</sup>

The mechanics of contact induced damage in optical fiber has been studied extensively through the use of artificial flaws.<sup>52,53</sup> Flaws are imparted to the glass surface using a Vickers or Knoop diamond indenter. More recently, flaws produced by a cube-corner indenter have been used for the study of fatigue in proof stress level flaws.<sup>54,55</sup> Indentation produces some of the same features found in process and handling induced flaws with less complexity. For example, plastically deformed glass is generated at the contact site and subsurface cracks emanate from this zone of contact. One important feature with flaws produced by Vickers indentation is that there appears to be a threshold load for median/radial crack formation. Below some indentation load, these strength controlling crack systems do not form and only a plastic zone beneath the indenter tip is present after indentation. Due to the effects of fatigue median/radial cracks can “pop-in” in a delayed fashion from an indent that was initially subthreshold. In the case of optical fiber, Matthewson has created subthreshold Vickers indentation flaws initially stronger than the typical proof stress of 700 MPa (~100 kpsi) that suddenly become weaker than the proof stress when these flaws “pop-in”.<sup>56</sup> The assertion is that proof testing does not assure a minimum strength as flaws could “pop-in” after proof testing and be weaker than the proof stress. However, after the installation of hundreds of millions of kilometers of fiber there are few, if any, documented occurrences of fiber failure that can be attributed to this phenomenon. There are a several possible explanations;

1. Delayed flaw development appears to be best achieved with a Vickers indenter. A cube-corner indenter has a much lower flaw generation threshold and a Knoop has a higher threshold. The distribution and magnitude of localized residual stresses in naturally occurring flaws may infrequently match that of the Vicker’s flaw. This is simply a probability argument.
2. The initial inert strength of flaws that showed delayed flaw development in Matthewson’s study was 1200 MPa (~175 kpsi). Fatigue during proof testing at a typical stress level of 700 MPa (100 kpsi) will grow and fail flaws with pre-proof test strength approaching 1000 MPa (145 kpsi). The point being that flaws prone to delayed inducement are strongly tempted to induce during proof testing itself. An interesting follow-up study would be to proof test these indentation flaws to see if they can pass such an event.
3. The inert strength after flaw development is estimated to be at least 500 MPa (70 kpsi). This is still strong enough to withstand most in-service applied stresses on fiber and fiber-terminations.

### 3.3 Environmentally Induced Flaws

Several studies in the 1980’s found that the strength of pristine optical fibers could be degraded if exposed to severe environments like immersion in hot water or a combination of high temperature and high humidity.<sup>57,58</sup> Matthewson and Kurkjian<sup>59</sup> performed 2-pt bend strength tests on fibers aged in 100°C water for 12 days and observed strength degradation of almost 50%, see Figure 22. Figure 23 shows static fatigue results from Chandan and Kalish<sup>57</sup> on pristine fiber in a similarly harsh environment. A clear “knee” is created where the  $n$  value, determined from the slope of  $\log(\text{time-to-failure})$  and  $\log(\text{applied stress})$  drops well below the typical value of 20. Kennedy et al.<sup>60</sup> demonstrated that strength degradation for a given fiber was dependent on the test environment, Figure 24. Atomic force microscopy of aged fiber revealed nanometer sized pits on the glass surface.<sup>61</sup> The prevailing explanation is chemical etching of pristine surfaces. Introduction of surface pits creates the fatigue knee found in static fatigue data of pristine fibers. These, along with other studies, created concern that fiber life could be limited for reasons other than the well-known fatigue phenomenon and associated lifetime models were generated.<sup>62,63,64,65</sup>

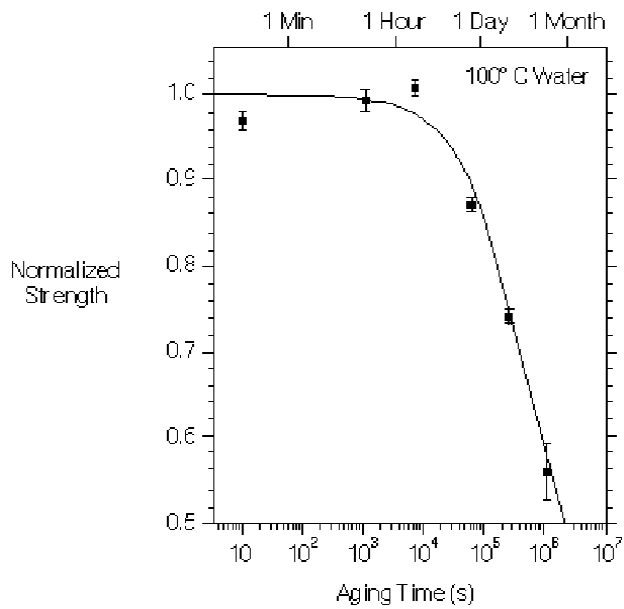


Figure 22. Effect of Aging in 100°C water on the Strength of Optical Fiber.<sup>59</sup>

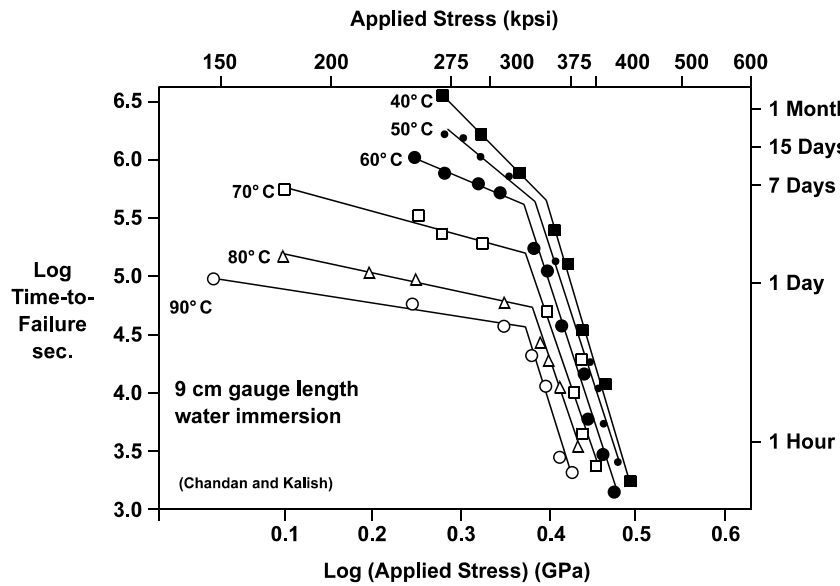


Figure 23. Static fatigue of pristine fiber lengths in tension and immersed in water.<sup>57</sup>

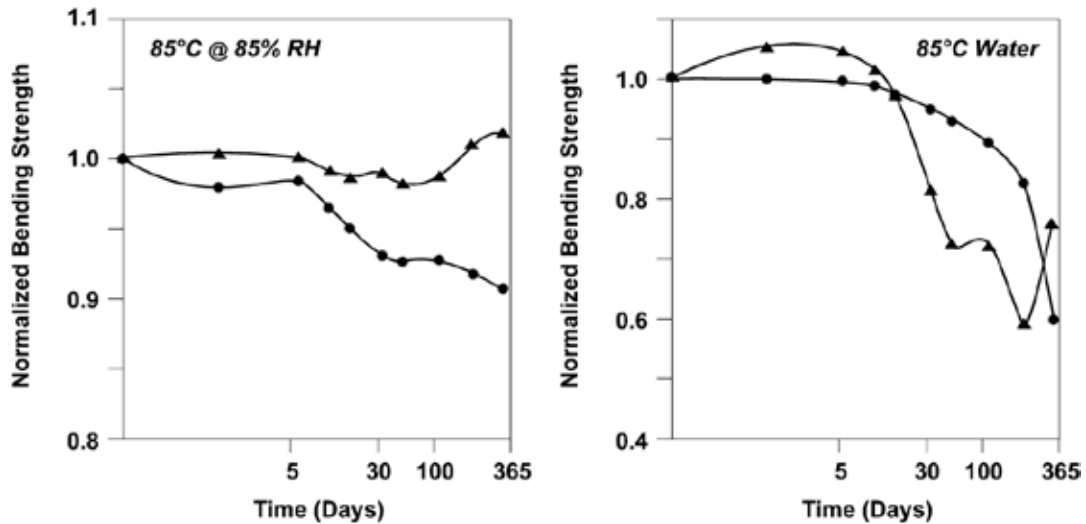


Figure 24. Strength of two different fibers measured in 2-point bending after aging.<sup>60</sup>  
The symbols represent optical fiber from different manufacturers.

Concern that installed fiber would fail prematurely due to this phenomenon reached its height in the 1990's. Two studies found strength degradation after extended exposure to moisture after years of service.<sup>66,67</sup> Griffioen et al.<sup>67</sup> found it difficult to attribute that such strength degradation solely to field aging from surface pitting due to the fact that these early fibers were difficult to handle after such aging. Other field studies, on more modern fibers, failed to find any fiber strength degradation or surface pitting.<sup>68,69,70</sup> It should be noted that preexisting flaws near the proof stress level are not affected even in the most severe aging environments.<sup>71</sup> This is because "weathering" or aging is a flaw-introduction process for pristine fibers, but a flaw tip rounding process for preexisting flaws. Concern over this issue has subsided as coatings were reformulated to suppress this phenomenon. Note, however, that there are special applications where the environment is severe enough to warrant concern over this phenomenon.

### 3.4 Fracture Mechanics

Fracture mechanics is the theoretical framework used to relate flaw depth to fiber strength. The simplest form of this relationship is for a flaw of depth  $a$  in uniform tension,  $\sigma$ ,

$$K_I = Y\sigma \sqrt{\pi a} \quad (7)$$

where  $K_I$  is the mode I stress intensity factor and  $Y$  is a factor determined by the geometry of the flaw as well as the type of loading on the flaw. The stress intensity factor increases with increasing stress or flaw depth through growth or both. When  $K_I$  reaches a critical value,  $K_{IC}$ , the flaw propagates rapidly to failure.  $K_{IC}$  is a measure of a material's resistance to fracture and is a material property known as the fracture toughness. Silica has a relatively low fracture toughness of  $0.8 \text{ MPa}\cdot\text{m}^{1/2}$  and compares with alumina ceramic with  $K_{IC} = 2$  to  $6 \text{ MPa}\cdot\text{m}^{1/2}$  or 4340 steel with a high fracture toughness of  $90 \text{ MPa}\cdot\text{m}^{1/2}$ .

The stress at failure is the strength,  $\sigma_f$ , and Eq.(7) becomes,

$$\sigma_f = \frac{K_{IC}}{Y\sqrt{\pi a}} \quad (8)$$

Equation (8) describes one's intuition of lower strength with a larger flaw. It is important to realize that the failure of brittle materials, like glass optical fiber, is not governed by a strength threshold, as though strength was a property. Rather, stress and flaw size combine in the form of  $K_I$  and when it reaches its limit for that material,  $K_{IC}$ , failure occurs. Furthermore, for the same size flaw, a material with higher fracture toughness has a proportionally higher strength. Glass happens to have a relatively low fracture toughness compared to most other materials. Glass receives damage and propagates it to failure more easily than, say, 4340 steel which has a fracture toughness about an order of magnitude higher than that of glass.

Important constraints for the use of Eq. (8) are that the flaw be sharp at its tip and oriented normal to the direction of applied stress. Due to the wide variety of flaw sources and orientations, meeting these constraints appears unlikely. However, environmentally assisted slow crack growth occurs prior to failure in almost every fiber failure circumstance. This crack growth allows a more well-defined and sharp crack front to emerge from complex damage sites. In addition, the crack front will tend to reorient normal to the direction of applied tension prior to failure.<sup>72</sup> Therefore, most fiber failures occur under the mode I loading conditions of Eq. (8). For a surface flaw with a uniform stress intensity across the crack front,  $Y$  in Eq. (8) is approximately 0.7.<sup>46</sup> Figure 25 is a plot of predicted strengths for a range of flaw depths in silica. To pass the typical proof stress level of 700 MPa (100 kpsi), a flaw must be less than  $\sim 1 \mu\text{m}$  in depth. It is debatable whether or not fracture mechanics applies to short lengths of fiber where the surfaces are likely to be pristine and strengths approach 14,000 MPa (2000 kpsi), near the theoretical strength of silicon-oxygen bonds.

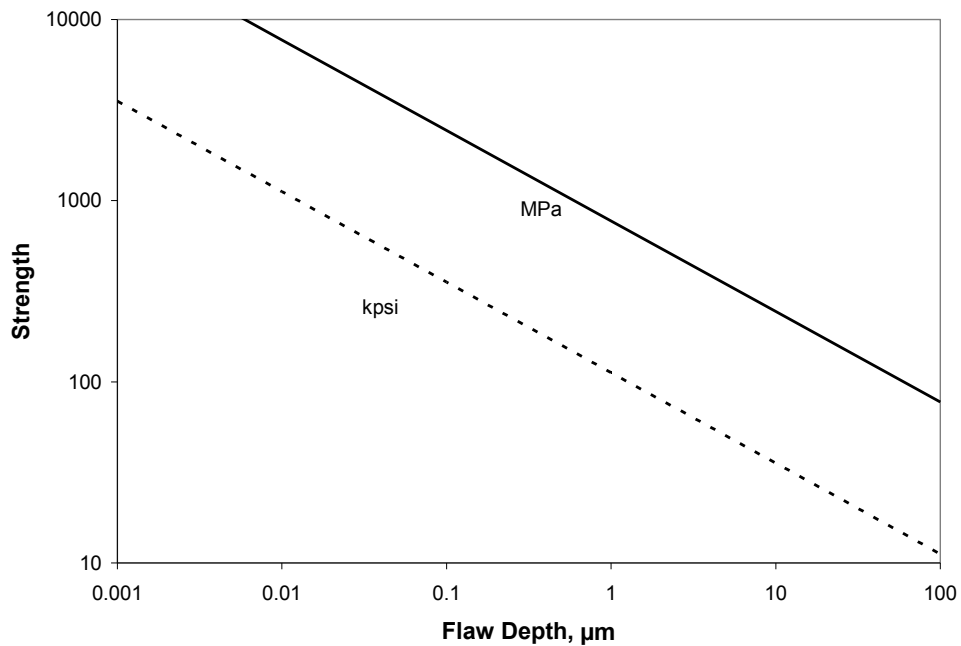


Figure 25. Estimated strength for a range of flaw depths.

### 3.5 Fractography

The mechanical failure of optical fiber, like glass and ceramic materials, generates new surfaces with markings that can be read and interpreted to either explain the cause of failure or inform the researcher about material properties.<sup>73,74</sup> The associated discipline is known as “fractography.” The physics behind the formation of these surface markings has been studied extensively over several decades with steady progress in understanding. Our purpose here is to use this knowledge as a tool for informed judgments about the failure history of optical fiber.

At failure, the crack propagates through the material, creating fracture features known as mirror, mist, and hackle shown in Figure 26. The crack front initially produces what appears to be a smooth “mirror” region. As the crack front accelerates, it creates a dimpled surface known as “mist”. At higher speeds the crack front forms the rough hackle region. The hackle region is characterized by elongated ridges that proceed in the direction of crack propagation. The hackle markings point back to the flaw origin. Beyond the hackle region, the crack front reaches about half the speed of sound in glass and becomes unstable enough to branch into two crack fronts and then into four and so on.

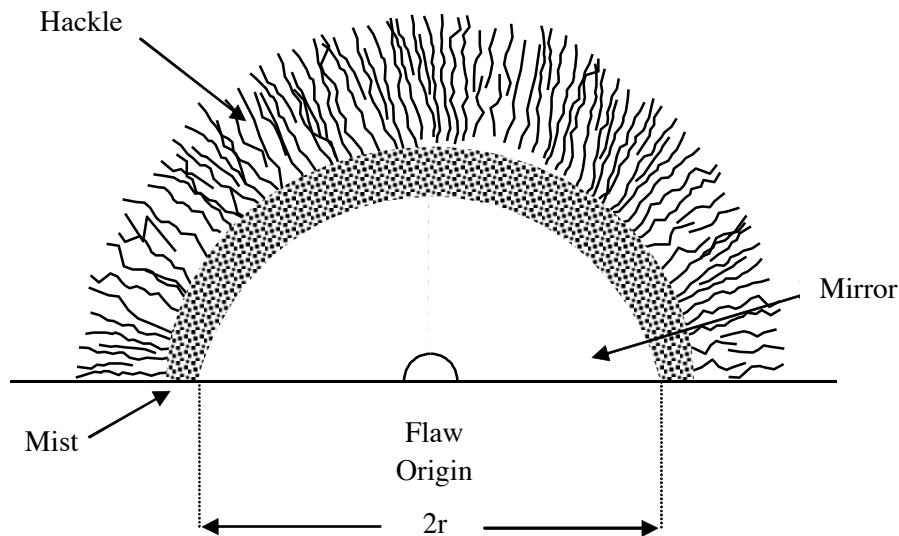


Figure 26. Schematic showing typical glass surface features that form during failure.

The failure stress,  $\sigma_f$ , of glasses and ceramics is related to the distance from the origin to the boundary between one surface feature and another,  $r$ , through the same square root dependence as strength and flaw size in Eq. (8),<sup>75,76</sup>

$$\sigma = \frac{A_i}{\sqrt{r_i}} \quad (9)$$

where  $A$  is the mirror constant for a given material and  $i=1,2,3$  is for the mirror-mist boundary, mist-hackle boundary, and crack branching location, respectively. The mirror-mist boundary,  $i=1$ , is typically measured at the intersecting points where the mist meets the material surface, as indicated by  $2r$  in Figure 26. The mirror constant,  $A$ , is empirically determined from strength and mirror measurement data. Measured mirror constants for the mirror-mist boundary for flaws in silica are shown in Table 1. Comparing Eq. (8) to Eq. (9) the mirror is a factor of 6 or 7 larger than the flaw responsible for failure.

Table 1. Mirror constant,  $A_1$ , for flaws in silica fibers.

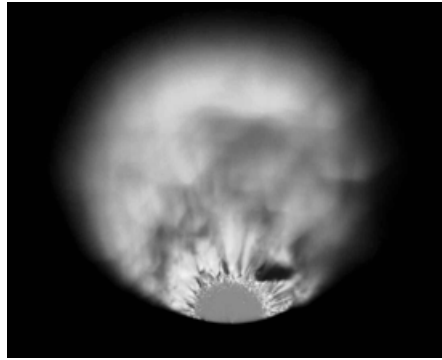
Study	MPa√m	kpsi√μm
Kerper and Scuderi <sup>77</sup>	1.89	275
Gulati et al. <sup>78</sup>	1.97	285
Baker and Glaesemann <sup>79</sup>	1.96	284
Choi and Gyekenyesi <sup>80</sup>	2.1	304
Chandan and Parker <sup>81</sup>	2.224	322
Mecholsky and Rice <sup>82</sup>	2.2	319

Estimating failure stress from mirror measurements is as much art as science. The pattern of an ever rougher fracture surface is found when one examines the mirror surface at high magnification. Thus, one's interpretation of, say, the mirror-mist boundary will depend on the magnification and quality of the microscope objective as well as the person performing the evaluation. This is illustrated by the range of mirror constant values in the above table. Nevertheless, the ability to determine the mode of loading and even roughly predict failure stress from fracture surface features has proven to be a powerful tool for identifying the root cause of fiber failures. For those estimating failure stress from fracture surface markings on a routine basis, it is, therefore, recommended that one measure mirror constant on fiber using the same equipment and person that will be used in performing the mirror measurements. A wide range of mirror dimensions should be used in making this determination.

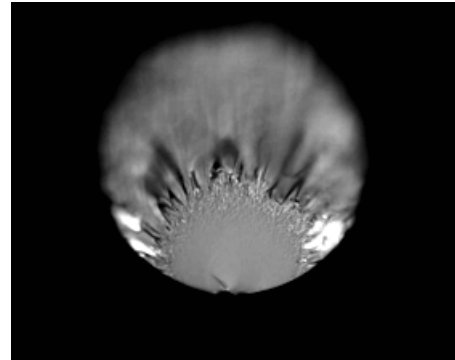
The fracture surface images in Figure 27 show the progression of surface features for ever decreasing fiber strength. In Image A, the mirror is well contained within the cross-section of the fiber and the progression through mirror, mist, and hackle is clear. Note that the mirror in Image A is almost semi-circular except near the glass surface where the mirror-mist boundary curves in slightly. Shand<sup>83</sup> believed that surface damage artifacts can destabilize the crack front enough to prematurely initiate mist and hackle. However, this isn't the case for these optical fiber specimens because their surface is pristine away from the fracture origin. By extending fracture mechanics to this dynamic crack situation, Kirchner et al.<sup>84</sup> attributed the distortion of the mirror to a higher stress intensity factor at the surface.

As the mirror becomes a larger portion of the fracture surface, at lower failure stress levels, several interesting features can be observed. In Image D the crack front transitions from mist-hackle back to mist and then finally to mirror near the furthest edge from the origin (see arrow). This transition back to mirror suggests that the crack front decelerates just before final glass separation. At the lower stress level of 186 MPa (27 kpsi) in Image E, the crack front reaches a velocity across the depth sufficient only to form mist before decelerating back to mirror as in Image D. At 145 MPa (21 kpsi) in Image F, the mirror appears to extend across the entire depth of the fracture surface. Notice that mist and hackle still form at the outermost width of the mirror on these specimens in Images E and F. This may be explained by the argument of a higher stress intensity factor at the surface. Finally, at stress levels below 145 to 172 MPa (21 to 25 kpsi) there is only a mirrored surface for 125 μm diameter fiber and the crack front never reaches the critical velocity for mist formation.

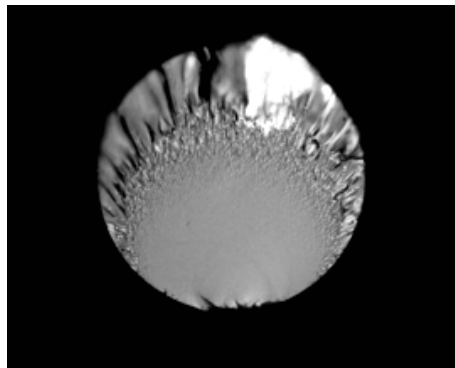
The images in Figure 27 demonstrate that failure stress can be determined from mirror dimensions over a wide failure stress range. Researchers have found that Eq. (9) holds for both bulk and fibrous silica.<sup>85,81</sup> However, there is less data available for the special case where mirrors are of the size of the fiber. This mirror size region is particularly important from a reliability point of view. For example, say a fiber is found to be broken after processing or installation and the fracture surface shows primarily mirror with a trace of mist. Quantifying the failure stress in this situation is critical to determining the location and root cause of the failure event. Recent research, see Figure 28 below, found that for mirrors larger than 30 to 40  $\mu\text{m}$  the log-log plot of strength versus mirror width departs from linearity. This suggests that Eq. (9) may not be appropriate for such large mirrors.



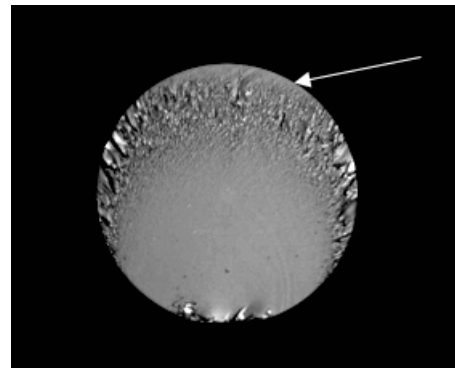
A) 538 MPa (78 kpsi)



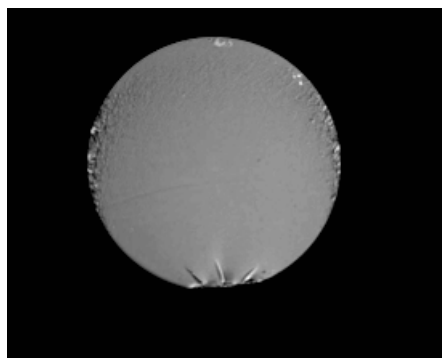
B) 324 MPa (47 kpsi)



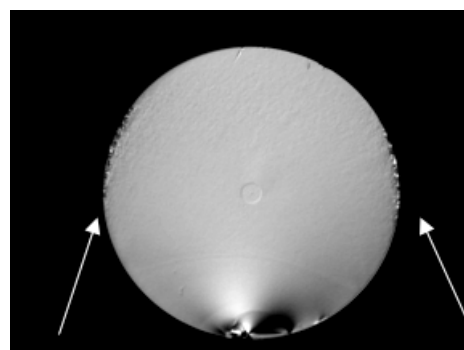
C) 248 MPa (36 kpsi)



D) 214 MPa (31 kpsi)  
Arrow shows reformation of mirror



E) 186 MPa (27 kpsi)



F) 145 MPa (21 kpsi)  
Arrows show mist region

Figure 27. Optical microscope images showing fracture surfaces for various failure stress values.<sup>86</sup>

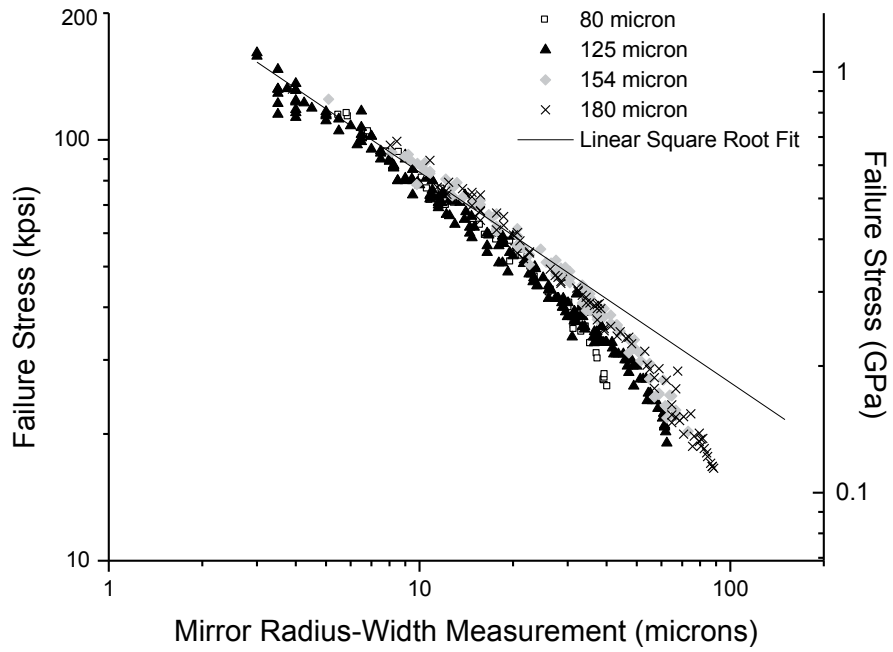


Figure 28. Mirror radius-width ( $r_w$ ) measurement values versus failure stress for various diameter fibers. Note that the departure from the classic relationship was more pronounced for the smaller diameter fibers.<sup>86</sup>

It was hypothesized that when the mirror becomes the size of the specimen the width of the mirror is interrupted by the curvature of a circular object like fiber. This is shown schematically in Figure 29. The dimension  $r_x$  represents a continuation of the circular mirror to a plane even with the origin and is related to the mirror width measurement,  $r_w$ , by;

$$r_x = \sqrt{r_w^2 + \left(R_f - \sqrt{R_f^2 - r_w^2}\right)^2} \quad (10)$$

where  $R_f$  is the fiber radius.

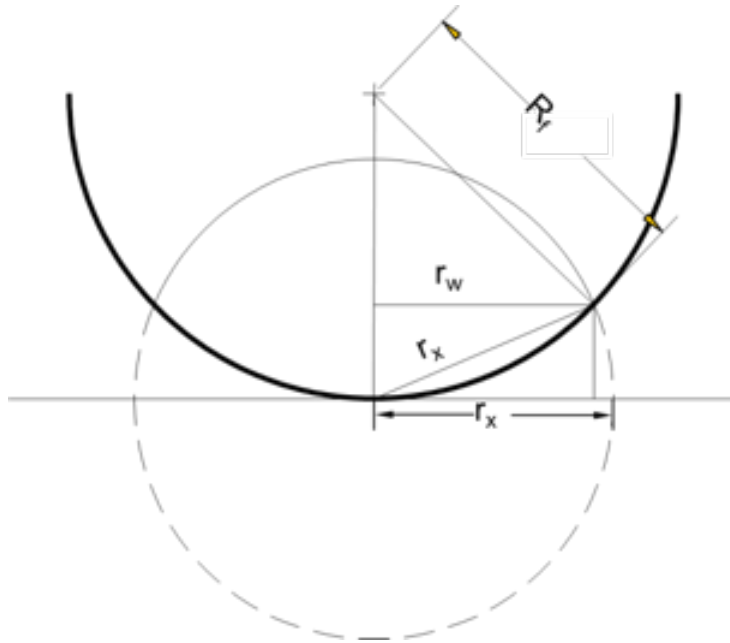


Figure 29. Schematic showing the extended mirror radius ( $r_x$ ) determined from the radius-width ( $r_w$ ) measurements on a fiber break end.

The strength results in Figure 28 are re-plotted in Figure 30 with the extended mirror radius,  $r_x$ , from Eq. (10). Using the extended mirror,  $r_x$ , the data from all four fiber diameters lie on a single curve. There is still some non-linearity at the lowest strength levels. A simple curve fit can account for this effect and can make meaningful failure stress predictions down to low stress levels,

$$\sigma = \frac{A}{\sqrt{r_x \cdot \exp(B \cdot r_x)}} \quad (11)$$

where  $r_x$  is the extended radius-width from Eq. (10), and B is the non-linear mirror factor. The mirror constant A was determined from the strength and mirror data from the high strength region, where the mirror is small compared to the fiber diameters, as  $A = 265 \text{ kpsi} \cdot \mu\text{m}^{1/2}$  ( $1.83 \text{ MPa} \cdot \text{m}^{1/2}$ ). A regression of strength and mirror data from all four fiber diameters in Figure 28 yielded a B value of 0.0074. The results from this analysis are shown in Figure 30 to give a reasonable representation of failure stress as a function of mirror radius for a wide range of failure stress and fiber diameter.

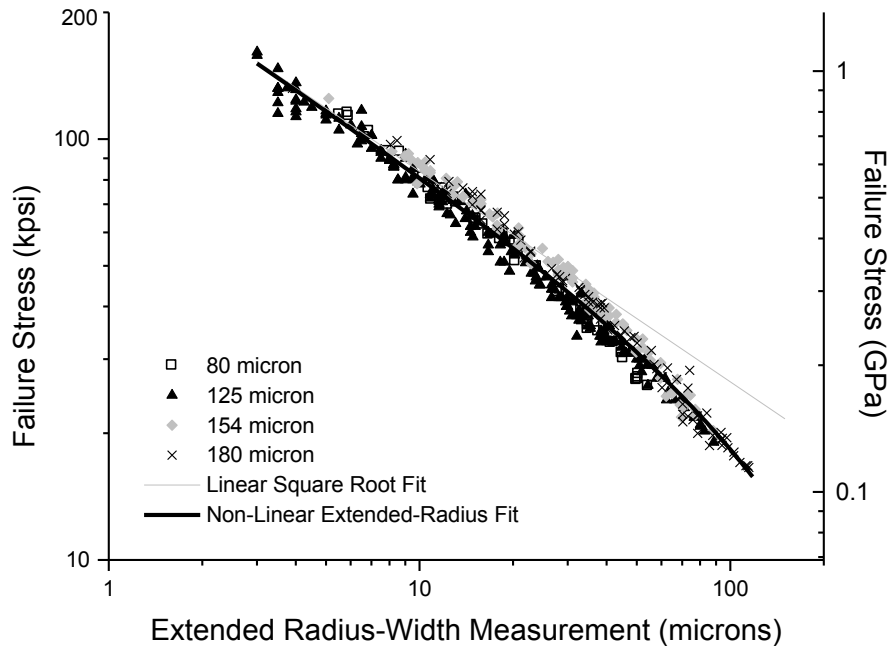


Figure 30. Mirror radius-width ( $r_w$ ) measurement values versus failure stress for various diameter fibers.

Procedures and techniques for failure analysis of brittle materials can be found in references 73, 74, and 87. For the subset of measuring mirror dimensions on optical fiber, the following suggestions are made;

- Ensure that the procedures used in making a mirror measurement are consistent with those used during the development of the mirror constant.<sup>83</sup> Before using published mirror constants it is advisable to perform at least a preliminary experiment to calibrate mirror measurement procedures against published values.
- Sufficient magnification is needed to adequately determine the onset of mist.<sup>88</sup>
- Residual stress and bending can alter the mirror shape.<sup>75,89</sup>
- For surface origins, mirror measurements should be taken several microns away from the specimen surface as the mirror curves in at the surface.
- Strength estimates from mirror dimensions are best made on mirrors that are small compared to the specimen size. However, the above discussion demonstrates that failure stresses can be made from large mirrors, provided that one has sufficient data.
- In the event where the failure stress exceeds approximately 1400 MPa (200 kpsi), the crack branches almost immediately and no mirror is created. Due to the violent nature of high stress failures, the origin is often lost.
- The effects of torsion distort the mirror size. Thus, one can use such an observation to determine the presence of fiber twist; however, it is difficult to predict failure stress from mirrors distorted by torsional stresses.

## 4 Fatigue and Optical Fiber

Subcritical flaw growth in window glass as a function of time, or “fatigue”, is shown in Figure 31 from the now classic work of Wiederhorn.<sup>90</sup> Crack growth is shown to be minimal over most of the crack’s life and increases appreciably just before failure. “Subcritical” refers to the fact that the stress intensity factor for the flaw has yet to reach the critical level for rapid failure. Michalske and Freiman<sup>91</sup> describe this fatigue mechanism as, “the slow extension of a crack due to a specific chemical reaction between strained silica bonds and water.” Bond breakage and crack advancement is shown as a three step process in Figure 32. The first step is where a water molecule attaches to a bridging Si-O-Si bond at the crack tip. Next, water reacts with the strained Si-O-Si bond to form two new bonds and, finally, bond rupture and the formation of surface hydroxyls. This process is illustrated in Figure 33 where mobile water reacts with the strained glass network at the tip of the crack.

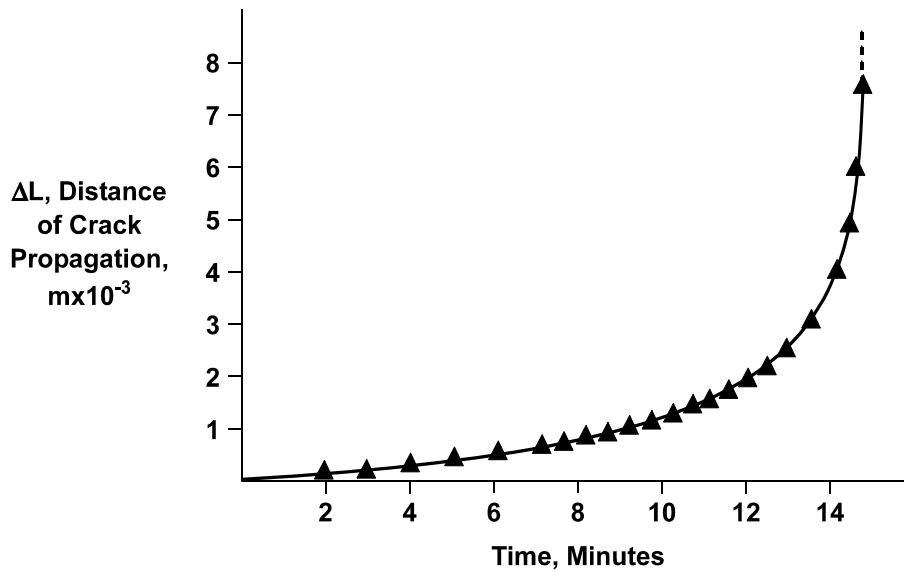


Figure 31. Subcritical crack growth in window glass in air and under a constant load.<sup>90</sup>

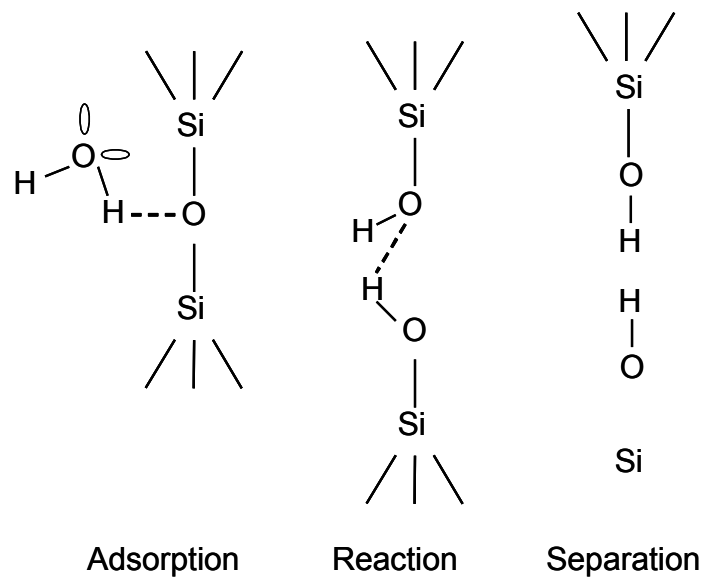


Figure 32. Michalske and Freiman’s model for the interaction between water and strained silica bonds.<sup>91</sup>

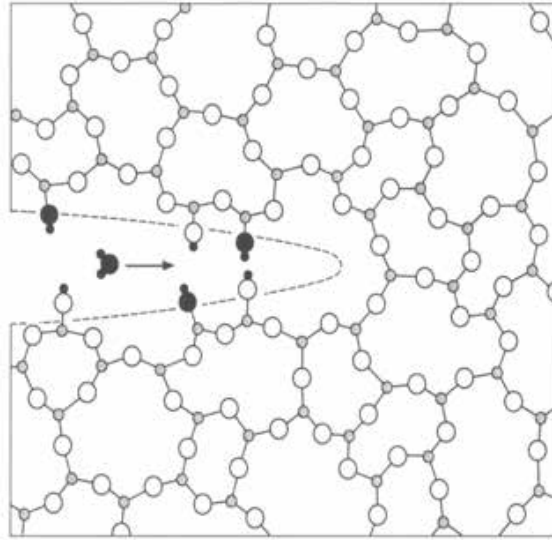


Figure 33. Representation of water-induced bond rupture in silica glass.<sup>49</sup>

As the flaw grows, the stress intensity factor slowly increases. This is shown as Region I behavior in the well-known crack velocity diagram shown in Figure 34. Wiederhorn's measurements on space shuttle windows show crack velocity increasing with increasing stress intensity factor up to a point where the reaction kinetics are believed to be limited by the speed at which moisture can find its way to the crack tip.<sup>90</sup> This is shown as Region II in Figure 34. Region III is when  $K_I$  approaches  $K_{IC}$  the crack advances rapidly to fast fracture through the glass. Since fatigue is dominated by slow growth in Region I, this region is usually all that is incorporated into lifetime models. Even though region I crack growth dominates the lifetime of the flaw, Fuller et al.<sup>14</sup> predicted that region II behavior may occur during short term stress events like proof testing.

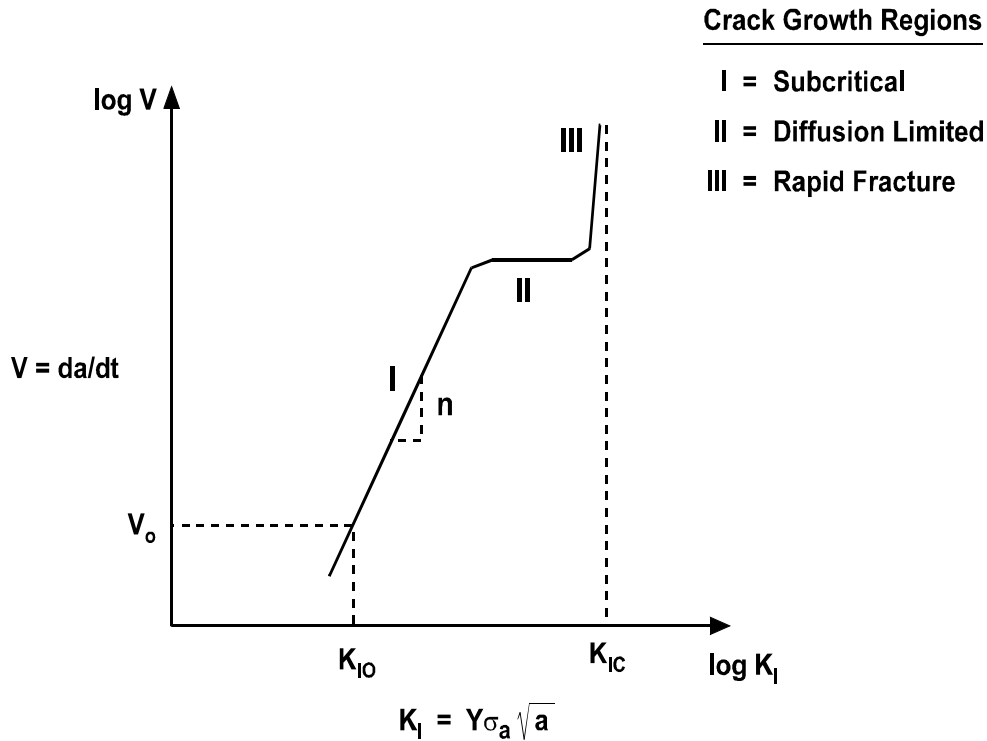


Figure 34. Crack velocity – stress intensity factor diagram illustrating the regions of subcritical crack growth in glass.

Models for crack velocity as a function of the stress intensity factor in region I are many.<sup>92,93,94,95</sup> In general, exponential forms are preferred due to their basis in chemical kinetics or atomistic modeling. The engineering community has almost exclusively used the more empirical power law relationship,

$$V = AK_I^n \quad (12)$$

where  $A$  and  $n$  are crack growth parameters. The power law has been criticized for its lack of theoretical underpinning, however, Fett has attempted a theoretical explanation for crack growth based on a power law model.<sup>96</sup> The power law is more optimistic in its prediction of lifetime than most other models. Said otherwise, one is allowed to place more stress on the glass with this model than with other models. The reasons for the almost exclusive use of the power law in making lifetime predictions for optical fiber are its mathematical simplicity, usage during the forming years of optical fiber technology, and the fact that remarkably few fatigue failures in optical fiber have occurred over the past three decades.

Ritter describes fatigue in terms of strength degradation when he states that “time-dependent strength behavior (fatigue) of glass is generally believed to be the result of subcritical crack growth of a flaw to a dimension critical for spontaneous failure.”<sup>97</sup> Flaw size is translated into strength through fracture mechanics; and therefore, flaw extension from fatigue corresponds to a reduction in strength. This is convenient for optical fiber because strength can be measured much more easily than flaw size.<sup>9</sup> From the power law model, strength degradation for any applied stress history is,

$$\sigma_f^{n-2} - S_i^{n-2} = \frac{AY^2 (n-2)K_{IC}^{n-2}}{2} \int_{t_0}^{t_f} \sigma^n(t) dt \quad (13)$$

or

$$\sigma_f^{n-2} - S_i^{n-2} = \frac{1}{B} \int_{t_0}^{t_f} \sigma^n(t) dt \quad (14)$$

where  $B = \frac{2}{AY^2 (n-2)K_{IC}^{n-2}}$ ,

$S_i$  is the initial inert strength or the strength prior to fatigue and  $\sigma_f$  is the final stress at failure or the fatigue strength. Said otherwise, the fatigue represented by the right side of Eq. (14) generates a decrease in strength on the left side of Eq. (14).

#### 4.1 Fatigue Measurements for Optical Fiber

Two test methods have evolved for determining fatigue parameters,  $n$  and  $B$  for optical fiber. The static fatigue test is where one subjects a length of fiber to a dead weight and simply tracks the time to failure. In this case, the flaw advances toward  $K_{IC}$  by flaw growth alone. The dynamic fatigue test consists of gradually loading the fiber to failure. During the test, both stress and crack extension raise the stress intensity factor to the point of failure.

For the case of static fatigue, Eq. (14) reduces an expression of time-to-failure,  $t_f$ , in terms of applied stress,  $\sigma_a$ ,

$$t_f = BS_i^{n-2} \sigma_a^{-n} \quad (15)$$

where  $S_i$  is the inert strength. The inert strength is the strength in the absence of fatigue, the strength before any flaw growth, and is typically measured at low temperatures or in inert environmental conditions.

Figure 35 is a schematic of strength degradation with time under static loading conditions. Because of the nature of the fatigue crack growth shown in Figure 31, the glass does not weaken appreciably until just before failure. Figure 36 is an early example of static fatigue data on optical fiber from the work of Schonhorn et al. for 61 cm lengths measured in tension.<sup>98</sup> The fatigue parameter  $n$  is determined from the slope of  $\ln t_f$  and  $\ln \sigma_a$ , and  $B$  is obtained from the intercept of the same as well as knowledge of the inert strength,  $S_i$ . Obtaining  $B$  on as-drawn fiber can be problematic as strength measurement in an inert environment is limited to the two point bend method. To statistically resolve crack growth

<sup>9</sup>Although crack velocity measurements on optical fiber have been attempted, see Muraoka et al., J. Am. Ceram. Soc. 76 [6] 1545-1550 (1993).

parameters, an inert strength distribution with a Weibull modulus near 100 is needed. Consequently, static fatigue testing has traditionally been limited to pristine as-drawn fiber. A recently developed indentation technique has produced a sufficiently high Weibull modulus for static fatigue testing and is discussed below. Static fatigue testing of as-drawn fiber requires high loads to generate failure and, consequently, premature failures where the fiber is gripped can be problematic. Two-point bending has been used extensively for static fatigue testing, but one must be mindful that only a very short length, about 20  $\mu\text{m}$ , is under test. One of the primary reasons static fatigue testing is performed on fiber is that it simulates the long term stress state of the fiber in-service.

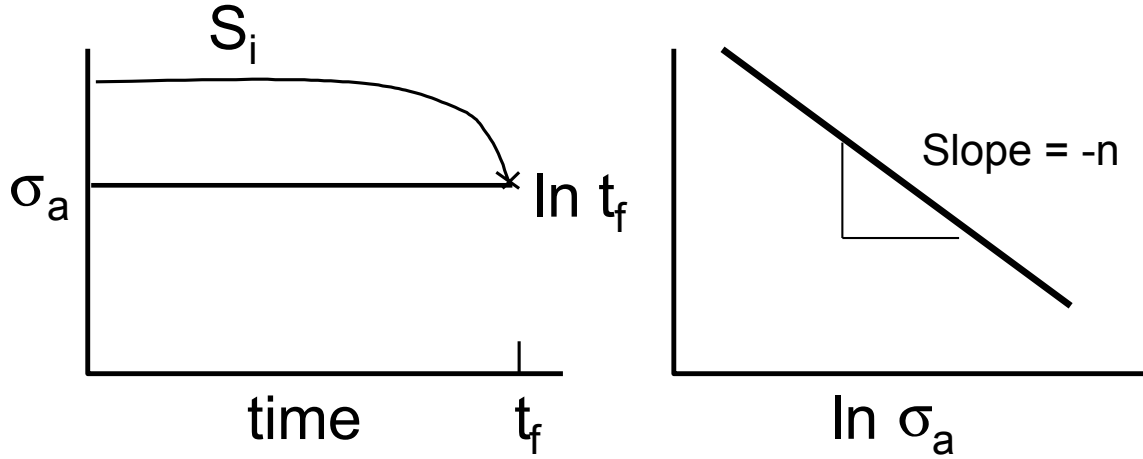


Figure 35. Static fatigue testing.

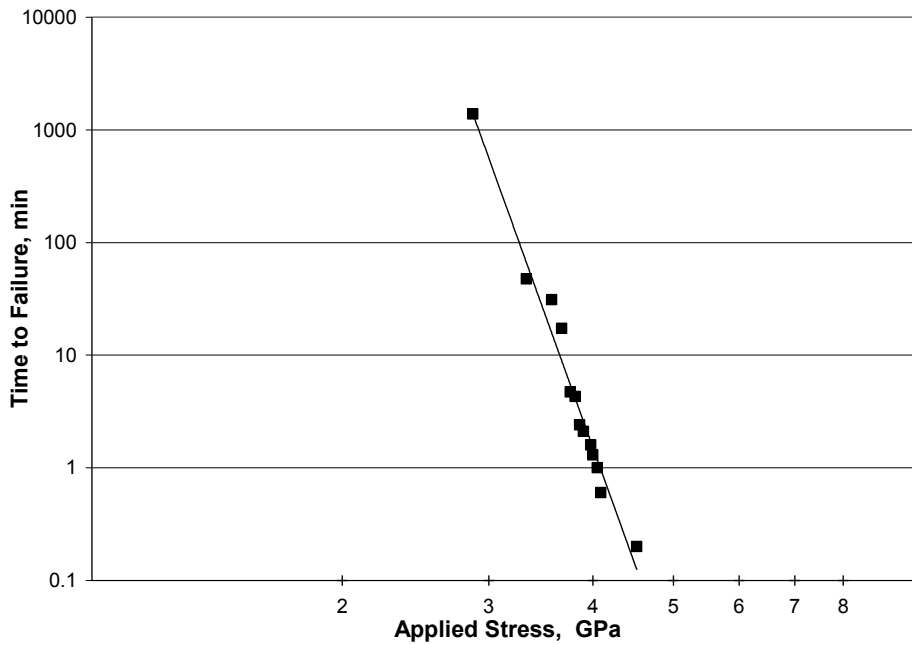


Figure 36. Static fatigue testing of optical fiber by Schorhorn et al.<sup>98</sup>  
Testing performed at 23°C and 50% RH using a gauge length of 61 cm.

Dynamic fatigue testing consists of loading glass to failure for a variety of stressing rates, usually an order of magnitude apart. Figure 37 illustrates that most strength degradation occurs just before failure. If the fatigue behavior follows the power law crack velocity model, the strength depends on the stressing rate by

$$\sigma_f^{n+1} = (n+1)BS_i^{n-2} \dot{\sigma} \quad (16)$$

The fatigue parameter  $n$  is obtained from the slope of  $\ln \sigma_f$  versus  $\ln \dot{\sigma}$ , and  $B$  is obtained from the intercept and knowledge of the inert strength. An example of dynamic fatigue test results on optical fiber is shown in Figure 38. Dynamic fatigue has fewer gripping issues and one has a higher degree of confidence in the resulting crack growth parameters than with static fatigue testing. The crack growth parameters determined from dynamic fatigue testing are less sensitive to variability in the inert strength than the static method. Because dynamic fatigue testing continues to load the fiber until failure, it is more suited for shorter term testing. To capture fatigue behavior over long time periods, special equipment must be built to achieve the necessary slow stressing rates.<sup>99</sup>

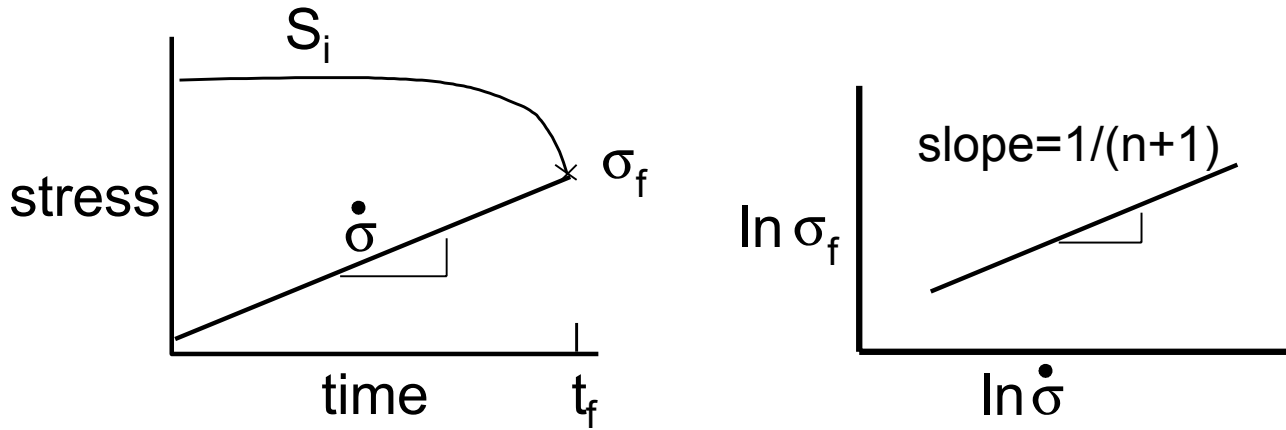


Figure 37. Schematic of dynamic fatigue testing.

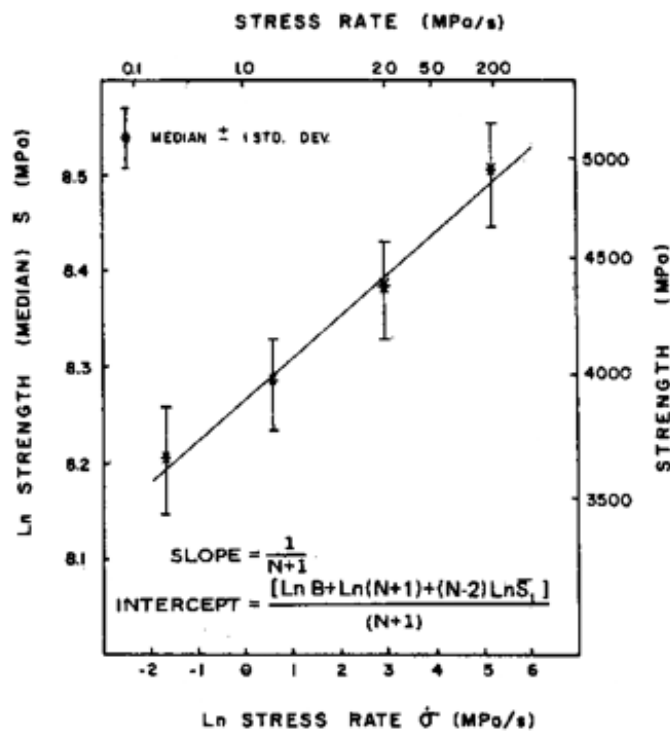


Figure 38. Example of dynamic fatigue data on optical fiber taken from Ritter et al.<sup>100</sup>

Matthewson<sup>101</sup> reminds us that since the crack growth parameters are obtained from the regression parameters of strength and stressing rate or time to failure and applied stress, they are correlated. This means that one should not simply use fatigue parameters from separate sources in making reliability predictions. This is particularly true for the  $B$  value, which can only be deduced from knowledge of the strength,  $S_i$ , and  $n$  from the same test data. Table 2 shows static and dynamic fatigue results from several early studies on short lengths of as-drawn optical fiber. The measured  $n$  values center around 20, but  $B$  ranges by several orders of magnitude. Note that the inert strength values are significantly lower than the value of 11 to 14 GPa one should find on gauge lengths less than 1 meter. This is likely due to difficulties in creating the necessary inert environment for strength in tension and explains much of the variability in  $B$ . Hence, some prefer to treat the regression parameter  $\ln BS_i^{n-2}$  as a fatigue parameter.

Table 2. Room temperature fatigue parameters for optical fiber. Gauge lengths are shown for the tensile tests and “static” and “dynamic” refer to the fatigue test method.

	Test Conditions	% RH	n	$S_i$ GPa	$\ln BS_i^{n-2}$	B GPa <sup>2</sup> s
Schonhorn et al. <sup>98</sup>	61 cm static	50	20.5	8.74	28.9	$1.2 \times 10^{-5}$
Schonhorn et al.	61 cm dynamic	50	21.5	8.74	35.2	$8.3 \times 10^{-4}$
Ritter et al. <sup>100</sup>	30 cm dynamic	55	22.2	5.67	35.5	1.6
Kalish and Tariyal <sup>102</sup>	61 cm static	97	14.3	6.16	21.4	0.38
Kalish and Tariyal <sup>102</sup>	5 cm dynamic	97	15.9	6.76	22.7	0.022
Kalish and Tariyal <sup>102</sup>	6 cm dynamic	45	25.5	6.76	39.2	$3.4 \times 10^{-3}$
Duncan et al. <sup>103</sup>	2 pt. bend dynamic	50	25.3	17.6% strain		$2.9 \times 10^{-8}$
Duncan et al. <sup>103</sup>	2 pt. bend dynamic	water	22.8	17.6% strain		$1.9 \times 10^{-5}$

## 4.2 Fatigue of Proof Stress Level Flaws

Optical fiber is most easily tested in short lengths in tension or 2-point bending and is usually flawless over these lengths. However, the flaws of greatest reliability risk are those near the proof stress level and the rarity of such defects makes fatigue characterization inconvenient. Figure 39 illustrates this point. Dynamic fatigue of 20 meter gauge length specimens was obtained using 5 stressing rates and 10 kilometers of fiber at each rate.<sup>99</sup> The higher strength region is well characterized, but there are too few flaws near the proof stress level to characterize the fatigue behavior in this region. In order to characterize the fatigue behavior of flaws of greatest reliability risk, researchers place artificial flaws on the surface of optical fiber. These flaws are intended to mimic the rare flaws that occur during fiber manufacturing and handling. The methods for placing artificial flaws on the fiber surface allow one to control both the strength level and distribution of flaws. The ability to concentrate the strength at a predetermined level greatly aids in resolving the behavior of the flaws at that strength level. Table 3 summarizes the results from a variety of studies employing flaws intentionally placed near the proof stress level of 700 MPa (100 kpsi). Results from as-drawn fiber and bulk fused silica are also included in Table 3 for comparison.

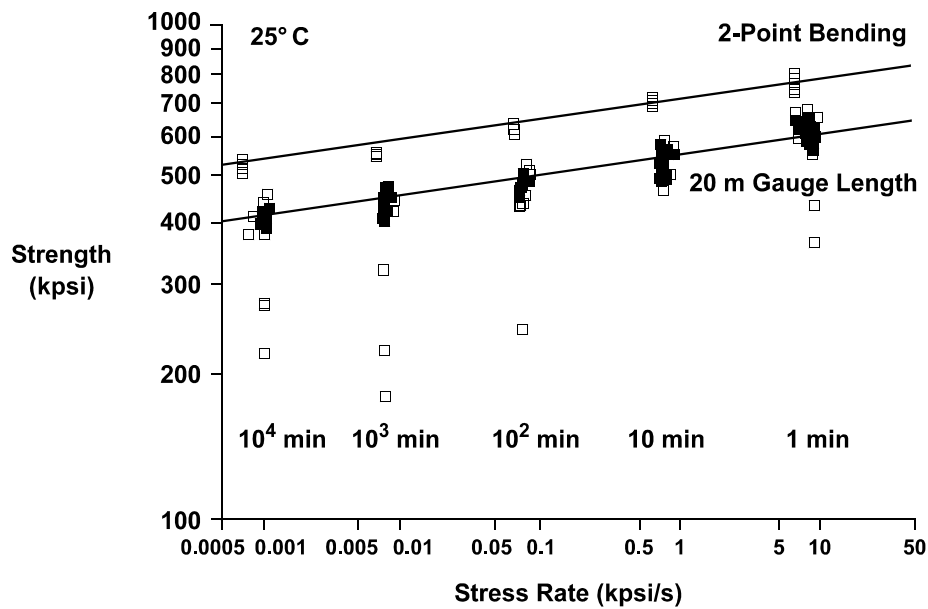


Figure 39. Dynamic fatigue of silica-clad optical fiber at room temperature using 20 meter gauge lengths in tension and 2-point bending. Ten kilometers of fiber was tested at each stressing rate for the tensile tests.<sup>99</sup>

As discussed previously, there are two basic flaw types, abrasions and contamination. Early fiber studies used diamond indentation to create an abrasion-like defect. Typical  $n$  values with the Vickers indentation method in Table 3 are in the range of 20. However, Matthewson has recorded an  $n$  value as low as 14 and attributed it to the effects of contact residual stress.<sup>111</sup> The  $n$  values obtained on optical fiber are about half that of bulk fused silica. This is more clearly shown in Figure 40 where fiber results in Table 3 are plotted with bulk fused silica and crack velocity data. Note that  $n$  values close to that of bulk glass were achieved in experiments where the strength of fiber was lowered close to that of bulk glass. This suggests that  $n$  has a flaw size dependency, but the reason for this behavior is not clear.

Table 3. Summary of fatigue studies on silica-clad fiber and bulk glass. Table modeled after Kurkjian.<sup>104</sup>

Silica Form	Surface Condition	Strength (kpsi)	n			H (%)	Comments	Ref.
			Crack Velocity	Dynamic Fatigue	Static Fatigue			
Fiber	As-drawn	700		15.9	14.3	97	Tension	102
Fiber	As-drawn	800		25.5		Amb.	Tension	
Fiber	As-drawn	800		22.5		Water	Tension	105
Fiber	As-drawn	700		22		Water	Tension	
Fiber	As-drawn	700		21.1	19.7	45	Tension	
Fiber	As-drawn	700		22.1		Water	Bending	99
Fiber	As-drawn	530		29.9		Water	Bending	99
Fiber	As-drawn	600		20.8		100	Tension	99
Fiber	As-drawn	420		25.5		100	Tension	99
Fiber	As-drawn	700		21.7		Amb.	Tension	100
Fiber	Abraded	180		22.1	19.8	50	Tension	
Fiber	Abraded	150		22.3	20.2	45	Tension	107
Fiber	Abraded	80		26	22.2	45	Tension	107
Fiber	Abraded	50		33.7		45	Tension	107
Fiber	Abraded	50			35.6	Water	Tension	
Fiber	Abraded	50		42.6		60	Tension	109
Fiber	Abraded	100		20.5		Water	Tension	105
Fiber	Abraded	100		25.5		Amb.	Tension	105
Fiber	Abraded	70		23.4		100	Tension	71
Fiber	Abraded	50		20.4		100	Tension	71
Fiber	Abraded	20		32		100	Tension	71
Fiber	Indented	70		19		Water	Tension	
Fiber	Indented	140		14-23		Amb.	Sub-threshold	
Bulk	Indented	10		30.7		Water	Sub-threshold	110
Bulk	Abraded	14		37.8		Water		
Bulk	Abraded	10		45		Water		
Bulk	Compact Tension		42			Water		109
Bulk	DCB		36			100		
Bulk	Compact Tension		36-44			0 to Water	24 to 70°C	

\*Test temperatures 20 to 25°C except where otherwise noted.

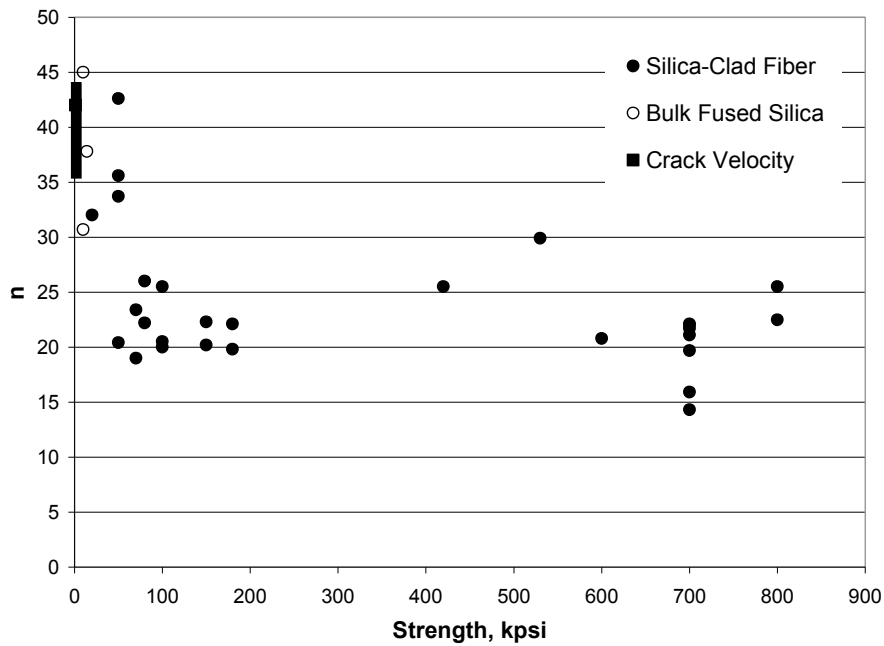


Figure 40. Fatigue parameter  $n$  for optical fiber for a range of strengths and compared to that from strength velocity experiments on bulk fused silica. Plot modeled after Kurkjian.<sup>104</sup>

An indentation method that employs a cube-corner indenter and nano-indentation has demonstrated Weibull moduli,  $m$ , between 50 and 100.<sup>54</sup> Cube corner indentation creates reproducible cracks emanating from the corners of the indent, shown in Figure 41, with few secondary crack systems. With these Weibull moduli values, static fatigue testing of proof test level flaws is possible. Figure 42 shows the results of both dynamic and static fatigue testing of cube corner indents plotted in dynamic fatigue coordinates.<sup>116</sup> The dynamic fatigue testing was obtained over 8 orders of magnitude in stressing rate to allow for a substantial overlap between the results of both test methods. The results at longer test times, slow rates for dynamic fatigue, demonstrate that fatigue is independent of the test method. However, at high speeds there is a significant departure from the slow speed behavior. This non-linearity in the fatigue curve is attributed to Region II-type crack growth behavior and will be discussed in more detail later.

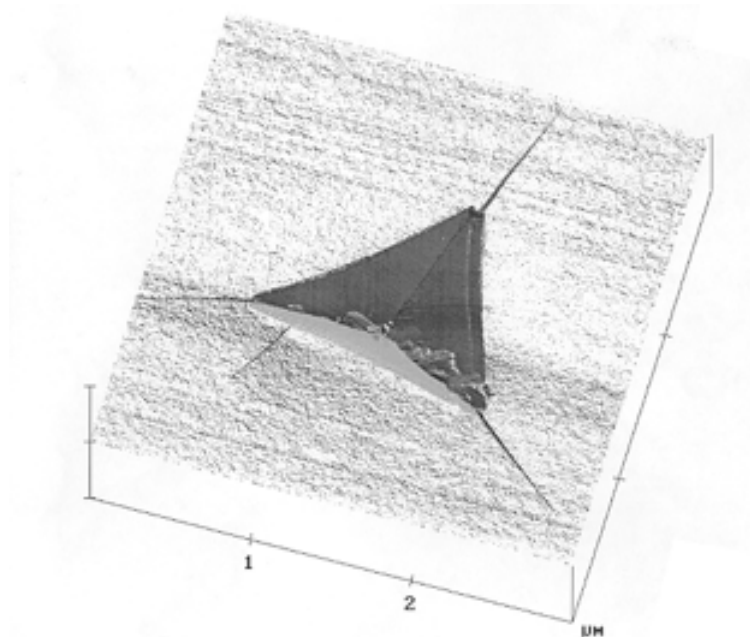


Figure 41. AFM image of a cube-corner indenter pressed into the surface of silica-clad optical fiber with a load of 1 gram.<sup>55</sup>

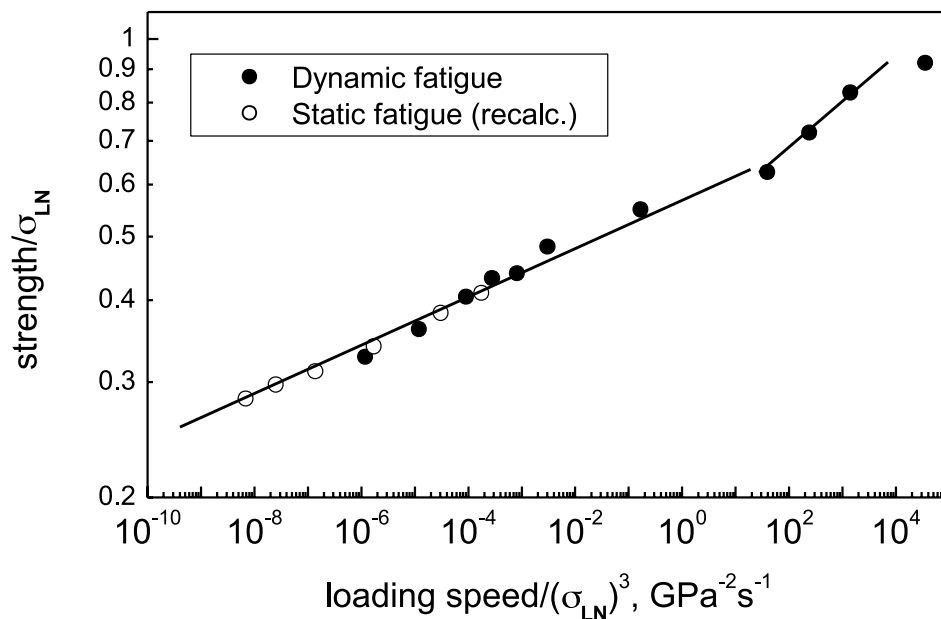


Figure 42. Combined plot of dynamic fatigue and recalculated static fatigue results obtained for indented fibers in a laboratory environment (50% RH, 23°C).<sup>116</sup>

Surface abrasion has also been simulated by dropping abrasive particles on the fiber,<sup>71,105</sup> by passing bare fiber over abrasive pulleys during draw,<sup>109,117</sup> and by placing abrasives in the coating.<sup>107</sup> The difficulty with such abrasion methods is control over the strength distribution. Rubbing the glass surface during fiber drawing with another piece of fiber can generate Weibull modulus values near 20.<sup>71</sup>

Studies on the fatigue behavior of fiber with surface contamination are few, limited primarily by the difficulty in generating sufficiently high Weibull moduli.<sup>118</sup> Semjonov created a technique for placing ZrO<sub>2</sub> particulate on the fiber surface to yield a Weibull modulus of about 20 and the resulting strength distributions for a wide range of stressing rates are shown in Figure 43.<sup>119</sup>

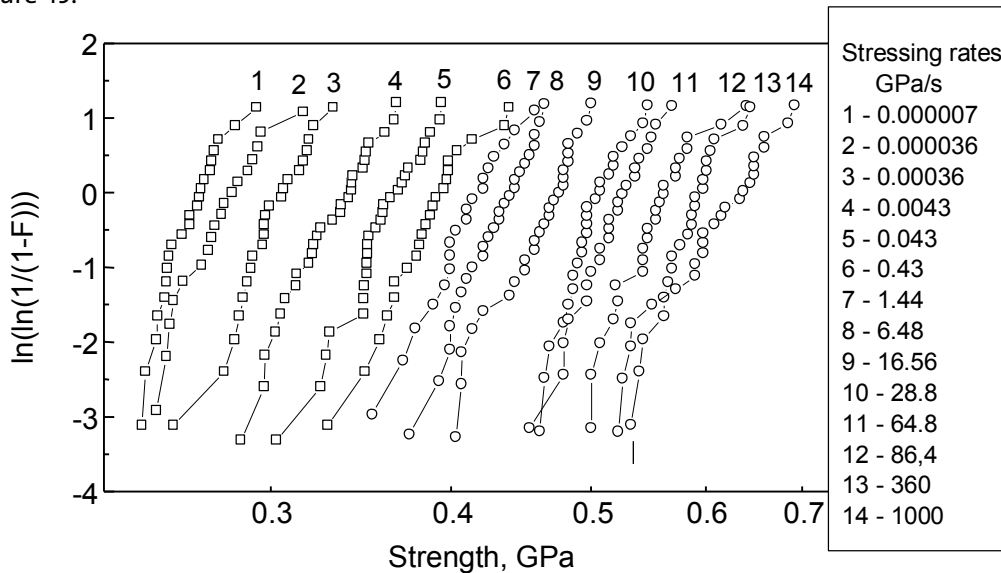


Figure 43. Weibull distributions from zirconia seeded fiber measured at different stressing rates in laboratory ambient environment.<sup>119</sup>

The fatigue behavior of fiber with different flaw sources and initial inert strengths can be compared using universal coordinates  $(\sigma_d/S_i) - (\sigma'/S_i^3)$ .<sup>120,121</sup> Here  $\sigma_d$  is the median strength of a fiber at stressing rate  $\sigma'$ , and  $S_i$  is the initial inert strength of the same fiber. The dynamic fatigue for indented, draw-abraded, and seeded fibers is shown in Figure 44 along with similar results on pristine fibers. The initial inert strength,  $S_i$ , for the low strength fibers was measured using a liquid nitrogen environment. Previously published values of 12 GPa and 14 GPa were used for the pristine fiber.<sup>36,122</sup>

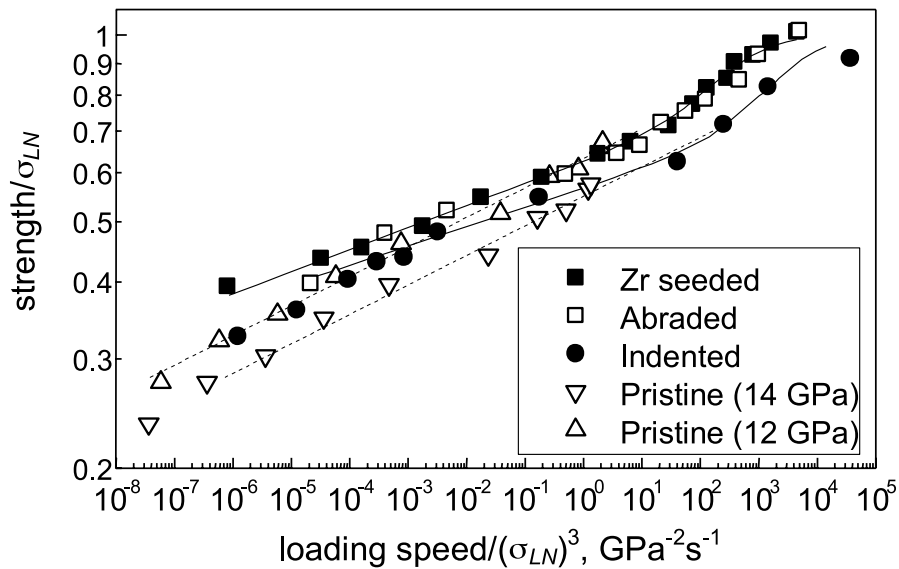


Figure 44. Joint plot of dynamic fatigue results obtained for different types of weak fibers and pristine fiber.<sup>119</sup>

Overall these fibers exhibit similar fatigue behavior over a wide range of stressing rates, but there is also a noticeable difference in fatigue between pristine and low strength fibers at slow stressing rates. However, this difference is within the range of fatigue results in Figure 40. Of particular importance is the observation that fatigue for low strength fibers at slow stressing rates appears to be independent of flaw source. This is somewhat unexpected as there are significant differences in residual stress profiles for seeded and indented flaws.<sup>4</sup> If long-term fatigue is independent of flaw source, then the same lifetime model can be used for all flaw types. All fibers in Figure 44 show a change in the fatigue behavior at fast stressing rates. It has been hypothesized that the non-linear fatigue behavior at the fast stressing rates can be attributed to the influence of region II crack growth.

### 4.3 Fatigue During High Speed Events and Associated Modeling

During manufacturing and cabling, optical fiber is subjected to several high speed events. Most notably is the high stress event of proof testing where processing speeds of 20-30 m/s is routine. Coloring is also performed at these speeds albeit at a lower stress. Establishing a post proof strength distribution is key to modeling long-term reliability and considerable work has been done to model fatigue during this high stress event.<sup>15,123,124</sup> As shown previously in Figure 42 and Figure 44, the fatigue behavior of low strength fibers subjected to high speed strength testing is different than that at slower test times. Note that several laboratories have observed this phenomenon on optical fiber.<sup>125</sup> Typical proof test loading and unloading rates are in the range of 0.01 seconds with dwell times on the order of 0.1 seconds.<sup>33</sup> This places fatigue during proof testing in the non-linear region of the fatigue curves for the low strength fiber. Based on fatigue studies and associated modeling by Fuller et al.,<sup>14</sup> Hanson and Glaesemann<sup>126</sup> attributed this behavior to an effect of region II type crack growth. The predicted effect of region II crack growth on dynamic fatigue test results is illustrated in Figure 45.

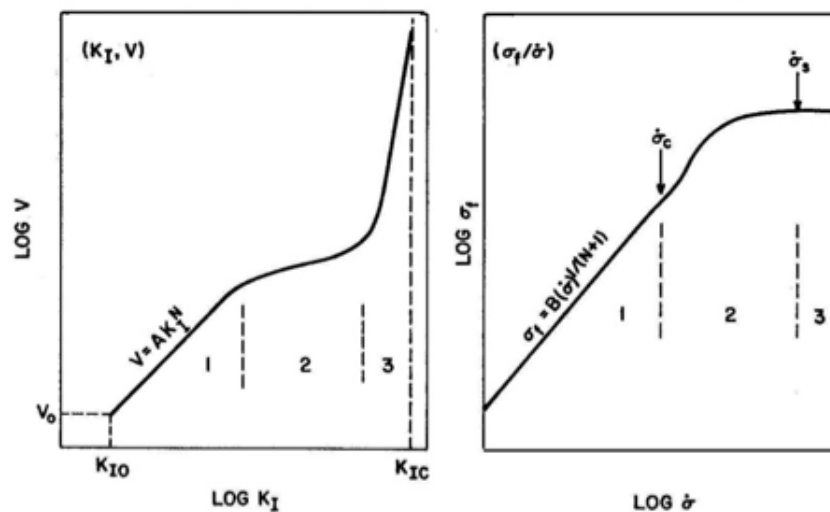


Figure 45. Influence of Region II and III crack growth on failure strength and loading rate dependence, from Chandan et al.<sup>127</sup>

A simple mathematical description of Region I and II is the joining of two power law equations,<sup>126,128</sup>

$$\frac{da}{dt} = v_1 \left( \frac{K_I}{K_{IC}} \right)^{n_1} \quad \text{for } K_I \leq r K_{IC} \quad (17a)$$

$$\frac{da}{dt} = v_2 \left( \frac{K_I}{K_{IC}} \right)^{n_2} \quad \text{for } K_I \geq r K_{IC} \quad (17b)$$

where  $K_I$  is the stress intensity factor,  $K_{IC}$  is the critical stress intensity factor,  $da/dt$  is the flaw growth rate,  $v_1$ ,  $v_2$ ,  $n_1$  and  $n_2$  are the fatigue parameters of the respective curves. The parameter  $r$  and the relation characterize the point of transition of flaw growth rate from Region I to Region II shown in Figure 46 below.

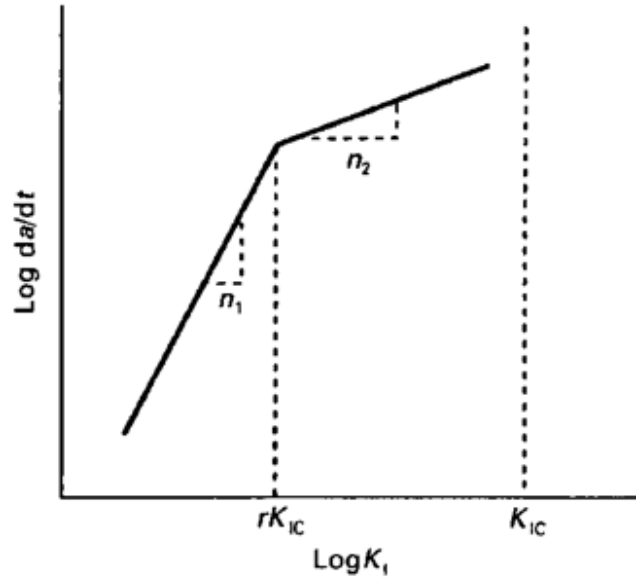


Figure 46. Description of the two-region power law model.

The following strength degradation equations are then derived for the case of dynamic fatigue,

$$S_i^{n_1-2} = S_r^{n_1-2} + \frac{\sigma_r^{n_1+1}}{B_1 (n_1 + 1) \dot{\sigma}} \quad \text{for flaw growth through Region I} \quad (18a)$$

$$S_r^{n_2-2} = \sigma_d^{n_2-2} + \frac{\sigma_d^{n_2+1} - \sigma_r^{n_2+1}}{B_2 (n_2 + 1) \dot{\sigma}} \quad \text{for flaw growth through Region II} \quad (18b)$$

where  $S_i$  is the inert strength before any loading or fatigue,  $S_r$  and  $\sigma_r$  are the inert strength and applied stress when  $K_I/K_{IC} = \sigma_r/S_r = r$ ,  $\sigma_d$  is the dynamic fatigue strength for stress rate  $\dot{\sigma}$ ,  $1/B_2 = v_2 (Y/K_{IC})^2 (n_2 - 2)/2$  and  $B_1 = B_2 \cdot r^{(n_1 - n_2)(n_2 - 2)}/(n_1 - 2)$ .

A physical description of failure for the two region model is that while loading under a constant stress rate a flaw with initial strength,  $S_i$ , experiences typical Region I growth as expressed by Eq. (18a) and degrades to strength,  $S_r$ . At strength,  $S_r$ , the growth behavior transitions to that of Region II and the flaw degrades to the final strength  $\sigma_d$  in Eq. (18b). Note that  $\sigma_r$  in Eq. (18b) is the applied stress at the transition from Region I to Region II, when the flaw is at strength  $S_r$ .

Dynamic fatigue data for abraded fibers was fitted to this model and the crack growth parameters in Table 4 were obtained. Figure 47 shows the predicted crack velocity curves for these parameters along with crack velocity data on optical grade bulk silica by Hibino et al.<sup>129</sup> Consistent with the earlier discussion, the Region I  $n$  values are lower than what is typical for bulk glass. The transition from Region I to Region II for optical fiber occurs at the same  $K_{IC}$  values as that for bulk silica. The Region II fiber behavior shows reasonable agreement with the crack velocity data.

Table 4. Fitted fatigue parameters for the two-region power law model.

	Ambient	100% RH
$n_1$	21.2	21.2
$n_2$	2.4	3.2
$r$	0.635	0.66
$B_1$ (GPa <sup>2</sup> s)	$4.99 \times 10^{-5}$	$4.09 \times 10^{-6}$
$B_2$ (GPa <sup>2</sup> s)	$5.52 \times 10^{-3}$	$4.53 \times 10^{-4}$
$A_1$ m/s	1.97	2.95
$A_2$ m/s	$3.90 \times 10^{-4}$	$1.66 \times 10^{-4}$

$K_{IC} = 0.87 \text{ MPa m}^{1/2} \quad Y = 0.73/\pi$

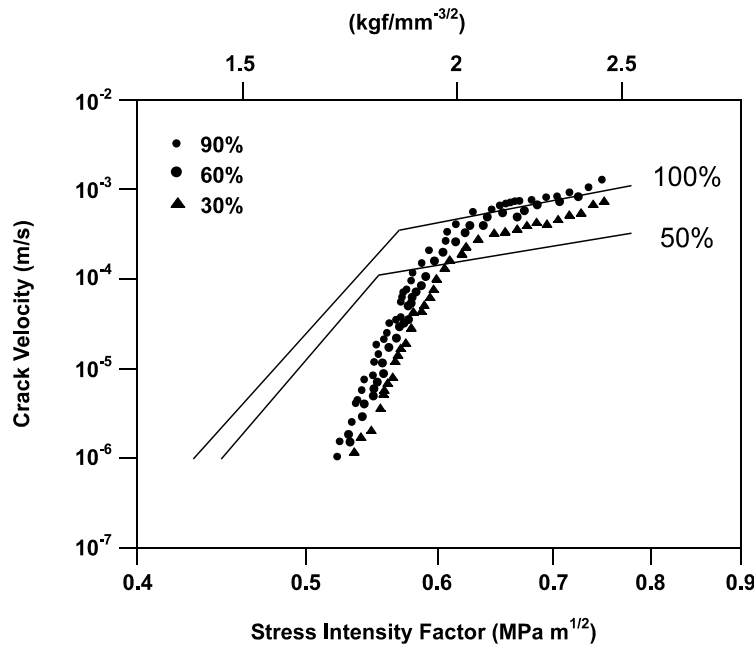


Figure 47. Predicted K-V Diagrams from the Abraded Fiber Data in Table I.

Crack Velocity Measurements on Fused Silica for a Range of Humidity Levels by Hibino et al.<sup>129</sup>

One of the important outcomes of the change in fatigue behavior at fast stressing rates is that a single set of crack growth parameters do not describe both proof testing and long term life. This should influence the construction of lifetime models for fiber. Furthermore, in characterizing the fatigue behavior of fiber through strength testing, one should combine data from longer-term static fatigue tests, slow rate dynamic fatigue tests as well as high speed dynamic tests. Finally, this behavior settles a long standing argument over the value of B, see references 125 and for more details.

#### 4.4 The Effect of Environment on Fatigue in Fiber

There are numerous studies on the effect of environmental conditions concerned with the fatigue of optical fiber (for examples, see 57, 59, 62, 103, 131, 132, 133, 134, 135, 136, 137 and 138). It is generally accepted that fiber lifetime decreases with increased temperature and humidity. As the pH of the test environment changes from acid to base (a pH increase) the lifetime decreases.<sup>59,131</sup> Matthewson and coworkers<sup>133,134</sup> have done the most to incorporate these factors into predictive models, but there is still much to be done in this area. The technology has obviously moved forward without a comprehensive fatigue model incorporating these environmental factors. Engineers tend to conduct fatigue tests in the environment they expect the fiber to experience in-service. For proof testing, fatigue tests performed in an ambient environment are appropriate. For fiber in cable, a higher humidity test environment mimics the case where water is allowed to permeate the cable. Tests at elevated temperatures are performed on fiber intended for down-hole oil exploration or some aircraft applications, for example.

## 4.5 Resisting Fatigue

There are several strategies for reducing the effect of fatigue on fiber lifetime. One is to eliminate moisture from reaching the glass surface by placing a hermetic layer next to the glass surface. The most used hermetic coating is amorphous carbon.<sup>139,140,141</sup> Fibers with little to no dependence of strength on stressing rate have been mass produced. There is little point in performing static fatigue tests on this fiber as specimens that did not fail during application of the static load would never fail. An  $n$  value between 100 and 200, as measured by the dynamic test method, is sufficient for claiming hermeticity. The allowable stress for such fiber could be any stress up to the proof stress, however, an allowable stress of 80 to 90% of the proof stress is recommended. This is for the practical reason that it is difficult to control applied stresses. Note that the strength of carbon-coated hermetic fiber is lower than that of typical non-hermetic fiber. The carbon layer fails first when stretching the composite to failure and in doing so damages the pristine glass.<sup>142</sup> Typical inert initial strengths are 600 to 800 kpsi, which is enough for most fiber processing and handling events. Special care needs to be taken when splicing carbon coated fiber.<sup>143</sup>

Metal coatings have been successfully applied to fiber as a hermetic layer.<sup>141</sup> The strength can be maintained over short lengths, but longer length strength distributions are generally poor. Cleaving can be an issue with metal coated fibers. For a good review of the history of this technology, see the paper by Filas.<sup>144</sup>

Another strategy for minimizing fatigue effects is to make the surface of the glass itself more resistant to fatigue. Doping the outer surface of the silica cladding with titania has been used commercially, yielding  $n$  values greater than 30.<sup>99,113,145</sup> Note that the use of low expansion titania also places the surface of the glass in compression during cooling after draw. Although less convincing, high fatigue resistance from specially designed polymer coatings has been claimed.<sup>146</sup>

## 5 Optical Fiber Strength

Figure 48 shows the evolution of optical fiber strength with time. Fiber strength distributions have always been distinctly bimodal with a high strength, high Weibull modulus region and a low strength, low Weibull modulus region. Figure 48 shows that the number of flaws in the lower strength region decreased over time as proof stress requirements increased and manufacturers pushed to improve proof test selects. Today fiber proof tested at 700 MPa (100 kpsi) can be purchased in 50 km lengths. Some applications, like submarine, require fiber to be proof tested at 1400 MPa (200 kpsi). The ability to establish a minimum strength through proof testing over long fiber lengths has been key to the reliability success of optical fiber. The infrequency of flaws also allows for discrete handling events in excess of the minimum allowable applied stress. Handling events like splicing, routing of pigtails and patch cords, and fiber-based device packaging routinely bend the fiber sharply and rely on the infrequency of flaws. With knowledge of the strength distribution, stresses in excess of the proof stress may be permanently applied in these shorter length applications. In addition to quantifying the spatial density of flaws for reliability prediction, strength testing is used for investigations into the structural properties of glass, development of processes and products, and characterizing delayed failure modes.

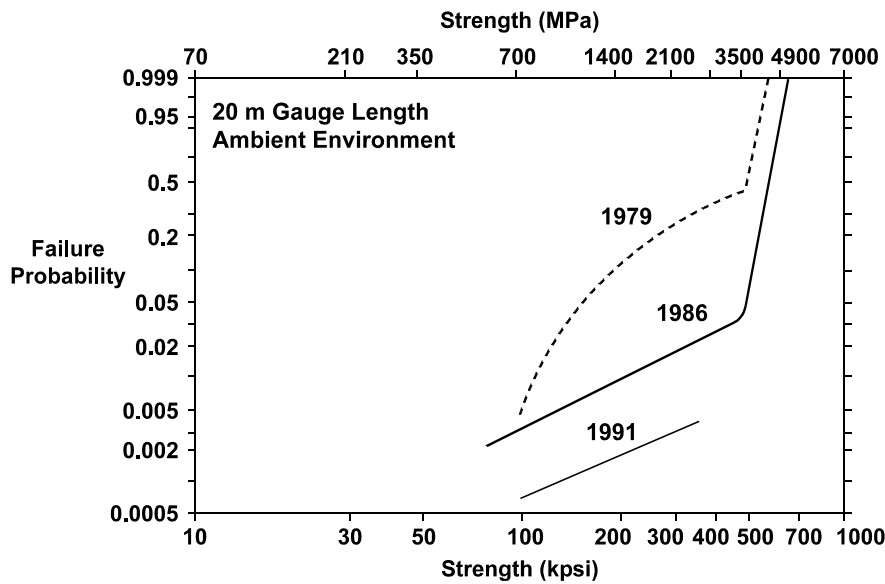


Figure 48. Evolution of fiber strength distribution, see also Kurkjian et al.<sup>104</sup>

Table 5 summarizes some of the early publications on optical fiber strength. Soon after achieving attenuation of 20 dB/km, then regarded as the threshold for a practical medium for optical communication, a comprehensive examination into optical fiber strength characteristics had been completed. Long lengths were tested for reliability prediction, the effect of various processing steps on fiber strength was researched, and strength testing was used to characterize strength degradation by flaw introduction or growth of preexisting flaws. Most of the work in fiber strength since then consists of either test method improvement or the specific examination of novel fibers.

There is a considerable number of fiber strength testing methods owing to the variety of strength investigations over the past thirty years. Matthewson discusses many of these test methods in his excellent review of the topic.<sup>12</sup> In this chapter, test methods will be discussed as they pertain to specific strength information of interest.

Table 5. Early fiber strength assessments.

Author	Year	Summary
Maurer <sup>147</sup>	1975	Strength of 60 cm length specimens compared to screening kilometer lengths at various stress levels
Kurkjian et al. <sup>148</sup>	1976	Strength of 0.04 to 50 m lengths combined to describe high strength to near proof stress level strength distribution
Olshansky and Maurer <sup>149</sup>	1976	Strength distribution created from range of gauge lengths and incorporated into lifetime model
Schonhorn et al. <sup>150</sup>	1976	Process for making high strength fiber
Justice <sup>151</sup>	1977	Statistical aspects of fiber strength
Snowden <sup>152</sup>	1977	Effect of gauge length on strength distribution, early fatigue work
Tariyal and Kalish <sup>153</sup>	1977	Strength distribution extrapolations based on long gauge lengths, proof testing, and effect of coating on fatigue behavior
Justice and Gulati <sup>154</sup>	1978	Technique for quickly measuring 20 to 50 m lengths
Maurer <sup>155</sup>	1979	100 m gauge length distribution and statistical model for strength degradation during screening
DiMarcello et al. <sup>156</sup>	1979	Guidance on drawing high strength optical fiber

## 5.1 Fiber Strength after Drawing

The first opportunity to characterize the strength distribution of optical fiber is after drawing and coating application. However, most strength distributions are generated after proof testing because this is a convenient point to benchmark strength, before fiber deployment into a variety of cable processes and applications. The 1979 distribution in Figure 48 exhibits classic truncation as the proof stress is approached. The 1986 strength distribution was created by tensile testing individual 20 meter lengths in ambient air. At that time, fiber was proof tested at 350 MPa (50 kpsi). This distribution is typical in that it is multimodal beginning with a uniform high strength region above 3500 MPa with a Weibull modulus,  $m$ , of 20 to 30 and transitioning to a lower strength region with Weibull modulus in the range of 2-5. In the past, the variability in the higher strength region was attributed to diameter fluctuations,<sup>157</sup> but with the high degree of diameter control in modern optical fiber processing another explanation is needed. Over 90% of the 20 meter lengths are in this region, meaning that most of the fiber volume is, for practical purposes, flawless. The region below 3500 MPa (500 kpsi) consists of a wide range of strengths and a corresponding low Weibull modulus of 2-5. Flaws in this region originate from slight surface damage and contamination sites that are small enough to pass proof testing. Note that failure source identification is difficult for failure stresses above 150 kpsi as fiber tends to fragment above this stress level and the origin is lost. By 1991 the strength distribution had improved as evidenced by the shift in the lower strength region to lower failure probabilities. More recent strength distributions will be shown later in Figure 53.

## 5.2 The Intrinsic Strength

Gupta and Kurkjian<sup>38</sup> define the intrinsic strength as the strength in the absence of flaws. The intrinsic strength of silica optical fiber can be easily observed by strength testing short lengths of optical fiber in tension or 2-point bending. The room temperature distribution in Figure 49 shows the strength of tensile and 2-point bend strength of silica-clad fiber specimens tested in air.<sup>158</sup> These distributions are typical of modern fiber tested in this fashion; high strength and a near single-valued distribution signified by a Weibull modulus near 100. A bi-modal distribution on short test lengths like those used for Figure 49 may be found on developmental or some specialty fibers, but is sub-par for standard commercial fiber.

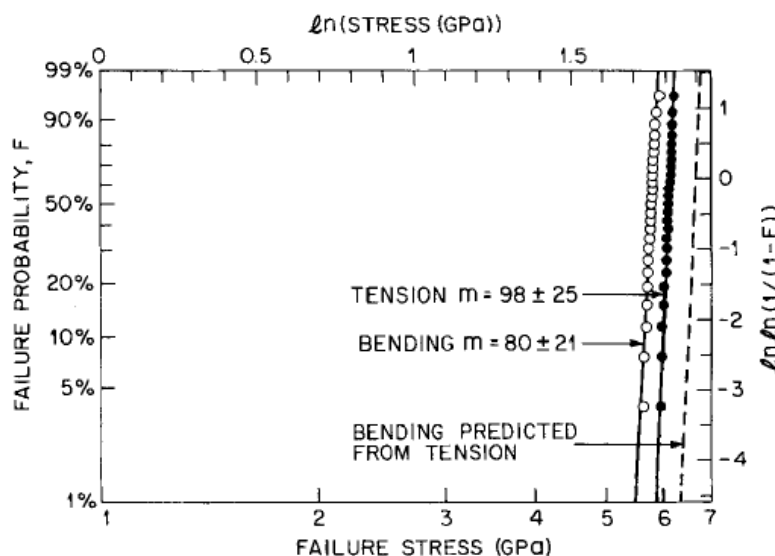


Figure 49. Strength of silica-clad optical fiber in two-point bending and 25 mm gauge lengths in tension from Matthewson et al.<sup>158</sup> The dashed line represents their prediction of tensile strength from the bending data.

The distributions in Figure 49 are fatigued strengths. Testing was performed in ambient room air leading to the fiber's strength degrading from its inert value because of subcritical crack growth that occurs just before failure. The inert intrinsic strength is defined as the strength in the absence of flaws and strength degrading phenomena like fatigue. The primary aim of measuring the inert intrinsic strength is to inform on the structure of the glass.<sup>159</sup>

Early strength studies found that glass in fiber form could be made flawless and this allowed researchers to gain understanding of structure of silica and multicomponent glasses.<sup>36,37</sup> For these studies, testing was performed at liquid nitrogen temperatures or high vacuum with short fiber lengths tested in tension or two-point bend testing to avoid preexisting flaws. For example, Figure 51 shows the tensile and two-point bend strength of sodium borosilicate glass fiber measured in air and liquid nitrogen<sup>160</sup>. The high strength and Weibull modulus indicate that the initial strength is being tested and the liquid nitrogen ensures no crack growth during the test.

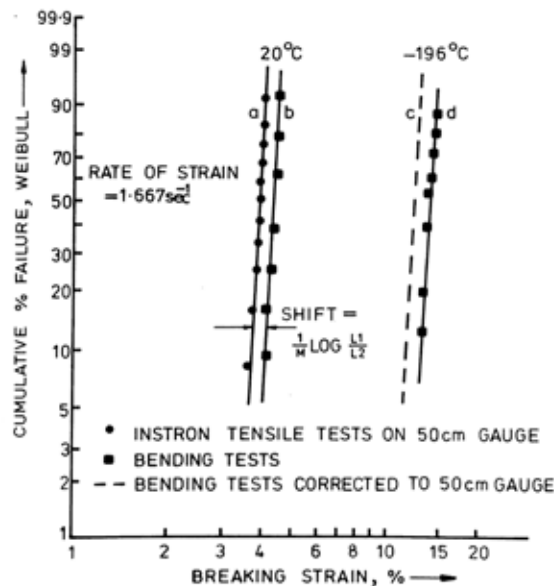


Figure 50. Strength distributions of sodium borosilicate glass fiber in air and liquid nitrogen from France et al.<sup>160</sup>

Two point bending is the most popular method for measuring the inert intrinsic strength of optical fiber. Shown schematically in Figure 51 this test method samples a small volume of glass and, by virtue of placing the glass in bending, emphasizes the surface of the glass. Thus, small changes to the glass surface can be easily detected. From a practical point of view, placing fiber in two-point bending avoids the complication of grip failures. The two-point bend test also facilitates the immersion of the stressed glass region in various environments or high vacuum.<sup>161</sup> One difficulty with two-point bending is that it is a strain-based test. The failure stress is calculated from the measured failure strain and knowledge of Young's modulus. The strain dependence of Young's modulus is known for strain levels to only 6%.<sup>11</sup> With inert intrinsic failure strains on the order of 16 to 18% the inert intrinsic strength is obtained by extrapolating Young's modulus to failure strains of 16 to 18%. As an aside, Young's modulus is known to decrease approximately 4% for liquid nitrogen temperatures<sup>162</sup> and its strain dependence at this temperature is unknown. With this method, Kurkjian and Gupta<sup>38</sup> calculate the inert intrinsic strength of silica in liquid nitrogen to be about 14 GPa ( $\sim 2 \times 10^6$  psi). In addition to testing in liquid nitrogen and vacuum, high speed testing in two point bending has demonstrated strength near that in liquid nitrogen.<sup>163</sup>

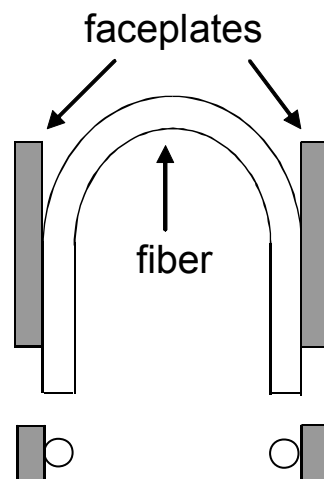


Figure 51. Schematic of two point bend test.

Proctor et al.<sup>36</sup> and Hillig<sup>37</sup> pulled filaments of silica glass in tension at low temperatures and achieved strengths of about 14 GPa ( $\sim 2 \times 10^6$  psi). These inert intrinsic tensile strength measurements of silica are in the range of predicted values.<sup>164</sup> High speed tensile testing in air has yet to achieve the inert intrinsic strength of silica glass fiber.

### 5.3 Strength Distributions for Reliability Predictions

The strength distribution is a key input for models attempting to predict optical fiber lifetime. One would prefer to have a post-proof test strength distribution collected from a length sufficient for predicting failure rates from stress events like coloring, cabling, installation, and the in-service life. Ideally, if thousands of kilometers of fiber are processed and installed, thousands of kilometers should be sampled and tested. With a few exceptions, the flaws of greatest reliability risk fall in the low strength region of the distributions in Figure 48. Note that standardized methods for strength testing only test the intrinsic strength, sampling 15 meters in tension<sup>166</sup> or a few millimeters in 2-point bending.<sup>167</sup> Whereas these tests are useful for scientific purposes, they do not provide sufficient data for making reliability predictions to failure probabilities on the order of  $10^{-4}$  to  $10^{-6}$ .

Like the distributions in Figure 48, some have characterized the strength of kilometers of fiber by testing individual 10 to 40 m lengths to failure. With the quality of today's fiber, testing 10's or 100's of kilometers by this method would be prohibitively time consuming. Maurer<sup>168</sup> demonstrated that the method of multiple proof tests matched that of tensile strength data. Here, one proof tests fiber at ever increasing stress levels and, by counting the breaks at each level, the failure probability for each stress level is determined. Whereas this method more efficiently tests many kilometers of fiber in a relatively short period of time, it is difficult to quantify subtleties in the curvature of the strength distribution. Another method for characterizing the fiber strength distribution is to strength test until some discernible "knee" in the distribution is observed. A Weibull,  $m$ , between 2 and 5 is then assumed for the region below the "knee". Enough fiber must be tested for the "knee" to be representative of what is manufactured. With the latter two methods, one will have to use some judgment in establishing a strength distribution and should choose one that leads to more conservative predictions.

Another method for creating a long length strength distribution is to count the number of breaks during proof testing, to establish the failure probability at that stress level, and then use an estimate of the Weibull modulus to obtain the shape of the distribution near the proof stress.<sup>14,124</sup> This method does not require extra strength testing; however, it assumes that the distribution of flaws failing proof testing is predictive for those that survive, that they come from the same distribution. Unless proven to be true with strength data, this assumption should be viewed with caution as it can easily provide an inaccurate prediction of the surviving flaw population.<sup>169</sup> As discussed earlier, optical fiber, like most glasses, has multiple flaw populations. A fiber with a high concentration of surface particulate weak enough to fail proof testing will generate a pessimistic estimation of the post proof strength distribution. Conversely, it is possible to have a high density of small surface abrasions pass proof testing undetected.

Many years ago a novel suspended test method was created for obtaining long-length strength distributions. A schematic of the testing equipment is shown in Figure 52 and the details surrounding this test have been previously published.<sup>170,171</sup> In this test, sequential 20-meter sections of fiber are stretched to a predetermined stress level. A load cell monitors the load as the stress is being applied. If the fiber survives the stress pulse, another 20 meter length is indexed and the load is again applied to the next section of fiber. When a break occurs, the break stress is recorded, the machine is reloaded and testing resumes until another failure occurs. Testing of multiple reels of fiber is performed until enough breaks are recorded to accurately describe the region between the proof test and the maximum stress. Whereas this method provides the desired distribution of weaker flaws in a relatively short period of time, its deficiency is that one must build test equipment just for this purpose.

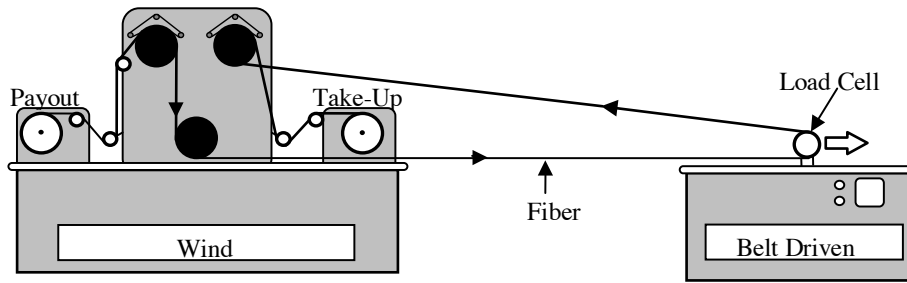


Figure 52. Schematic of the suspended test method for strength testing long lengths of fiber.

Individual 20 meter lengths are loaded to a predetermined stress level.

The failure stress is measured on specimens failing this stress level and those that survive are accounted for.

Figure 53 shows a strength distribution of 3,800 km of optical fiber obtained in the above manner.<sup>172</sup> The maximum stress level for the strength test was set to 2400 MPa (350 kpsi) as flaws with strengths above this level are generally of lesser reliability concern. The flaws that pass the test are accounted for statistically. For this reason, only failure probabilities below 0.01 are shown.

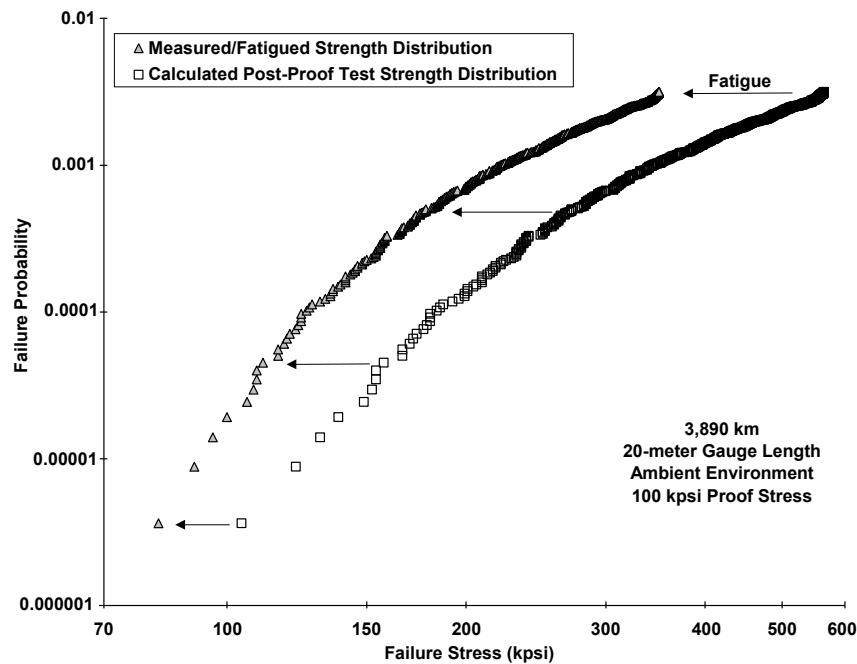


Figure 53. Strength distribution of almost 4000 kilometers of fiber using the suspended strength test method.<sup>172</sup> All failures below ~2400 MPa (350 kpsi) are shown. A fiber length passing this stress level is recorded and accounted for when determining the failure probability of the failures. The diamonds represent the measured fatigue strength and the squares are the predicted strength before strength testing, i.e., the post proof-test strength distribution.

The data in Figure 53 shows 609 failures in 3,850 kilometers, one break every 6.3 kilometers, below the maximum test stress of 2400 MPa (350 kpsi). The probability of encountering a flaw with strength near that of the proof stress is one in 30,000 attempts. This demonstrates the rarity of such flaws in modern fiber.

A feature of any proof-tested fiber is the truncation of the strength distribution near the proof stress level. This truncation occurs statistically as flaws which have been eliminated by the proof test. Note that this fiber was proof tested at 700 MPa (100 kpsi) in accordance with FOTP-31C.<sup>16</sup> However, the measured strength distribution in Figure 53 appears to truncate below this proof stress level. As with most strength measurements, testing for Figure 53 was performed in a fatigue environment. In this case the test environment was ambient air with a strain rate of 200%/minute. The consequence of strength testing under these conditions is that flaws grow subcritically during the test itself causing the stress at failure to be lower than the pretest strength. By accounting for fatigue during strength testing one obtains the initial strength and, in this case, the desired post proof test strength distribution for reliability predictions. Based on the high speed strength

test data presented in the fatigue section it is possible to estimate the pre-test or inert strength distribution. The predicted pre-test inert strength distribution is shown in Figure 53 and is an estimate of the actual post-proof strength distribution.

Once the post proof strength distribution is obtained, it is useful to scale the distribution to lengths used in actual fiber deployments.<sup>21,158,173</sup> Figure 54 shows the predicted post proof strength distribution from Figure 53 scaled to lengths representative of short and long length applications for the case of pure tension. A 100 meter riser cable places the entire fiber length in tension due to the weight of the cable. The probability of encountering a flaw with strength less than 1400 MPa (~200 kpsi) is quite low, about 0.0005. The probability of encountering a flaw weaker than 2000 MPa (~300 kpsi) is only 0.001.

If cabling or installation requires the fiber be placed in a bent configuration, the failure probability is reduced by a factor of 5 to 10 below the tensile predictions.<sup>130,173,173</sup> As was discussed earlier, bending places fewer flaws in tension. The predicted strength distribution for the case of pure bending is shown in Figure 55 for a range of lengths. Short lengths of about one meter are representative of, say, a coiled length of pigtail or patch cord fiber. From the data in Figure 55, the probability of encountering a flaw with strength below 4000 MPa is extremely low. Thus, for installed lengths on the order of 1 kilometer or less, it is not always necessary to design around the proof stress. Depending on the quality of the strength distribution, the proof stress can have little effect on the overall reliability of the fiber for applications using short lengths. As fiber comes closer to the home and business there are more instances where short lengths are being deployed or short sections of longer cables are pulled or bent.

The longer lengths are representative of fiber in a loose tube or buffer tubes stranded about a central member. For lengths greater than 1 kilometer, it is best to design around the lowest strength, the proof stress.

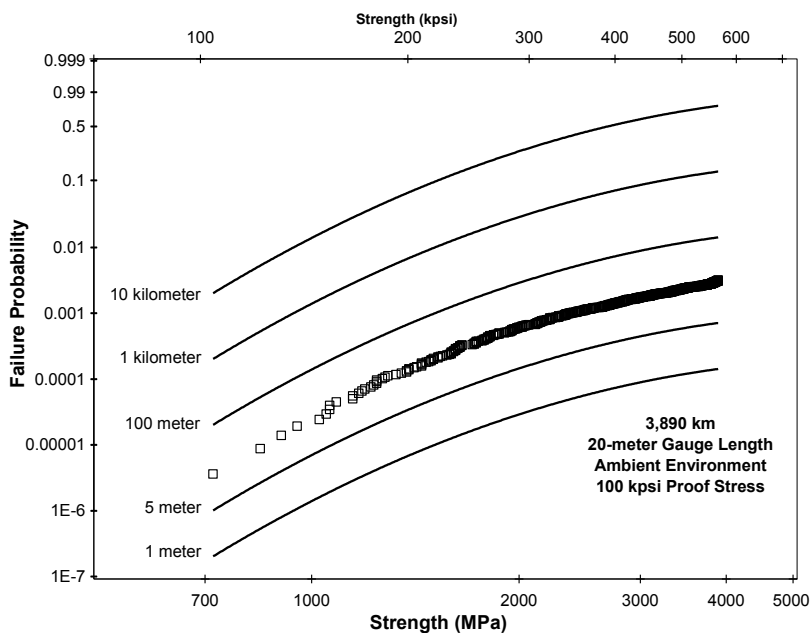


Figure 54. Predicted strength distributions for a range of fiber lengths in tension.

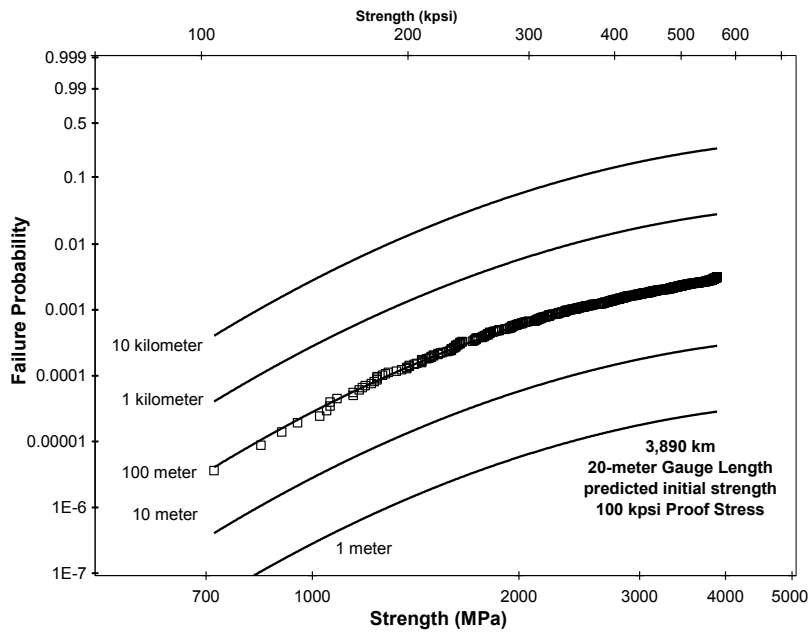


Figure 55. Predicted strength distribution for lengths of fiber in bending.

#### 5.4 Strength Testing to Characterize Damage Inducing Events

Optical fiber is unique in that minute contact or contamination on the glass surface can be detected by strength testing. A one micron flaw reduces the strength from near pristine levels to about 700 MPa (100 kpsi). It may be difficult to visibly see the damage, but strength testing can reveal it. A few examples of studies where strength testing was used to assess the impact of a particular process or handling event on fiber strength are shown in Table 6.

For mechanically induced flaws, tensile testing short fiber lengths on a universal testing machine is the easiest and most common method for assessing the effects of the contact event. Strength testing at various stages of a handling process is useful for uncovering the process step or handling procedure responsible for inducing damage. This technique is especially useful when developing processes for splicing, connectorization, making couplers and splitters, fiber Bragg gratings, and general fiber packaging for photonic applications. Splicing is a good example for this test strategy because it consists of handling coated fiber, stripping, cleaning, cleaving, splicing and protection of the spliced region. By strength testing after each step, one might find that clamping directly on the glass when holding the fiber for cleaving is the weak link in the process, for example.

Table 6. Strength testing as a tool for investigating handling or process-induced fiber damage.

<b>Strength Study</b>	<b>Description</b>	<b>Reference</b>
Mechanical stripping	Effect of tools, personnel, wiping and leaning on stripped fiber strength	Wei et al. <sup>174</sup>
Mechanical stripping	Weak link model evaluated for stripped lengths tested in tension and bending	Kurkjian <sup>175</sup>
Terminations	Location and characterization of damage from flaws induced during termination	Wagner <sup>176</sup>
Chemical Stripping	Stripping with acid and Methylene Chloride has no effect on fiber strength	Rondinella and Matthewson <sup>177</sup>
Chemical Stripping	Retaining intrinsic strength through acid stripping	Matthewson et al. <sup>178</sup>
Cleaving	Optimizing cleaving tools and procedure	Field <sup>51</sup>
Splicing	Controlling impingement of silica particles during arc fusion splicing increases splice strength	Krause et al. <sup>179</sup>
Splicing	Splices with intrinsic strength made with flame fusion process	Krause and Kurkjian <sup>180</sup>
Splicing	Optimizing arc fusion conditions for single fiber and ribbons	Pitassi <sup>181</sup>
Splicing	Principle factors affecting arc fusion splice strength reviewed	Krause et al. <sup>182</sup>
Splicing carbon coated fiber	Arc fusion splice settings optimized for splice strength	Yoshizawa et al. <sup>183</sup>
Hermetic splices	Hermetic behavior of proof stress level flaws coated with carbon	Estep et al. <sup>184</sup>
Hermetic splices	A process for reconstituting carbon coating provides high strength and hermeticity	Inniss et al. <sup>185</sup>
Hermetic joints	Evaluation of the fatigue behavior of metallized fiber pigtailed	Orcel <sup>186</sup>
Devices	Frit bonding optical fiber to a substrate	Srinivasan and Webb <sup>187</sup>
Fiber Bragg grating	The effect of irradiation dose on fiber strength	Limberger et al. <sup>188</sup>
Bragg grating	The effect of laser type on fiber strength	Barber et al. <sup>189</sup>
Laser induced defects	Laser-induced cavities form as a result of damage wave propagation	Sidorin et al. <sup>190</sup>
Connector	Reliability assessment of a novel connector design	Baker et al. <sup>30</sup>

## 6 Optical Fiber Reliability

The classic reliability “bathtub” diagram in Figure 56 shows the stages of product lifetime. First, there is the early failure period, better known as “infant mortality”. For fiber, this period represents premature mechanical failures from handling and process induced damage. For example, contamination in a coloring die punctures through the fiber’s polymer coating and contacts the glass, creating a flaw below the proof stress level. During subsequent buffering or stranding, the fiber fails from this flaw. This example illustrates early failure due to flaw introduction, but failures can also occur from overstressing the fiber during processing or installation. The second stage represents failures due to incidental events such as failures from severe ice loading or dig-ups. Finally, there is the wear-out period. For optical fiber, the mechanical wear-out failure mode of greatest concern is fatigue. In this section, guidance is given, from an engineering point of view, for avoiding failures early in the fiber’s life as well as minimizing the probability of fatigue failure during the intended lifetime.

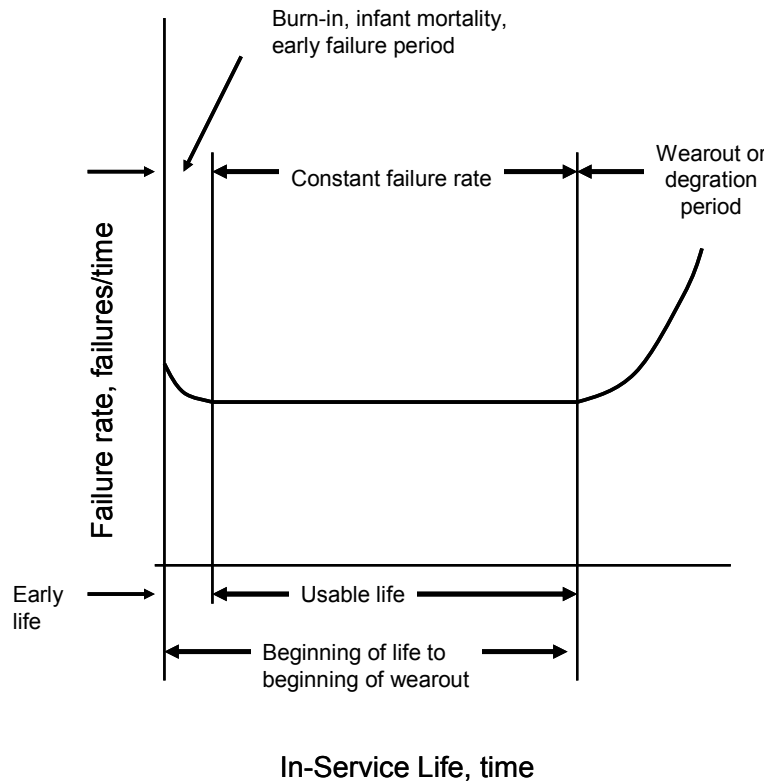


Figure 56. Reliability “bathtub” diagram showing stages to product life.<sup>191</sup>

### 6.1 Avoiding Early Failures From Glass Damage Through the Coating

One of the most persistent failure modes for optical fiber is glass damage through the protective polymer coating during fiber processing and handling. Fiber, with typical coating dimensions of 242  $\mu\text{m}$  outer primary over a 190  $\mu\text{m}$  inner primary, can be handled without damaging the coating; however, it is necessary to regularly clean and maintain pulleys and rollers that contact the fiber. With the advent of fiber-based photonic devices, fibers are handled significantly more than in cabling. Coating damage resulting in fiber breaks can be a significant cost of manufacturing.

The ability of protective optical fiber coatings to resist damage to the underlying glass has historically received little attention. Exploration into thinner coatings in the 1990’s prompted research into test methods aimed at quantifying the protective capability of the coating. One test strategy has been to damage the coating surface with an increasingly abrasive surface until the glass is damaged. In 1993 Oishi et al.<sup>192</sup> published a test method whereby fiber in tension is passed over a roller covered with sandpaper. A schematic of this test method is shown in Figure 57. Coating thickness is plotted versus the grit size of the sandpaper in Figure 58. They concluded that particle sizes greater than twice the secondary coating thickness cause the fiber to break in this test.

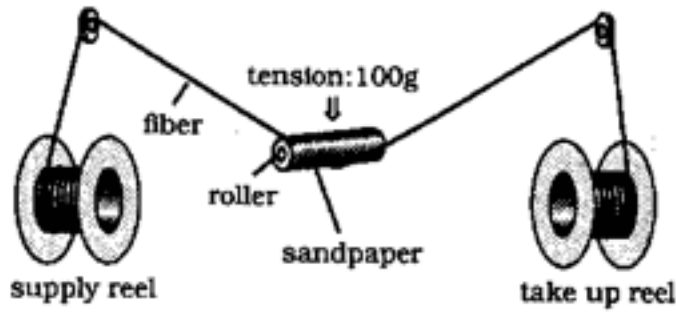


Figure 57. Oishi et al. fiber coating abrasion test<sup>192</sup>

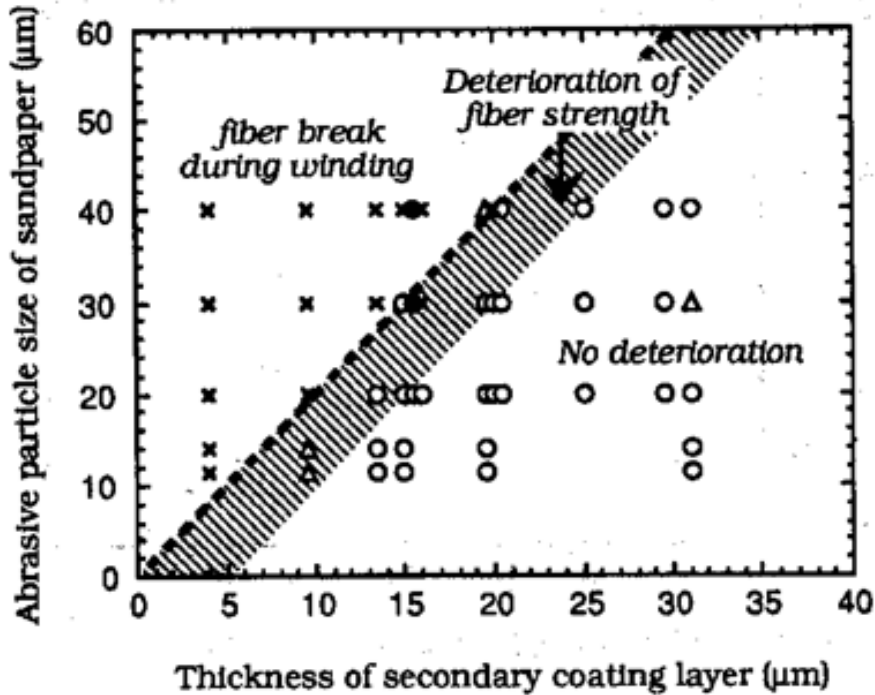


Figure 58. Dependence of secondary coating thickness on abrasive particle size.<sup>192</sup>

In 1994, a “pulse” test was used to evaluate the damage resistance of fibers with a range of coating dimensions.<sup>193</sup> The strategy here was to use a constant surface roughness and to increase the lateral load of the fiber against that surface until the coating ruptured. Fiber was tensioned around a rough aluminum pulley and pulsed to ever increasing loads until the secondary coating fractured. The results summarized in Figure 59 show good agreement between the threshold load for damage and the cross-sectional area of the coating. Delamination always preceded coating fracture in this test. This test, though crude, was useful at the time in establishing a correlation between coating dimensions and a threshold for coating damage. It should be noted that delamination itself does not damage the glass, but it is an indication that mechanical contact has been made with the coating surface.

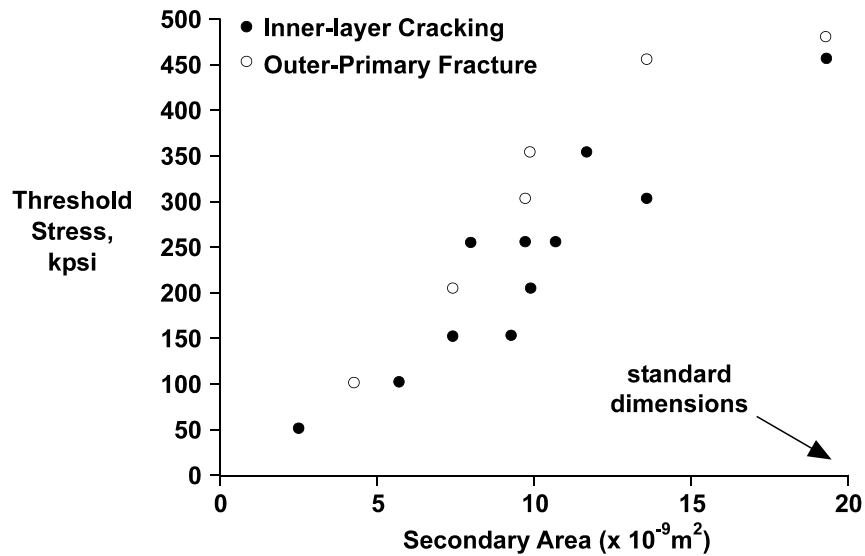


Figure 59. Thresholds for delamination (inner-layer cracking) and secondary fracture using the pulse test.<sup>193</sup>

In 1998 Wissuchek et. al.<sup>194</sup> were able to isolate the fracture energy of secondary coatings using an indentation test directly on coated optical fiber. This was the first study to quantify the protectability of fiber coatings in fracture energy or fracture toughness terms. A key feature of this test method was the use of two different microhardness indenters. A Vickers diamond pyramid indenter and a diamond wedge indenter, with an included angle of 75°, were driven into the coated fiber resulting in a load drop when the secondary coating ruptured. The schematic of an indented fiber in Figure 60 shows three mechanisms for strain energy absorption: (1) plastic deformation of the secondary coating, (2) fracture of the secondary coating, and (3) fracture of the glass/primary interface.

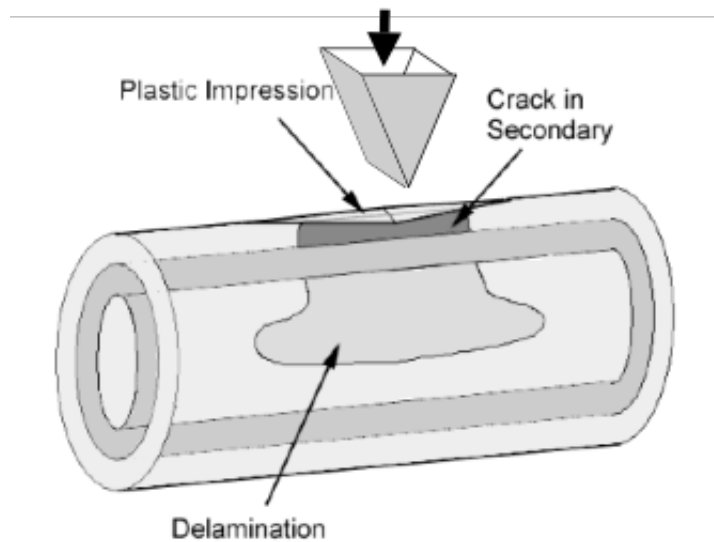


Figure 60. Schematic of coating indentation event.<sup>194</sup>

It was determined that most of the fracture energy went into fracture of the secondary. The fracture energy of delamination was found to be about 15 to 20% of the fracture energy of the secondary. Plasticity of the secondary coating comprised about 1% of the total strain energy. More recently a simplified version of this test method was used to quantify the puncture resistance of fiber coatings.<sup>195</sup> It was found that the threshold load for puncture through the coating correlates well with the cross-sectional area of the outer-primary fiber coating as shown in Figure 61. This study included both single and dual coated fibers and the fact that both coating configurations show the same dependence illustrates the small contribution to mechanical protection provided by the inner-primary coating.

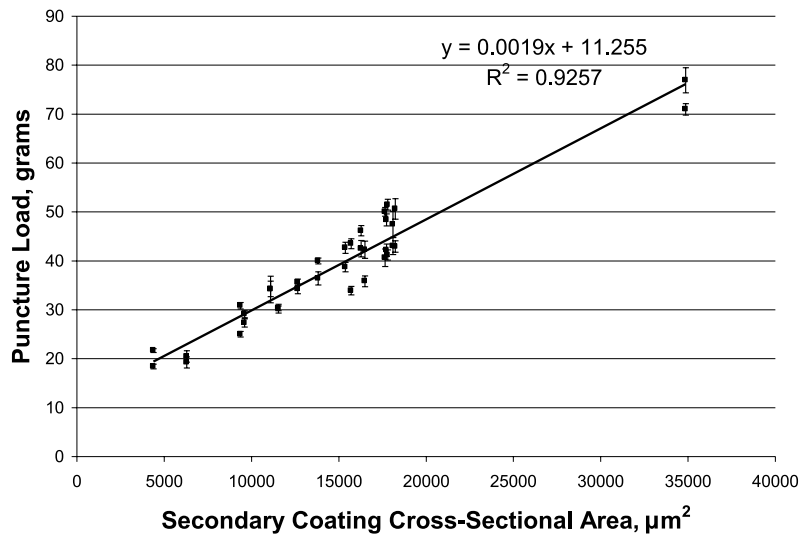


Figure 61. The dependence of puncture load on cross-sectional area of the secondary coating.<sup>195</sup>

Guidance for avoiding coating damage or excessive tension during fiber processing include the following:

- Minimize the number of pulleys and guide rollers in the fiber path. Minimize contact with stationary fiber guides.
- Avoid use of soft metal pulleys as they can be damaged or polymer pulleys as they wear.
- Regularly clean all pulleys and dies in the fiber path.
- Replace pulleys and guide rollers before they fail.
- Belts in contact with fiber should be set to the lowest tension without fiber slippage and should be changed regularly.
- Avoid cutting fiber before a die, pulley or belt as glass debris will collect and damage subsequent fiber.
- Protect fiber surfaces from abrasive particulate tracked into processing area by operators, ceiling and piping insulation, broken pieces of fiber, etc. Recommend performing a process audit for such contamination.
- Fiber reels should be stored in a vertical orientation; stacking reels horizontally can cause the fiber pack to cascade.
- Keep covers on fiber reels until immediately before loading onto the processing line to protect the outer winds from dirt, debris, and damage.
- Avoid sudden “jerks” or high tension events during processing as fiber can bury into the fiber pack and break.
- Keep fiber twist to no more than three 360° turns per meter as fiber can knot and break in bending.
- Reduce contamination on fiber surface by static charge eliminators, this technology is readily available.
- Ground equipment in contact with fiber. It is rare, but fiber can be damaged by electrostatic discharge under dry processing environments.

Guidelines for handling fiber include:

- Regularly clean work surfaces.
- Avoid breaking fiber over work surface.
- Minimize contact between tools used to strip, clean, and splice and fiber, especially when they share the same work surface.
- Wear clean gloves when manually handling fiber as normal contamination on fingers is enough to damage coating.
- When clamping during cleaving or similar processes constraining the fiber it is preferred that contact be made with the coated fiber rather than bare glass. Of course, this pertains to useful fiber and not ends being removed.
- Fiber pigtailed are often stored in a coiled configuration. Manually coiling fiber requires a significant amount of contact with the coating surface and is a primary source of fiber damage. If automated coiling cannot be used, clean gloves should be worn and operators should be trained on fiber handling.
- Tape is often used to contain fiber in some configuration for future handling. The act of placing tape on the fiber should be carefully examined. It is best if the tape does not stick to the coating surface. Upon removal it will leave adhesive residue or, worse, take the coating with it. Avoid pressing the tape against the fiber.

## 6.2 Practical Guidance on Fiber Lifetime Estimations

### Minimum Strength Design

Establishing a fiber lifetime that exceeds the expected in-service life begins with the static fatigue equation,

$$t_f = BS_i^{n-2} \sigma_a^{-n} \quad (19)$$

The allowable stress,  $\sigma_a$ , for, say, a 25-year lifetime of a flaw with a pre-fatigue strength,  $S_i$ , can be calculated provided the crack growth parameters are known. The most conservative approach to reliability modeling, known as the “minimum strength design”, is to assume that a proof test level flaw will experience the maximum applied stress.<sup>123</sup> The strength,  $S_i$ , is set to the proof stress,  $\sigma_p$ , and the allowable stress is expressed as a fraction of the proof stress,

$$\frac{\sigma_a}{\sigma_p} = \left( \frac{B}{t_f \sigma_p^2} \right)^{1/n} \quad (20)$$

Using the region I crack growth parameters in Table 4, the applied stress is about 25% of the proof stress for a 25-year lifetime. Because of the known difficulties in determining the crack growth parameters, Glaesemann and Gulati<sup>196</sup> developed a model based on the simple assumption that a low crack velocity is equivalent to a threshold for crack growth. Their ratio of applied stress to proof stress is shown in Figure 62 for a range of n values.

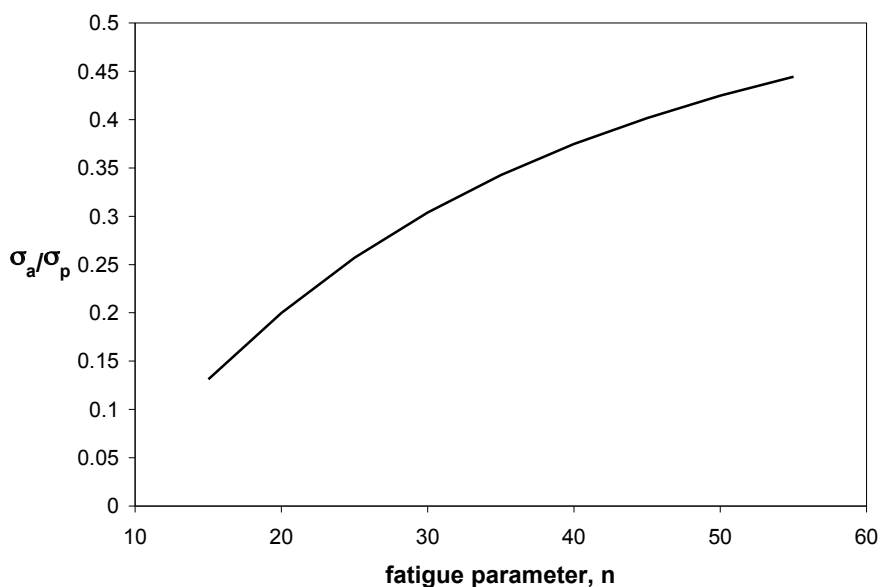


Figure 62. Allowable safe stress to proof stress ratio for proof stress level flaws in optical fiber.<sup>196</sup>

For silica-clad optical fiber with an n value of approximately 20, the applied stress is 1/5<sup>th</sup> the proof stress for 20 to 40 year life. The two-region power law model described above gives a similar design guideline for long-term life and is extended to include short term process events and installation in Figure 63 below. One can load the fiber to about half the proof stress during processing (the 1 second line in Figure 63) and 1/3<sup>rd</sup> the proof stress during installation or submarine recovery events (the 4 hour line). These guidelines are shown in terms of bend radius in Figure 64. The minimum bend radius for, say, stranding of loose tubes of 700 MPa (100 kpsi) proof tested fiber about a central member is 32 mm.

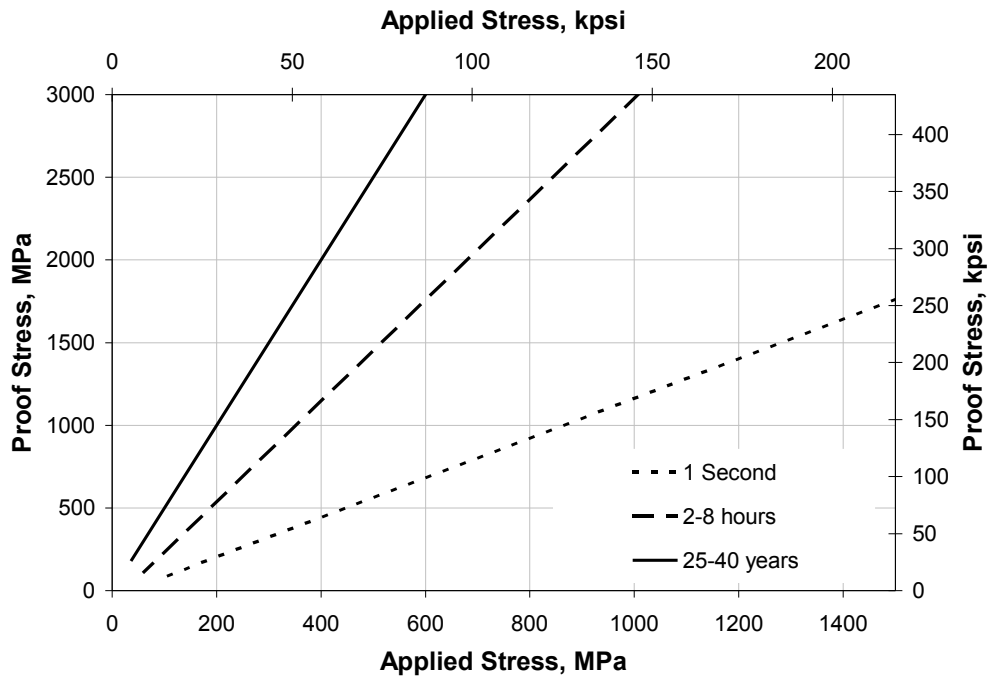


Figure 63. Allowable stress as a function of proof stress for several common stress events.

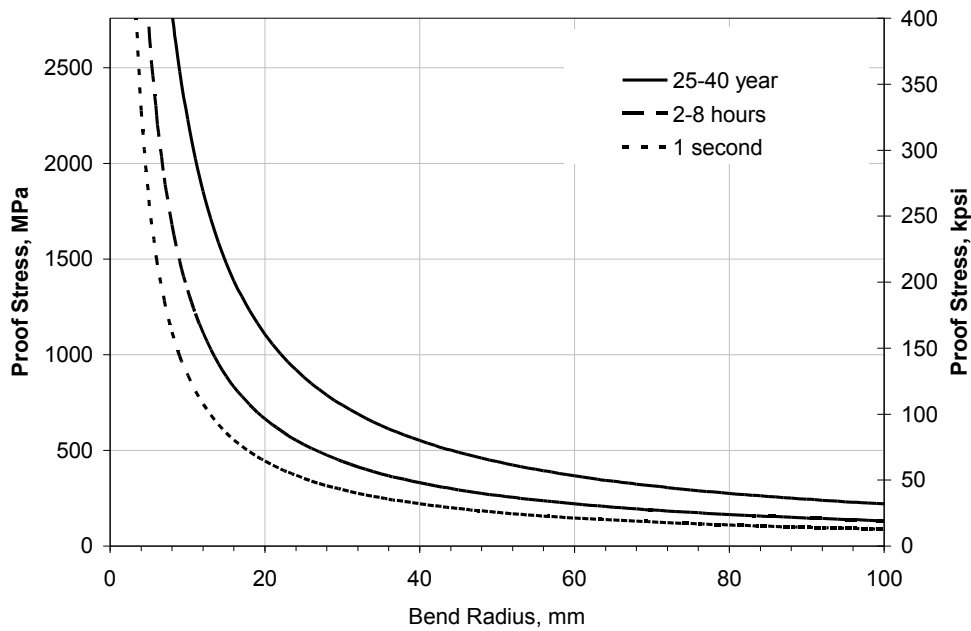


Figure 64. Allowable bend radius for common stress events.

In photonic applications, significant lengths of fiber can be permanently coiled. Examples include Er-doped fiber for amplifiers and fiber for dispersion compensating modules. Here fiber is wound under tension into a coiled configuration. In the case where the wind tension is relieved, the allowable bend radius can be determined from Figure 64 above. If the wind tension is permanent, then it is simply added to the bend-induced stress as shown in Figure 65.

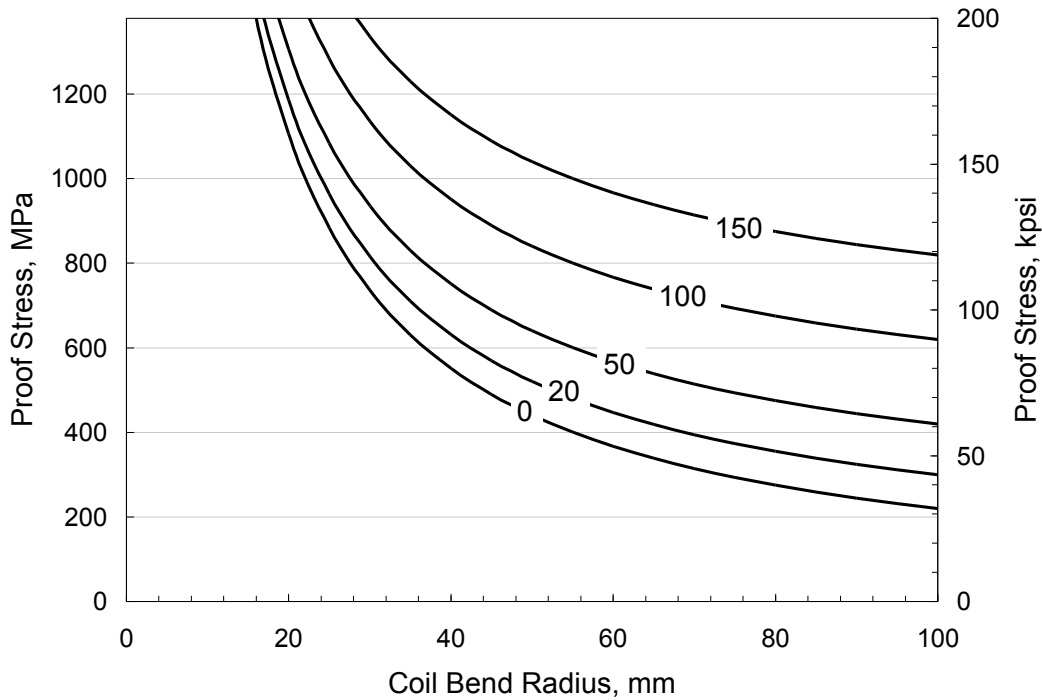


Figure 65. Allowable bend radius for permanently coiled fiber for a range of wind tensions (grams).

Now, consider the choice of pulley dimensions for fiber processing under tension. The maximum stress is a combination of processing tension and bending about pulleys and is to be no more than 50% of the proof stress level. Figure 66 shows the allowable pulley size for a range of wind tensions and proof stress levels for this short-term stress event.

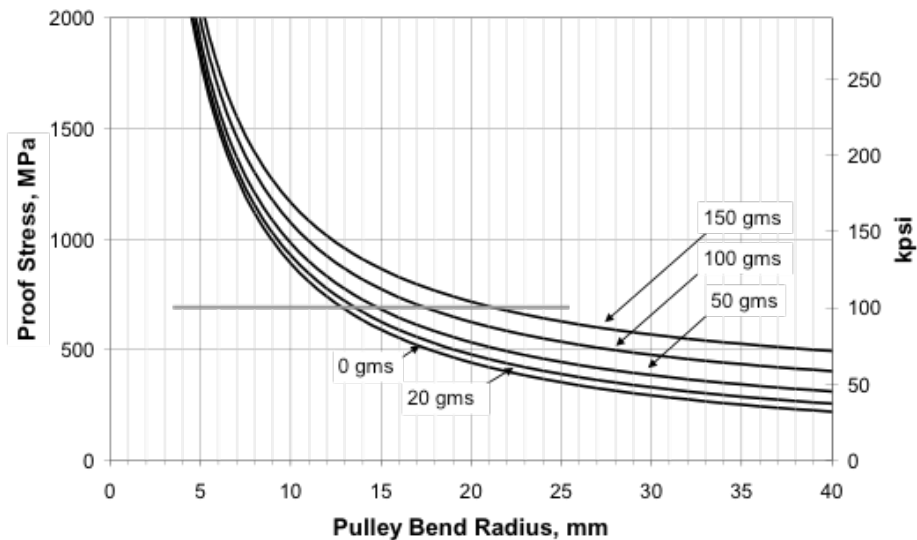


Figure 66. Allowable pulley dimensions for a range of proof stress and wind tension levels.

These applied stress guidelines apply to fiber terminations and packaging for photonic devices as well. Any application where the protective polymer coating is removed will result in damage and weakening of the glass. The choices are to deploy such fiber in an unstressed state or to reproof and deploy using the guidelines presented here. A common approach for determining connector and splice reliability is to measure the strength of a few specimens in a laboratory environment and deploy if the perceived risk is sufficiently low. The difficulty with this approach is that the actual strength distribution of manufactured pieces can vary widely depending on operator, tools, cleaning methods, etc. Obtaining a statistically significant sample size can be expensive and time consuming. Proof testing after reconstitution of glass protection is the best method for assuring reliability of fiber deployed in a stressed state.

## Failure Probability Design

If the deployed length is less than a kilometer, one can consider using a failure probability design methodology. For shorter deployed lengths, the risk of encountering a flaw that will grow and fail may be at an acceptably low level. Failure probability is incorporated into Eq. (19) through the inert strength,  $S_i$ ,

$$t_f = B \left( F \{ S_i \} \right)^{n-2} \sigma_a^{-n} \quad (21)$$

When such modeling was being developed in the 1970's and early 1980's it was recognized that one should account for fatigue during processing events as well as in-service life. The most important process stress event is proof testing and in recent years the Telecommunications Industry Association has captured these developments into reliability guideline based on the power law crack velocity model.<sup>130</sup> The basic reliability model for proof tested fiber is given as,

$$t_f = \left\{ \left[ B^{\frac{m}{n-2}} S_o^m \frac{L_o}{L} \ln \frac{1}{(1-F)} + (\sigma_p^n t_p)^{\frac{m}{n-2}} (1+C)^{\frac{m}{n-2}} \right]^{\frac{n-2}{m}} - \sigma_p^n t_p \right\} \sigma_a^{-n} - \frac{B}{\sigma_a^2} \quad (22)$$

where  $C = \frac{\frac{B}{\sigma_p^2} - \frac{t_u}{n+1}}{t_p}$  when,  $t_u \leq (n-2) \frac{B}{\sigma_p^2}$  fast unloading rates typical of most fiber processes,

$t_p = t_d + \frac{t_l + t_u}{n+1}$  where  $t_d$  is the proof test dwell time,  $t_u$  and  $t_l$  and are the loading and unloading times for proof testing, respectively,  $L_o/L$  and is the test gauge length divided by the in-service length being modeled.

In addition to use of the power law crack velocity model, two assumptions in Eq. (22) are worth noting. The first is that the fiber strength can be described by a unimodal Weibull distribution. Some practical obstacles accompany this assumption. As discussed previously, it requires considerable effort to measure the strength distribution near the proof stress level. The best method is that used to obtain the nearly 4000 kilometer strength distribution previously shown in Figure 53, but special equipment must be built for this test. Second, use of the above lifetime model also implies that crack growth during high speed events is the same as during slow speed events. Fatigue data obtained from experiments mimicking proof test speeds clearly shows a departure from region I type behavior.

Mitsunaga et al. simplified complex Eq. (22) into the following model based on fiber break rate,<sup>124</sup>

$$F = 1 - \exp \left( -N_p L \frac{m}{n-2} \frac{\sigma_a^n t_a}{\sigma_p^n t_p} \right) \quad (23)$$

where  $N_p$  is the proof test break rate and  $L$  is the installed length of interest.

Note that production failure rate data is considered proprietary information by most fiber manufacturers. The Weibull modulus,  $m$ , is that of the pre-proof test strength distribution. Figure 67 shows the predicted failure probability for a range of installed lengths. A typically low Weibull modulus was chosen and an  $n$  value of 20. The break rate was taken to be 0.01/kilometer.

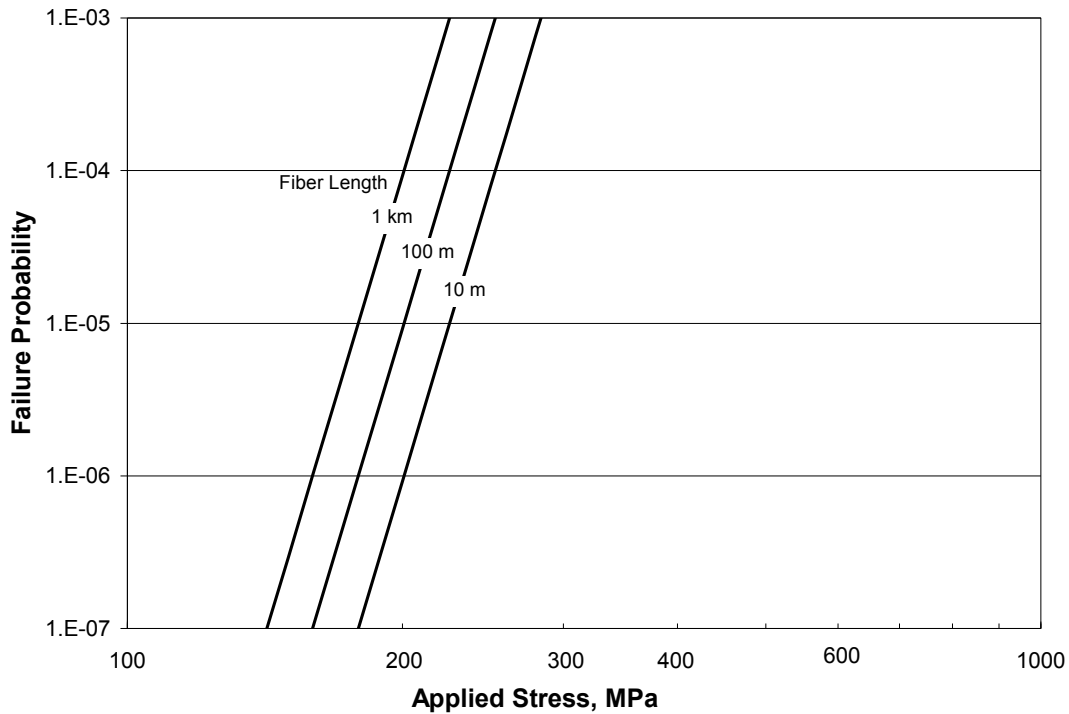


Figure 67. Predicted failure probability for range of fiber lengths based on Mitsunaga et al.<sup>124</sup>

Inputs include a proof stress of 700 MPa (100 kpsi), fatigue parameter  $n=20$ , assumed break rate of  $N_p=0.01/\text{kilometer}$ , Weibull modulus of  $m=2$  and the measured proof test parameters in Figure 10.

The popularity of this model is based on its ease of use, but it has a deficiency worth noting. The method uses failure rate data from proof testing to describe the strength distribution of the surviving flaws. In other words, the flaws that fail proof testing are assumed to describe those that survive. Given the enormity of defect sources in the low strength region this assumption has been questioned.<sup>169</sup> The predictive capability of this approach to modeling fiber life is enhanced by confirming the strength distribution through direct strength testing.

There are many fiber lifetime models in the literature. It is common for engineers to choose a lifetime equation and attempt to input crack growth and strength parameters from their own laboratory data or published values. How can one assess the predictive capability of a fiber lifetime model? If the fiber cladding is silica and the application is close to room temperature in a moist environment, then consider the following suggestions. Set the failure probability in the model to a low value of, say,  $1 \times 10^{-6}$  and compare the determined allowable stress against the applied stress to proof stress ratios for the “minimum strength design” in Figure 63. In other words, the failure probability model should approach the minimum strength design at low failure probabilities.

The existence of the ultra-long length initial strength distribution in Figure 53 enables one to create a simple failure probability design diagram. Assume the previous guidelines for applied stress that one can stress a flaw to  $1/5^{\text{th}}$  of its inert strength,  $S_i$ , for 25 year life,  $1/3 S_i$  for 4 hours, and  $1/2 S_i$  for one second. The value for  $S_i$  can be any inert strength and for the previous discussion of proof test level flaws,  $S_i$  was simply set to the proof stress. Thus, for example, a flaw with an initial strength of 1400 MPa (200 kpsi) can be loaded to 40 kpsi long term, 70 kpsi during installation and 100 kpsi for short handling event. A design diagram for allowable stress can be made directly from the predicted inert strength distribution in Figure 53 by applying the above fatigue ratios. This is shown in Figure 68 for various lengths of fiber subjected to pure tension and Figure 69 for fibers in constant radius bending. It is important to note that the recommendations regarding tight bends in this analysis are for mechanical reliability reasons only as optical performance may be affected by bending to small radii.

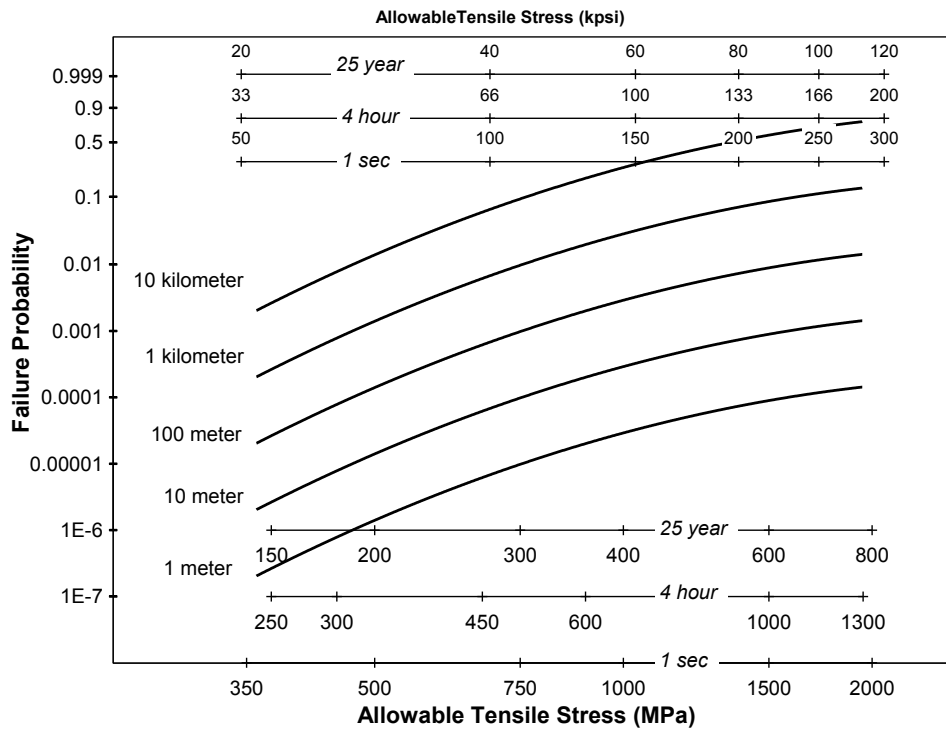


Figure 68. Design diagram for various fiber lengths subjected to tensile loading. 125 um silica-clad fiber proof tested to 100 kpsi.

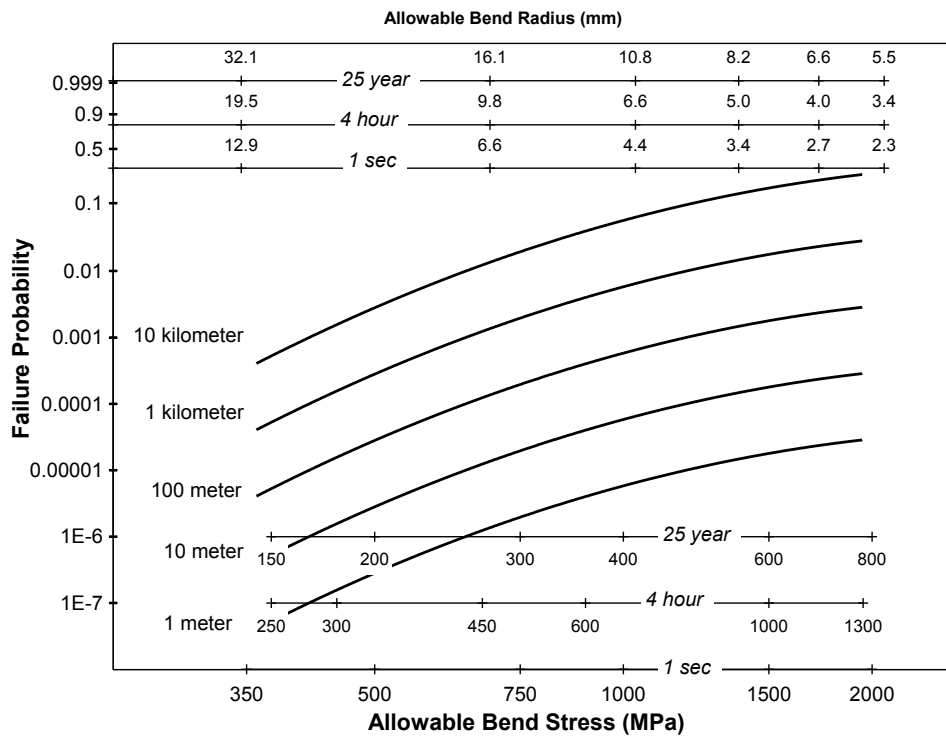


Figure 69. Design diagram for various fiber lengths subjected to bending. 125 um silica-clad fiber proof tested to 100 kpsi.

Depending on installation and environmental conditions, aerial, drop, and riser cable applications can place significant lengths of fiber under tensile loadings. Figure 68 shows that for lengths less than about one kilometer the failure probability is low enough that one can exceed the guidelines of the above minimum strength design. Most optical fiber is cabled, but in recent years significant amounts of fiber are coiled for storage, routed through a package, and bent to connect devices components together. Each of these situations can place tight bends on the fiber. Furthermore, the trend in the industry is to make storage space, components, connections, etc. ever smaller. Tight bends can place high levels of stress on the fiber, posing a possible reliability risk. However, for fibers in these relatively short-length applications, where the lengths tend to be in meters instead of kilometers, one can exceed the proof stress guidelines with acceptable reliability risk. This is because the probability of encountering flaws near the proof stress level is low for these short-length applications.

## 7 Closing Comments

Since large-scale fiber deployments commenced in the early-1980s, optical fiber has proven its reliability despite the fact that there are many unanswered questions about flaws, strength, fatigue, and aging. Early strength studies showed that fiber could be stressed provided a minimum strength could be established through proof testing and the loose tube cable design was key to deployment under minimal stress. Today, the number of cable designs and applications for optical fiber are too numerous to count. History has shown that perhaps optical fiber was more robust than initially thought. Nevertheless, as this technology pushes forward we need to continue to anticipate failure modes from fatigue, handling, etc. In this review the basics of these failure modes are presented from an engineering point of view.

## References

1. P.K. Bachmann, W. Hermann, H. Wehr, and D.U. Wiechert, "Stress in Optical Waveguides. 2: Fibers," *Appl. Opt.*, **26** [7] 1175-1182 (1987).
2. U.C. Paek and C.R. Kurkjian, "Calculation of Cooling Rate and Induced Stresses in Drawing of Optical Fibers," *J. Am. Ceram. Soc.*, **58** [7-8] 330-335 (1975).
3. G.W. Scherer and A.R. Cooper, "Thermal Stresses in Clad-Glass Fibers", *J. Am. Ceram. Soc.*, **63** [5-6] 346-347 (1980).
4. D.J. Wissuchek, C.W. Ponader, and J.J. Price, "Analysis of Residual Stress in Optical Fiber," *Proc. SPIE*, **3848** 34-43 (1999).
5. M.J. Li, X. Chen, and D.A. Nolan, "Effects of Residual Stress on Polarization Mode Dispersion of Fibers made with Different Types of Spinning," *Opt. Lett.*, **29** [5] 448 (2004).
6. D.J. Wissuchek, D.J. Walter, D.A. Clark, and G.S. Glaesemann, "Fracture and Abrasion Resistance Tests for Optical Fiber Coatings," *Mater. Res. Soc.*, **531**, 309-314 (1998).
7. B. Marshall and B.R. Lawn, "Residual Stress Effects in Sharp Contact Cracking: Part I. Indentation Fracture Mechanics," *J. Mater. Sci.*, **14**, 2001 (1979).
8. R.F. Cook and G.M. Pharr, "Direct Observation and Analysis of Indentation Cracking in Glasses and Ceramics," *J. Am. Ceram. Soc.*, **73** [4] 787-817 (1990).
9. D.H. Roach and A.R. Cooper, "Effect of Contact Residual Stress Relaxation on Fracture Strength of Indented Soda-Lime Glass," *J. Am. Ceram. Soc.*, **68** [11] 632-36 (1985).
10. F.P. Mallinder and B.A. Proctor, "Elastic Constants of Fused Silica as a Function of Large Tensile Strain," *Phys. Chem. Glasses*, **5** [4] 91-103 (1964).
11. J.T. Krause, L.R. Testardi and R.N. Thurston, "Deviations from Linearity in the Dependence of Elongation upon Force for Fibers of Simple Glass Formers and of Glass Optical Lightguides," *Phys. Chem. Glasses*, **20** [6] 135-139 (1979).
12. J.M. Matthewson, "Optical Fiber Mechanical Testing Techniques," *Proc. SPIE Critical Review Series CR50*, 32-59 (1993).
13. G.S. Glaesemann, "Optical Fiber Failure Probability Predictions from Long-Length Strength Distributions," *Proc. Int. Wire Cable Symp.*, **40**, 819-825 (1991).
14. E.R. Fuller, Jr., S.M. Wiederhorn, J.E. Ritter, Jr., P.B. Oates, "Proof Testing of Ceramics, Part 2: Theory," *J. Mater. Sci.*, **15**, 2282-2295 (1980).
15. TIA/EIA-455-31C, Proof Testing Optical Fibers by Tension, Telecommunications Industry Association (1999).
16. IEC 60793-1-30, Measurement Methods and Test Procedures – Fiber Proof Test, International Electrotechnical Commission (2001).
17. C.S. Ma, "Strain of an Optical Fiber in Undersea Cable Manufacture During Its Insulation Jacket Extrusion Process," *Proc. SPIE*, **4639**, 93-100 (2002).
18. Z. Gao, W. Pfandl, R. Engel, and A. Stingl, "A Study of the Fiber Strains in Central Tube Ribbon Cables," *Proc. Int. Wire Cable Symp.*, **48**, 61-65, (1999).

19. F. Sears et al., "Measurement of Discrete Strain Change in a High-Fiber Count Slotted-Core Ribbon Cable Using Bragg Gratings," *Proc. Int. Wire Cable Symp.*, **49**, 636-645, (2000).
20. B.J.G. Aragao, E.C. Longui, R.L. Leite, and P.J.P. Curado, "A Mathematical Model for Creep Estimation of OPGW Cables," *Proc. Int. Wire Cable Symp.*, **52**, 592-596 (2003).
21. K.G. Hodge, C.S. Pegge, G.S. Glaesemann, and M. Hopiavuori, "Predicting the Lifetime of Optical Fibre Cables using Applied Stress Histories and Reliability Models," *Proc. Int. Wire Cable Symp.*, **41**, 713-724 (1992).
22. W.E. Beasley, "Measurement of fiber strain in optical cables," *Proc. SPIE*, **2074**, 129-134 (1993).
23. M.R. Brininstool, "Measuring Longitudinal Strain in Optical Fibers," *Opt. Engr.*, **26** [11] 1112-1119 (1987).
24. T. Horiguchi, T. Kurashima, M. Tateda, K. Ishihara, and Y. Wakui, "Brillouin Characterization of Fiber Strain in Bent Slot-Type Optical-Fiber Cables," *J. Lightwave Tech.*, **10** [9] 1196-1201 (1992).
25. C.J. Sandwith, W.D. McCormick, J.A. Thornton, D.R. Wise, and R.I. Odom, "Fiber-Strain Measurement using Brillouin Optical-Fiber Time-Domain Analysis," *Proc. Int. Wire Cable Symp.*, **45**, 415-427 (1996).
26. R. Kashyap, *Fiber Bragg Gratings*, Academic Press, 1999.
27. G.P. Agrawal, *Fiber-Optic Communication Systems*, John Wiley & Sons, Inc. New York, 1997.
28. E. Denarie, V.E. Saouma, A. Iocco, and D. Varelas, "Concrete Fracture Process Zone Characterization with Fiber Optics" *J. Engr. Mech.*, **127** [5] 494 – 502 (2001).
29. L. Bjerkan, "Application of Fiber-Optic Bragg Grating Sensors in Monitoring Environmental Loads of Overhead Power Transmission Lines," *Appl. Opt.*, **39** [4] 554-560 (2000).
30. L. Baker, V. Bhatia, G.S. Glaesemann, M.A. Marro, and C. Mansfield, "Fiber Bragg Grating for Stress Field Characterization Inside a Connector," *Proc. SPIE*, **3848**, 207-211 (1999).
31. S. Capouilliet, J.A. Smith, D.J. Walter, G.S. Glaesemann, G.E. Kohnke and R. Irion, "A Fiber Bragg Based Measurement System for Monitoring Optical Fiber Strain," *Proc. Int. Wire Cable Symp.*, **50**, 240-248 (2001).
32. J.A. Smith and G.S. Glaesemann, "Design of a Fiber Bragg Based Measurement System for Strain and Temperature Monitoring," in *Review of Progress in Quantitative Nondestructive Evaluation*, **22**. Ed. D.O. Thompson, D.E. Chimenti, American Institute of Physics, Melville, NY, 2003.
33. J.A. Smith, G.S. Glaesemann, R. Johnson, and D.A. Clark, "In-process Stress Measurements Using Fiber Bragg Gratings," pp. 40-44 in proceedings of Lightwave Technologies in Instrumentation & Measurement Conference, Palisades, New York, USA, 19-20 October 2004.
34. G.S. Glaesemann, J.A. Smith, D.A. Clark, and R. Johnson, "Measuring Thermal and Mechanical Stresses on Optical Fiber in a DC Module using Fiber Bragg Gratings," *J. Lightwave Tech.*, **23** [11] 3461-3468 (2005).
35. W.B. Hillig, "Sources of Weakness and the Ultimate Strength of Brittle Amorphous Solids," in *Modern Aspects of the Vitreous State*, Volume 2. Edited by J.D. Machenzie. Butterworths, Washington, 1962.
36. B.A. Proctor, I Whitney and J.W. Johnson, "The Strength of Fused Silica," *Proc. Royal Soc. London, A*, **297**, 534-557 (1967).
37. W.B. Hillig, "The Factors Affecting the Ultimate Strength of Bulk Fused Silica," pp. 295-325 in Symposium sur la resistance mecanique du verre et les moyens de l'ameliorer. 1961. Union Scientific du Verre, Charleroi, Belgium.
38. C.R. Kurkjian and P.K. Gupta, "Intrinsic Strength and the Structure of Glass," *Proc. Int. Congr. Glass*, **1**, 11-18 (2001).
39. M.J. Winningham, M.D. Fabian, K.R. McCarthy, C.R. Dietrich, K.L. Simonton, J.T. Westbrook, and D.W. Hill, "Aged Fiber Strength and Adhesion Behavior of Fibers Containing Hydrophilic Primary Coatings," *Proc. Int. Wire Cable Symp.*, **53**, 288-295 (2004).
40. J.L. Mrotek, M.J. Matthewson, and C.R. Kurkjian, "Modeling of Diffusion through Optical Fiber Coatings," *Proc. SPIE*, **4215**, 144-149 (2001).
41. B.R. Lawn and R. Wilshaw, "Indentation Fracture: Principles and Applications," *J. Mater. Sci.*, **10**, 1049-1081 (1975).
42. D.B. Marshall and B.R. Lawn, "Surface Flaws in Glass," in *Fracture in Ceramic Materials*. Edited by A.G. Evans. Noyes Publications, N.J., 1984.
43. E.B. Shand, "Correlation of Strength of Glass with Fracture Flaws of Measured Size," *J. Am. Ceram. Soc.*, **44** [9] 451-455 (1961).
44. J.T. Hagan and S. Van Der Zwaag, "Plastic Processes in a Range of Soda-Lime-Silica Glasses," *J. Non-Cryst Solids*, **64**, 24-268 (1984).
45. J.T. Hagan, "Cone Cracks Around Vickers Indentations in Fused Silica Glass," *J. Mater. Sci.*, **14**, 462-466 (1979).

46. J.C. Newman and I.S. Raju, "An Empirical Stress Intensity Factor Equation for the Surface Crack," *Eng. Fract. Mech.* **15** [1-2] 185-192 (1981).
47. G.S. Glaesemann, K. Jakus, and J.E. Ritter, Jr., "Strength Variability of Indented Soda-Lime Glass," *J. Am. Ceram. Soc.*, **70** [6] 441-444 (1987).
48. J.T. Hagan and M.V. Swain, "The Origin of Median and Lateral Cracks around Plastic Indents in Brittle Materials," *J. Phys. D: Appl. Phys.*, **11** [15] 2091-2102 (1978).
49. B.R. Lawn, *Fracture of Brittle Solids*, Cambridge Univ. Press, 1993.
50. B.R. Lawn, B.J. Hockey and S.M. Wiederhorn, "Thermal Effects in Sharp-Particle Contact," *J. Am. Ceram. Soc.*, **63** [5-6] 356-357 (1980).
51. J. E. Field, B. Samuels, D. Townsend, and J. T. Hagan, "Cleavage of Optical Fibers Following Diamond-Wedge Indentation," *Philosophical Magazine*, **57** [2], 151-171 (1998).
52. T.P. Dabbs, D.B. Marshall, and B.R. Lawn, "Flaw Generation by Indentation in Glass Fibers," *J. Am. Ceram. Soc.*, **63** [3-4] C224-225 (1980).
53. K. Jakus, and J.E. Ritter, Jr., S.R. Choi and T.J. Lardner, "Failure of Fused Silica Fibers with Subthreshold Flaws," *J. Non-Cryst. Solids*, **102**, 82-87 (1988).
54. G.S. Glaesemann, D.A. Clark, and J.J. Price, "An Indentation Method for Creating Reproducible Proof-Stress Level Flaws in Commercial Optical Fiber," *Proc. SPIE*, **4639**, 21 (2002).
55. S.L. Semjonov, G.S. Glaesemann, C.R. Kurkjian, and M.M. Bubnov, "Modeling of Proof Test Level Flaws Using Cube Corner Indents," *Proc. Inter. Wire Cable Symp.*, **47**, 928-932 (1998).
56. J.M. Matthewson, "Optical Fiber Reliability Models," *Proc. SPIE Critical Review CR50*, 3-31 (1993).
57. H.C. Chandan and D. Kalish, "Temperature Dependence of Static Fatigue of Optical Fibers Coated with a UV-Curable Polyurethane Acrylate," *J. Am. Ceram. Soc.*, **65** [3] 171-173 (1982).
58. T.T. Wang and H.M. Zupko, "Long-Term Mechanical Behavior of Optical Fibres Coated with a U.V. Curable Epoxy Acrylate," *J. Mater. Sci.*, **13**, 2241- 2248 (1978).
59. M.J. Matthewson and C.R. Kurkjian, "Environmental Effects on the Static Fatigue of Silica Optical Fiber," *J. Am. Ceram. Soc.*, **71** [3] 177-83 (1988).
60. M.T. Kennedy, E. Cuellar, D.R. Roberts, and M.M. Stipek, "Stress-Free Aging of Optical Fiber in Water and Humid Environments: Part 2," *Proc. SPIE*, **1791**, 67-79 (1993).
61. R.S. Robinson and H.H. Yuce, "Scanning Tunneling Microscopy of Optical Fiber Corrosion: Surface Roughness Contribution to Zero-Stress Aging," *J. Am. Ceram. Soc.*, **74** [4] 814 (1991).
62. P.W. France, W.J. Duncan, D.J. Smith, and K.J. Beales, "Strength and Fatigue of Multicomponent Optical Glass Fibres," *J. Mater. Sci.*, **18**, 785-792 (1983).
63. P. Haslov, K.B. Jensen, and N.H. Skovgaard, "Degradation Study for Stressed Optical Fibres in Water. New Worst Case Time Estimation Model," *J. Am. Ceram. Soc.*, **77** [6] 1531-1536 (1994).
64. W. Griffioen, "Lifetime Model for Optical Fibers in Water," *Proc. SPIE*, **1973**, 150-160 (1993).
65. E. Cuellar, M.T. Kennedy, and D.R. Roberts, "Accelerated Static Fatigue Behavior of Optical Glass Fibers," *Proc. SPIE*, **1973**, 138-148 (1993).
66. A. Gouronnec, R. Goarin, G. Le Moigne, and M. Baptiste, "Optical Fiber Reliability Results from the BIARRITZ Field Trial," *Proc. SPIE*, **2290**, 191-203 (1994).
67. W. Griffioen, T. Volotinen, P. Wilson, A. Gouronnec, and T. Svensson, "Handleability of Aged Optical Fibers," *Proc. Inter. Wire Cable Symp.*, **44**, 857-864 (1995).
68. A. Dwivedi, G.S. Glaesemann, and C.K. Eoll, "Optical Fiber Strength, Fatigue and Handleability after Aging in a Cable," *Proc. Inter. Wire Cable Symp.*, **43**, 728-735 (1994).
69. K. Houser and S. Chahanovich, "Verification of Optical Fiber and Cable Reliability," *Proc. Inter. Wire Cable Symp.*, **47**, 468-474 (1998).
70. J.L. Smith, A. Dwivedi, and P.T. Garvey, "Mechanical Behavior of Optical Fibers Removed from a Field-Aged Cable," *Proc. Inter. Wire Cable Symp.*, **44**, 848-856 (1995).
71. G.S. Glaesemann, "The Mechanical Behavior of Large Flaws in Optical Fiber and Their Role in Reliability Predictions," *Proc. Inter. Wire Cable Symp.*, **41** 689-704 (1992).
72. G.S. Glaesemann, J.E. Ritter, Jr., and K. Jakus, "Mixed-Mode Fracture in Soda-Lime Glass Using Indentation Flaws," *J. Am. Ceram. Soc.*, **70** [9] 630-36 (1987).

73. V. Frechette, *Failure Analyses of Brittle Material; Advances in Ceramics – Volume 28*, The American Ceramic Society, Westerville, Ohio, 1990.
74. Derek Hull, *Fractography: Observing, Measuring and Interpreting Fracture Surface Topography*, Cambridge University Press, Cambridge, UK, 1999.
75. E.B. Shand, "Breaking Stress of Glass Determined from Dimension of Fracture Mirrors," *J. Am. Ceram. Soc.*, **42** [10] 474-477 (1959).
76. J.J. Mecholsky, R.W. Rice, and S.W. Freiman, "Prediction of Fracture Energy and Flaw Size in Glasses from Measurements of Mirror Size," *J. Am. Ceram. Soc.*, **57** [10], 440-443 (1973).
77. M.J. Kerper and T.G. Scuderi, "Modulus of Rupture in Relation to Fracture Pattern," *Ceram. Bull.*, **43** [9] 622-625 (1964).
78. S.T. Gulati, C.B. King, and F. Quan, "Some Recent Results on Fracture Stress and Mirror Size for Optical Fibers," *Proc. Int. Wire Cable Symp.*, **27** (1978).
79. L.K. Baker and G.S. Glaesemann, "Break Source Analysis, Alternate Mirror Measurement Method," *Proc. Int. Wire Cable Symp.*, **47**, 933-937 (1998).
80. S.R. Choi and J.P. Gyekenyesi, "Crack Branching and Fracture Mirror Data of Glasses and Advanced Ceramics," NASA Technical Report TM 1998-206536, 1998.
81. H.C. Chandan and R.D. Parker, "Fractography of Optical Fibers," in *Fractography of Glass*. Edited by R.C. Bradt and R.E. Tressler, Plenum Press, NY, 1994.
82. J.J. Mecholsky, and R.W. Rice, "Fractographic Analysis of Biaxial Failure in Ceramics," in *Fractography of Ceramics and Glass Failures*, ASTM STP 827. Edited by J. Mecholsky and S. Powell, ASTM, Westerville, OH, 1984.
83. E.B. Shand, "Breaking Stress of Glass Determined from Fracture Surfaces," *The Glass Industry*, **4**, 190-194 (1967).
84. H.P. Kirchner and J.W. Kirchner, "Fracture Mechanics of Fracture Mirrors," *J. Am. Ceram. Soc.*, **62** [3-4] 198-202 (1979).
85. J.J. Mecholsky, "Fracture Surface Analysis of Optical Fibers," in *Engineered Materials Handbook: Ceramics and Glasses*, ASM International, **4**, 663-668 (1991).
86. R.J. Castilone, G.S. Glaesemann, and T.A. Hanson, "Relationship Between Mirror Dimensions and Failure Stress for Optical Fibers," *Proc. SPIE*, **4639**, 11-20 (2002).
87. ASTM C1322-05b, "Standard Practice for Fractography and Characterization of Fracture Origins in Advanced Ceramics."
88. T.A. Michalske, "Quantitative Fracture Surface Analysis," in *Engineered Materials Handbook: Ceramics and Glasses*, ASM International, **4**, 652-662, (1991).
89. D.G. Holloway, "The Fracture Behavior of Glass," *Glass Technology*, **27** [4] 120-133 (1986).
90. S.M. Wiederhorn, "Influence of Water Vapor of Crack Propagation in Soda-Lime Glass," *J. Am. Ceram. Soc.*, **50** (8) 407-414 (1967).
91. T.A. Michalske and S.W. Freiman, "A Molecular Interpretation of Stress Corrosion in Silica," *Nature*, **295** (2), 511-12 (1982).
92. S.W. Freiman, "Fracture Mechanics of Glass," *Glass Science and Technology*, **5**, 21-79 (1980).
93. W.S. Hillig and R.J. Charles; pp. 682-705 in *High-Strength Materials*, Edited by W.F. Zackay. Wiley & Sons, New York, 1965.
94. S.M. Wiederhorn and L.H. Boltz, "Stress Corrosion and Static Fatigue of Glass," *J. Am. Ceram. Soc.*, **53** [10] 543-48 (1970).
95. A.G. Evans, "Slow Crack Growth in Brittle Materials under Dynamic Loading Conditions," *Inter. J. Fracture*, **10** (2) 251-259 (1974).
96. T. Fett, "A Fracture-Mechanical Theory of Subcritical Crack Growth in Ceramics," *Inter. J. Fracture*, **54**, 117-130 (1992).
97. J.E. Ritter, G.S. Glaesemann, K. Jakus, and P. Rampone, "Dynamic Fatigue of Soda-Lime Glass as a Function of Temperature," *Phys. Chem. of Glass.*, **27** [2] 65-70 (1986).
98. H. Schonhorn, T.T. Wang, H.N. Vazirani, and H.L. Frisch, "Static and Dynamic Fatigue of High-Strength Glass Fibers Coated with a UV-Curable Epoxy-Acrylate," *J. Appl. Phys.*, **49** (9) 4783-4787 (1978).
99. G.S. Glaesemann and S.T. Gulati, "Dynamic Fatigue Data for Fatigue Resistant Fiber in Tension vs. Bending," Technical Digest Series, *Optical Fiber Communication Conference*, **5**, 48 (1989).
100. J.E. Ritter, Jr., J.M. Sullivan, Jr., and K. Jakus, "Application of Fracture-Mechanics Theory to Fatigue Failure of Optical Glass Fibers," *J. Appl. Phys.*, **49** (9) 4779-4782 (1978).

101. Y.S. Shiue and M.J. Matthewson, "Stress Dependent Activation Entropy for Dynamic Fatigue of Pristine Silica Optical Fibers," *J. Appl. Phys.*, **89** [9] 4787-4793 (2001).
102. D. Kalish and B.K. Tariyal, "Static and Dynamic Fatigue of a Polymer-Coated Fused Silica Optical Fiber," *J. Am. Ceram. Soc.*, **61** [11-12] 518-523 (1978).
103. W.J. Duncan, P.W. France, and S.P. Craig, "The Effect of Environment on the Strength of Optical Fiber," in *Strength of Inorganic Glass*. Edited by C.R. Kurkjian. Plenum Press (1985).
104. C.R. Kurkjian, J.T. Krause, and M.J. Matthewson, "Strength and Fatigue of Silica Optical Fibers," *J. Lightwave Tech.*, **7** [9] 1360-1370 (1989).
105. S.P. Craig, W.J. Duncan, P.W. France, and J.E. Sodgrass, "The Strength and Fatigue of Large Flaws in Silica Optical Fibres," in *Proc. 8<sup>th</sup> ECOC*, (1982).
106. G.S. Glaesemann, Masters Thesis, University of Massachusetts, 1983.
107. H.H. Yuce, P.L. Key, and D.R. Biswas, "Investigation of the Mechanical Behavior of Low Strength Fibers," *Proc. SPIE*, **1174**, 272-278 (1989).
108. F.A. Donaghy and D.R. Nicol, "Evaluation of the Fatigue Constant n in Optical Fibers with Surface Particle Damage," *J. Am. Ceram. Soc.*, **66** [8] 601-4 (1983).
109. S. Sakaguchi and Y. Hibino, "Fatigue in Low-Strength Silica Optical Fibers," *J. Mater. Sci.*, **19**, 3416-20 (1984).
110. T.P. Dabbs and B.R. Lawn, "Strength and Fatigue Properties of Optical Glass Fibers Containing Microindentation Flaws," *J. Am. Ceram. Soc.*, **68** [11] 563-69 (1985).
111. M.J. Matthewson, "Strength and Reliability of Fused Silica Optical Fiber," *Proc. BROADBAND (FOC/LAN)*, (1990).
112. J.E. Ritter, Jr., and C.L. Sherburne, "Dynamic and Static Fatigue of Silicate Glasses," *J. Am. Ceram. Soc.*, **54** [12] 601-605 (1971).
113. S.T. Gulati, "Mechanical Properties of SiO<sub>2</sub> versus SiO<sub>2</sub>-TiO<sub>2</sub> Bulk Glasses and Fibers," in proceedings of 1991 MRS Fall Meeting, Boston.
114. S.M. Wiederhorn, A.G. Evans, and D.E. Roberts, "A Fracture Mechanics Study of Skylab Windows," pp. 829-41 in *Fracture Mechanics of Ceramics*, Vol. 2. Edited by R.C. Bradt, D.P.H. Hasselman, and F.F. Lange. Plenum Press, New York, 1974.
115. S. Sakaguchi, Y. Sawaki, Y. Abe, and T. Kawasaki, "Delayed Failure in Silica Glass," *J. Mat. Sci.*, **17**, 2878-2886 (1982).
116. S.L. Semjonov and G.S. Glaesemann, "High-Speed Tensile Testing of Optical Fibers – New Understanding for Reliability Prediction," in *Micro- and Opto-Electronic Materials and Structures: Physics, Mechanics, Design, Reliability, Packaging*, Edited by E. Suhir, C.P. Wong, and Y.C. Lee. Springer, Cambridge, MA, 2006.
117. H.H. Yuce, P.L. Key, and H.C. Chandan, "Aging Behavior of Low Strength Fused Silica Fibers," *Proc. SPIE*, **1366**, 120-128 (1990).
118. A.H.E. Breuls and T. Svensson, "Strength and Fatigue of Zirconia-Induced Weak Spots in Optical Fiber," *Proc. SPIE*, **2074**, 78-82 (1994).
119. S.L. Semjonov, G.S. Glaesemann, D.A. Clark and M.M. Bubnov, "Fatigue behavior of silica fibers with different defects," *Proc. SPIE*, **4215**, 28-35 (2000).
120. R.E. Mould and R.D. Southwick, "Strength and Static Fatigue of Abraded Glass under Controlled Ambient Conditions: II," *J. Amer. Ceram. Soc.*, **42**, 582-592 (1959).
121. S.L. Semjonov, G.S. Glaesemann, and M.M. Bubnov, "Fatigue behavior of Silica Fibers of Different Strength," *Proc. SPIE*, **3848**, 102-107 (1999).
122. C.R. Kurkjian, D. Biswas and H.H. Yuce, "Intrinsic Strength of Lightguide Fibers," *Proc. SPIE*, **2611**, 56-63 (1995).
123. J.E. Ritter, Jr., "Engineering Design and Fatigue Failure of Brittle Materials," in *Fracture Mechanics of Ceramics*, Vol.4. Edited by R.C. Bradt, D.P.H. Hasselman, and F.F. Lange. Plenum Publishing, 1978.
124. Y. Mitsunaga, Y. Katsuyama, H. Kobayashi, and Y. Ishida, "Failure Prediction for Long Length Optical Fiber Based on Proof Testing," *J. Applied Phys.*, **53** (7) 4847-4853 (1982).
125. T. Volotinen, A. Breuls, N. Evanno, K. Kemeter, C. Kurkjian, P. Regio, S. Semjonov, T. Svensson, and G.S. Glaesemann, "Mechanical Behavior and B-Value of an Abraded Optical Fiber," *Proc. Inter. Wire Cable Symp.*, **47**, 881-890 (1998).
126. T.A. Hanson and G.S. Glaesemann, "Incorporating Multi-Region Crack Growth into Mechanical Reliability Predictions for Optical Fibers," *J. Mat. Sci.*, **32**, 5305 – 5311 (1997).
127. H.C. Chandan, R.C. Bradt, and G.E. Rindone, "Dynamic Fatigue of Float Glass," *J. Am. Ceram. Soc.*, **61** [5-6] 207-210 (1978).
128. S.L. Semjonov and M.M. Bubnov, "On the Concept of Multi-Region Crack Growth," *Mater Res Soc.*, **531**, 243-248 (1998).

129. Y. Hibino, S. Sakaguchi, and Y Tajima, "Crack Growth in Silica Glass under Dynamic Loading," *J. Am. Ceram. Soc.*, **67** [1] 64-68 (1984).
130. IEC SC86A/WG1 NO-17A, "Technical Report on the Power-Law Theory of Optical Fibre Reliability," March 1997.
131. S. Sakaguchi and T. Kimura, "Influence of Temperature and Humidity on Dynamic Fatigue of Optical Fibers," *J. Am. Ceram. Soc.*, **64** [5] 259-262 (1981).
132. A.T. Taylor and M.J. Matthewson, "Effect of pH on the strength and fatigue of fused silica optical fiber," *Proc. Inter. Wire Cable Symp.*, **47**, 874-880 (1998).
133. Y.S. Shiue and M.J. Matthewson, "Stress Dependent Activation Entropy for Dynamic Fatigue of Pristine Silica Optical Fibers," *J. Appl. Phys.*, **89** [9] 4787-4793 (2001).
134. M.J. Matthewson, C.R. Kurkjian, C.D. Haines, N. Venugopal, "Temperature Dependence of Strength and Fatigue of Fused Silica Fiber in the Range 77 to 473 K," *Proc. SPIE*, **4940**, 74-79 (2003).
135. S.L. Semjonov, M.M. Bubnov, and O.V. Khleskova, "Susceptibility of static fatigue parameters of optical fibers to environmental conditions", *Proc. SPIE*, **2611**, 49-54 (1995).
136. S.L. Semjonov, G.S. Glaesemann, D.A. Clark, and M.M. Bubnov, "Effect of environmental conditions on fatigue of weak silica-clad optical fibers," *Proc. SPIE*, **5465**, 61-67 (2004).
137. D. Inniss, C.R. Kurkjian, and D.L. Brownlow, "Summary of Stress Dependent Activation Energy for Lightguide Fibers," *J. Am. Ceram. Soc.*, **75** [12] 3485-86 (1992).
138. J.E. Ritter, Jr., G.S. Glaesemann, and K. Jakus, "Effect of Temperature on the Strength and Fatigue Behavior of Optical Fibres," *J. Mater. Sci.*, **19** 4087-4092 (1984).
139. K.E. Lu, G.S. Glaesemann, R.V. VanDewoestine, and G. Kar, "Recent Developments in Hermetically Coated Optical Fiber," *J. Lightwave Tech.*, **6** [2] 240-243 (1988).
140. R.G. Huff and F.V. DiMarcello, "Hermetically Coated Optical Fibers for Adverse Environments," *Proc. SPIE*, **867** (1987).
141. C.R. Kurkjian, P.G. Simpkins, and D. Inniss, "Strength, Degradation, and Coating of Silica Lightguides," *J. Am. Ceram. Soc.*, **76** [5] 1106-1112 (1993).
142. M.M. Bubnov, E.M. Dianov, A.M. Prokhorov, S.L. Semjonov and C.R. Kurkjian, "Dual Hermetically Coated Optical Fibers with Strength of 9 GPa," *OFC post deadline paper* (1992).
143. N. Yoshizawa, H. Tada and Y. Katsuyama, "Strength Improvement and Fusion Splicing for Carbon-Coated Optical Fiber," *J. Lightwave Tech.*, **9** [4] 417-421 (1991).
144. R.W. Filas, "Metallization of Silica Optical Fibers," *Mater. Res. Soc.*, **531**, 263-272 (1998).
145. S.T. Gulati, J.D. Helfinstine, G.S. Glaesemann, D.R. Roberts, E. Cuellar and L.M. Middleman, "Improvements in Optical Fiber Reliability via High Fatigue Resistant Composition, Fiber Optics Reliability: Benign and Adverse Environments, *Proc. SPIE*, **842**, 22-30 (1987).
146. US Patent 5,181,269, Optical Fiber Including Acidic Coating System.
147. R.D. Maurer, "Strength of Fiber Optical Waveguides," *Appl. Phys Lett.*, **27** [4] 220-221 (1975).
148. C.R. Kurkjian, R.V. Albarino, J.T. Krause, H.N. Vazirani, F.V. DiMarcello, S. Torza, and H. Schonhorn, "Strength of 0.04-50 m Lengths of Coated Fused Silica Fibers," *Appl. Phys. Lett.*, **28** [10] 588-590 (1976).
149. R. Olshansky and R.D. Maurer, "Tensile Strength and Fatigue of Optical Fibers," *J. Appl. Phys.*, **47** [10] 4497-4499 (1976).
150. H. Schonhorn, C.R. Kurkjian, R.E. Jaeger, H.N. Vazirani, and R.V. Albarino, "Epoxy-Acrylate-Coated Fused Silica Fiber with Tensile Strengths >500 ksi (3.5 GN/m<sup>2</sup>) in 1-km gauge lengths," *Appl. Phys. Lett.*, **29** [11] 712-714 (1976).
151. B. Justice, "Strength Considerations of Optical Waveguide Fibers"; pp. 115-133, in *Fiber and Integrated Optics*, Vol. 1, Number 2. Edited by Henri Hodara, Crane, Russak & Company, Inc., New York, 1977-1978.
152. W.E. Snowden, "Surface Flaws and the Mechanical Behavior of Glass Optical Fibers"; pp. 143-159, in *Fracture Mechanics of Ceramics*, Vol. 3. Edited by R.C. Bradt, D.P.H. Hasselman and F.F. Lange, Plenum Press, New York, 1977.
153. B.K. Taryal and D. Kalish, "Mechanical Behavior of Optical Fiber"; pp. 161-175, in *Fracture Mechanics of Ceramics*, Vol. 3. Edited by R.C. Bradt, D.P.H. Hasselman and F.F. Lange, Plenum Press, New York, 1977.
154. B. Justice and S.T. Gulati, "Tensile Tester for Long Optical Fibers," *Ceram. Bull.*, **57** [2] 217-219 (1978).
155. R.D. Maurer, "Strength of Screen Tested Optical Waveguide Fibers," *Mat. Res. Bull.*, **14**, 1305-1310 (1979).
156. F.V. DiMarcello, A.C. Hart, Jr., J.C. Williams and C.R. Kurkjian, "High Strength Furnace Drawn Optical Fibers," *Fiber Opt.*, 125-135 (1979).
157. C.R. Kurkjian and U.C. Paek, "Single-Valued Strength of 'Perfect' Silica Fibers," *Appl. Phys. Lett.*, **42**, 251 (1983).

158. M.J. Matthewson, C.R. Kurkjian, and S.T. Gulati, "Strength Measurement of Optical Fibers by Bending," *J. Am. Ceram. Soc.*, **69** [11] 815-821 (1986).
159. N.P. Lower, R.K. Brow, C.R. Kurkjian, "Inert Failure Strain Studies of Sodium Silicate Glass Fibers," *J. Non-Cryst. Solids*, **349**, 168-172 (2004).
160. P.W. France, M.J. Paradine, M.H. Reeve, and G.R. Newns, "Liquid Nitrogen Strengths of Coated Optical Glass Fibers," *J. Mater. Sci.*, **15**, 825-830 (1980).
161. W. Griffioen, G. Segers, and E. van Loenen, "Two-Point Bending Apparatus, Fracturing Optical Fibres at Different Speeds in One Run: Measurements in Standard and Vacuum Environment," *Proc. Inter. Wire Cable Symp.*, **39**, 368 (1990).
162. C.R. Kurkjian and J. Kieffer, "Elastic Properties of Glasses," in *Handbook of Elastic Properties of Solids, Liquids, and Glasses*. Edited by Levy, Bass, and Stern. Academic Press, 2001.
163. W. Griffioen, T. Svensson, and B. Friderich, "Optical Fiber Inert Strength and B-Value," *Proc. Inter. Wire Cable Symp.*, **43**, 750-758 (1994).
164. N.H. Macmillian, "Review: The Theoretical Strength of Solids," *J. Mater. Sci.*, **7** 239-254 (1972).
165. J. Bjorkman and T. Svensson, "Quick-Access to Fracture Statistics at Ultra-Wide-Range Tensile Test of Optical Fibers," *Proc. Inter. Wire Cable Symp.*, **39**, 373-378 (1990).
166. TIA/EIA-455-28C, Measuring Dynamic Strength and Fatigue Parameters of Optical Fiber by Tension, (Telecommunications Industry Association, Arlington VA, 1999).
167. IEC 793-1-B7B, Dynamic Fatigue Parameters of Optical Fibers by Two Point Bending, (International Electrotechnical Commission, 1995).
168. R.D. Maurer, "Strength of Fiber Optical Waveguides," *Appl. Phys. Lett.*, **27** [4] 220-221 (1975).
169. A. Paul and G.S. Glaesemann, "An Appraisal of Mechanical Reliability Predictions for Optical Fibers Based on Break Rates," *Proc. Inter. Wire Cable Symp.*, **46**, 896-901, 1997.
170. G.S. Glaesemann and D.J. Walter, "Method for Obtaining Long-Length Strength Distributions for Reliability Prediction," *Opt. Eng.*, **30** [6] 746-748 (1991).
171. TIA/EIA ITM-1, "Characterization of Large Flaws in Optical Fibers by Dynamic Tensile Testing with Censoring," (1994).
172. R.J. Castilone, G.S. Glaesemann, and T.A. Hanson, "Extrinsic Strength Measurements and Associated Mechanical Reliability Modeling of Optical Fiber," *National Fiber Optics Engineers Conference*, **16**, 1-9 (2000).
173. G.S. Glaesemann, "Optical Fiber Failure Probability Predictions from Long-Length Strength Distributions," *Proc. Inter. Wire Cable Symp.*, **40**, 819-825 (1991).
174. T. Wei, H.H. Yuce, C.H. Hasz and P.L. Key, "Degradation of Fiber Strength during Coating Stripping," *Proc. Inter. Wire Cable Symp.*, **48**, 199-204 (1989).
175. C.R. Kurkjian, "Distribution of Stripping-Induced Flaws," *Proc. SPIE*, **4215**, 150-157 (2001).
176. W.R. Wagner, "Extrinsic fiber damage and its effect on the reliability of optical fiber connectors and splices," *Proc. SPIE*, **1580**, 168-185 (1992).
177. V.V. Rondinella and M.J. Matthewson "Effect of Chemical Stripping on the Strength and Surface Morphology of Fused Silica Optical Fiber," *Proc. SPIE*, **2074**, 52-58 (1994).
178. M.J. Matthewson, C.R. Kurkjian, and J.R. Hamblin, "Acid Stripping of Fused Silica Optical Fibers Without Strength Degradation," *J. Light. Tech.*, **15** [3] 490-497 (1997).
179. J.T. Krause, G.W. Kammlott, S.G. Kosinski, and R.S. Riggs, "Improved Strengths (3.7 GPa) of Arc Fusion Splices for High Yield-High Reliability," *Proc. ECOC*, 449-452 (1993).
180. J.T. Krause and C.R. Kurkjian, "Fibre Splices with 'Perfect Fibre' Strengths of 5.5 GPa,  $v < 0.01$ ," *Electron. Lett.*, **21**, 533-535 (1985).
181. S. Pitassi, "Effect of Arc Fusion Conditions on Strength of Single-Fiber and Ribbon Fiber Splices," *Proc. 10<sup>th</sup> NFOEC*, 257-270 (1994).
182. J.T. Krause and D. Stroumbakis, "Factors Affecting Arc Fusion Splice Strengths," *Proc. SPIE*, **2611**, 98-109 (1996).
183. N. Yoshizawa, H. Tada, and Y. Katsuyama, "Strength Improvement and Fusion Splicing for Carbon-Coated Optical Fiber," *J. Light. Tech.*, **9** [4] 417-421 (1991).
184. M.G. Estep and G.S. Glaesemann, "The Effect of Carbon Overcoating on the Mechanical Behavior of Large Flaws," *Proc. SPIE*, **1791**, 18-24 (1992).
185. D. Inniss and J.T. Krause, "Hermetic Splice Overcoating," *Opt. Eng.*, **30** [6] 776-779 (1991).

186. G.F. Orcel, "Dynamic Fatigue of Metallized Fiber Optics," *Proc. SPIE*, **1791**, 110-116 (1993).
187. G.V. Srinivasan and J.E. Webb, "Reliability of Fiber in Fiber Bragg Grating Devices," *Proc. SPIE*, **3848**, 186-194 (1999).
188. H.G. Limberger, D. Varelas, R.P. Salathé, and G. Kotrotsios, "Mechanical Degradation of Optical Fibers Induced by UV Light," *Proc. SPIE*, **2841** 84-93 (1996).
189. D.A. Barber and N.H. Rizvi, "Characterization of the Effects of Different Lasers on the Tensile Strength of Fibres during Laser Writing of Fibre Bragg Gratings," *Proc. SPIE*, **4876**, 321-329 (2003).
190. Y. Sidorin, S.L. Semjonov, and M.M. Bubnov, "Strength and Fatigue Measurements using the Fibers with Laser-Induced Glass Defects," *Opt. Mater.*, **10** [3] 79-83 (1998).
191. D. Kececioglu, *Reliability Engineering Handbook*, Volume 1, Prentice-Hall, Upper Saddle River, NJ, 1991.
192. K. Oishi, W. Katsurashima, T. Kakuta, Y. Matsuda, and S. Tanaka, "Coating Design of Thin Coated Fiber for Ultra-High-Count Optical Fiber Cable," *Proc. Inter. Wire Cable Symp.*, **42**, 687-693 (1993).
193. G.S. Glaesemann, "Process Handleability of Thin-Coated Optical Fibers," *OFC'94 Tech. Digest*, **5**, 243-244 (1994).
194. D.J. Wissuchek, D.J. Walter, D.A. Clark, and G.S. Glaesemann "Fracture and Abrasion Resistance Test for Optical Fiber Coatings," *Mat. Res. Soc.*, **531**, 309-314 (1998).
195. G.S. Glaesemann and D.A. Clark, "Quantifying the Puncture Resistance of Optical Fiber Coatings" *Proc. Inter. Wire Cable Symp.*, **50**, 240-248 (2003).
196. G.S. Glaesemann and S.T. Gulati, "Design Methodology for the Mechanical Reliability of Optical Fiber," *Opt. Eng.*, **30** [6] 709-715 (1991).

**Corning Incorporated**  
[www.corning.com/opticalfiber](http://www.corning.com/opticalfiber)

One Riverfront Plaza  
Corning, New York  
USA

Phone: (607)248-2000  
Email: [cofic@corning.com](mailto:cofic@corning.com)

Corning is a registered trademark of Corning Incorporated, Corning, N.Y.

© 2017, Corning Incorporated